Abiotic Mechanisms for Cyanobacteria Physiology and Distribution in Lakes: A Multi-Scale Approach

A THESIS
SUBMITTED TO THE FACULTY OF THE GRADUATE SCHOOL
OF THE UNIVERSITY OF MINNESOTA
BY

Anne Ahlvers Wilkinson

IN PARTIAL FULFILLMENT OF THE REQUIREMENTS
FOR THE DEGREE OF
DOCTOR OF PHILOSOPHY

Professor Michelle Guala, *advisor*
Professor Miki Hondzo, *co-advisor*

May, 2018

Acknowledgements

This dissertation represents work done by many many scientist, engineering, agencies and friends. I am ever grateful to my advisers Michele Guala and Miki Hondzo for not only coming out to the lake with me to help with sampling and maintenance; but most importantly providing me direction in not only my research but my personal and professional development.

I am grateful for the knowledge and input from other faculty members at the University of Minnesota. First to Shahram Missaghi who has mentored me from the start teaching me laboratory techniques and provided my laboratory culture. He has expanded my network with the HAB community by always including me in this outreach and workshops which has given me invaluable practical knowledge. Thank you to Dr Christine Salomon and her lab group at the Center for Drug Design for guidance and equipment for toxin analysis. I am grateful for Dr Bill Arnold for providing input on chemical analysis for the inorganic carbon flux quantification.

My dissertation research would not have been possible without the dedication and ingenuity of the technical staff, students and my lab mates. I am eternally grateful to Dr Chris Ellis for his guidance and genius which touches every part of the work outlined in this thesis. His tireless work for the faculty and students at SAFL has created a culture of excellence and creativity that has made SAFL a truly special place. Thank you to Ben Erickson, Chris Milleren and all the technical staff and students who have helped with all laboratory operations and particular the fabrication and maintenance of the research station.

Special thank you to Jiaqi You and Jacqueline Taylor for the help in the lab and in the field and your friendship. Thank you to all the SAFL students and staff that have supported me, listened to my practices, participated in planning community events. I am lucky to share this journey with you.

Thank you to Steven Heiskary, Isaac Marin and Pam Anderson and the staff at the MPCA for assistance with samples, data and research station deployment and maintenance. Thank to Adam Heathcoate, the Madison lake association, the city of Madison Lake and the Lindstrom sheriff's department and everyone in the MN HAB planning team for help with data collection, research station support and forming a strong HAB network

Funding was provided in part by the Legislative-Citizen Commission on Minnesota Resources (LCCMR), Environment and Natural Resources Trust Fund 2015-2016, Assessing the Increasing Harmful Algal Blooms in Minnesota Lakes, ID: 038-B. Data described in this paper are available online according to the journal guidelines. I am grateful for the National Science Foundation for the Graduate Research Fellowship and the University of Minnesota for the Doctoral Dissertation Fellowship for providing support for my stipend, travel and tuition.

Dedication

This thesis is dedicated with love and appreciation:

To Nikolas who spent many nights in the lab processing samples and editing with me to enable we to do this and many more night sitting with me, and convincing me that I could do this even when I didn't believe I could. You are my best friend and I love you.

To My family, the Ahlvers, the Tarkas and the Wilkinsons, who have continually supported me in achieving all my goals, never once doubting my potential and always encouraging me to push harder to achieve what you always believed I could. That backbone of support has allowed me to finish this journey and has given me the confidence to achieve any of my past and future goals. In particular, this thesis is dedicated to my grandfathers, Norman Fontaine and Donald Ahlvers, who both passed away during my tenure in graduate school. Their love and support provided a constant foundation for our family and I am proud to complete this journey knowing they are watching over me.

To all women and girls who have a dreams or interest in STEM, YOU CAN DO IT! I have been lucky to be inspired, challenged and mentored by some of the most amazing young women, that I am lucky to call my friends. To Brittany, you were my first lab partner in my science career and ever since our collaborations as two of the few women in our department we have achieved so much together. Our friendship is something that is beautiful and rare and I cherish it with all my heart. To the smiling flowers, our diverse scientific and life backgrounds made us an unstoppable force ever since our first "study sessions in the library". I never felt more capable, confident, beautiful and powerful as when we were all working together. I owe so much to you three, you not only made me a better scientist but a better person.

TO my SAFL family, I have learned that luckily I don't always have to know you can do it but you have a network of support from friends, family and mentors that will step in and hold you up when you feel like everything is falling apart. Most of all, Mirko was that person for me.

Abstract

Harmful Algal Blooms (HABs) are a ubiquitous ecological and public health hazard because they are comprised of potentially toxic freshwater microorganisms, called cyanobacteria. Cyanobacteria are capable of accumulating in large concentrations in fresh-water ecosystems during summer and producing a toxin (microcystin) that in high concentration can be harmful to humans and animals. The occurrences of toxic HABs are highly spatially and temporarily variable in freshwater ecosystems and are difficult to predict. These HABs can be governed by abiotic environmental conditions including water temperature structure, light, nutrient abundance, and mixing. This dissertation increases the understanding of abiotic environmental conditions, i.e. different mixing scales, on the physiology and distribution of cyanobacteria in nutrient invariant eutrophic systems using field and laboratory studies.

In the laboratory, we investigated the effect of small-scale turbulence on the growth and metabolism of *Microcystis aeruginosa*. The laboratory bioreactor setup included two underwater speakers, generating a quasi-homogeneous turbulent flow, comparable to field values in the lacustrine photic zone (Re_λ =0, Re_λ =33 and Re_λ =15). The results suggest that turbulence mediates the metabolism of *Microcystis aeruginosa,* quantified by the net oxygen production, oxygen uptake, and inorganic carbon uptake, which is not manifested in changes in growth rate.

In the field, we investigate the abiotic drivers for cyanobacteria and microcystin vertical distribution using a research station to quantify a wide range of local

meteorological conditions, water temperature, and water chemistry, including phycocyanin, in two different eutrophic stratified Minnesota lakes. The monitoring effort was coupled with discrete weekly sampling measuring nutrients, cyanobacteria composition, and microcystin concentrations. Our objective was to describe the distributions of cyanobacteria biovolume (BV) and microcystin concentrations (MC) using easily measurable physical lake parameters. The analysis of vertical heterogeneity of cyanobacteria in the entire water column revealed high positive correlations among BV stratification, surface water temperature, stratification stability, quantified by the Schmidt stability. During strong stratification, the MC and BV accumulated above the thermocline and were highly correlated. Although, the cyanobacteria BV is significant only above the thermocline during stratification where cyanobacteria are exposed to high phosphate, temperature and light, there is still further vertical variability to explain within this region. Two types of BV distributions were observed above the thermocline. The first distribution depicted BV uniformly distributed over the diurnal surface mixed layer (SL). The second BV distribution displayed local BV maxima near and under the surface in the SL. A quantitative relationship was developed to determine the probability of observing a uniform distribution as a function of the surface Reynolds number (Re_{SL}), the dimensionless ratio of inertial to viscous forces, over the SL. The uniform distribution was observed for $Re_{SL}>50{,}000$. The outcome of this analysis is the first step towards the quantification and prediction vertical stratification of cyanobacteria biovolume and microcystins as a function of local meteorological and physical conditions in a stratified lake.

Contents

List of Tables

List of Figures

Chapter 1

Introduction to Harmful Algal Blooms

Harmful Algal Blooms, HAB, or cyanobacteria blooms are being witnessed and monitored worldwide [1,2]. HAB are made up of large accumulations of microorganisms called cyanobacteria. Cyanobacteria are the world's oldest oxygenic photo-autrophs and are responsible in part for the oxygenation of the planet's atmosphere [3]. They also have special physio-ecological traits which distinguish them from other phytoplankton. Cyanobacteria cells are capable of regulating their buoyancy and moving through the water column presumably seeking favorable conditions [4]. This allows them to form surface or metalimnetic blooms and out compete other phytoplankton [2,5]. Cyanobacteria are colloquially named blue green algae because along with chlorophyll they produce an auxiliary pigment, phycocyanin, which allows them to harvest a broader range of wavelengths of incident light [3]. This pigment allows them to have specific spectral

signatures that can be exclusively monitored in water bodies by remote sensing or fluorescent probes [6,7]. Individual cells form diverse colonies or filaments of variable morphologies [4]. Individual cells have specialty strategies for dealing with variable nutrient conditions. For example, regulating inorganic carbon utilization to power their photosynthetic metabolism during times of high productivity, environmental stress and variable inorganic carbon [8,9]. Additionally, cyanobacteria are capable of fixing atmospheric nitrogen in order to persist in low nitrogen environments [4].

Figure 1.1: Images of HAB in lakes. The images are taken by Anne Wilkinson.

These adaptions allow cyanobacteria to dominate warm surface waters affecting the ecosystem, Figure 1.1. The surface blooms out compete other phytoplankton by removing nutrients, elevating pH, reducing light penetration into the water column, and locally increasing temperature from that light absorption [4,10,11]. On the macro scale large pockets of photosynthetic respiration can locally deplete dissolved oxygen, which can cause fish kills [12].

From a human perspective, the special cyanobacteria traits have present scientific and ecological significances. However, cyanobacteria blooms are capable of producing potent toxins, which pose significant public health and safety risk [1]. Cyanotoxins range in potency and structure including, hepatotoxins (affecting the liver), neurotoxins (affecting the brain) and dermatoxins (affecting the skin) [1,13]. However, hepatotoxins, microcystins are the only ones regulated by the world health organization and the Environmental Protection Agency (EPA). This may be because they are the most stable and potent of the cyanotoxins produced by freshwater cyanobacteria[1,2]. Microcystins are a secondary metabolite produced by cyanobacteria in that it is not necessary for primary metabolism and cell division [2]. They have been linked to internal and external functions in the ecosystem, however the role of microcystins is still speculative [2]. Some hypothesize they are used for intracellular processes such as carbon, nitrogen or light regulation or for extracellular protection i.e. metabolite inhibition in other phytoplankton or reduction of grazing pressure from zooplankton and protozoa [2,13,14]. Along with the effects of dominate biomass, cyanotoxins produced by some HABs affect the ecosystem in deleterious ways. Cyanotoxins have been shown to induce liver disease in fish [2,15].

Microcystin has been shown to be assimilated by terrestrial plants irrigated with contaminated water [15]. Beyond these ecological impacts, cyanotoxins are a human health concern. Microcystins can cause GI symptoms, blisters, liver disease and cancer [1]. Human exposure can come from recreational activities like accidental ingestion during swimming or inhalation from lake spray or aerosolization. Along with recreational exposure, populations can be exposed to cyanotoxins from drinking water contamination, since conventional water treatment or boiling does not remove microcystins from the influent [15].

Because of these ecological and public health concerns it is important to understand the causes or drivers of HAB formation. Prediction and management is difficult because cyanobacteria blooms are not caused by one parameter but are driven and sustained by a mix of interacting physical and biological parameters. Specifically, stably stratified waters with high epilimnetic concentrations of phosphate and inorganic nitrogen, and low grazing pressure from zooplankton [2,11]. Climate change has a role to play in the dominance of cyanobacteria as warmer water temperatures mean both conditions for optimal growth but also increases in bloom season and water column stability [10,11,16,17]. Additionally increases in CO_2 in the atmosphere would relieve C limitations in the epilimnion during high growth periods promoting more photosynthetic activity [4].

Cyanobacteria blooms are increasingly a concern worldwide and thus more monitoring efforts and management practices have been employed [1,2]. Current monitoring efforts range from remote sensing using satellites on the great lakes [18] to anchored buoy network with fixed point fluorometry to photic zone sampling [19]. These

efforts rely on the distinct pigments, phycocyanin, present in cyanobacteria which allow them to be distinguished from other phytoplankton or inorganic compounds. However, HAB distribution, both spatial and temporal, is not well understood. Thus sampling efforts must be optimized to capture the data that is representative of the HAB dynamics to direct efficient management strategies.

Current HAB management strategies for lake restoration include strategies to reduce nutrient inputs into the lake, however phosphate is a legacy nutrient and stays in the water column [20]. Other strategies for discouraging HAB development include the installation of artificial aeration to break stratification and by introducing mixing the water column to reduce the development of HAB [16]. Sonic waves and chemical additives have been used to encourage the growth of other phytoplankton and discourage cyanobacteria growth [21,22]. Strategies for removing HAB and cyanotoxins have already developed including flocculation by clay to absorb MC and cyanobacteria colonies in the water column, UV and microbial degradation [2]. However these strategies, especially the use of chemical treatments could induce cell lysis which has the potential to increase extracellular MC in the water column and have had mixed success [2,14].

HAB is a growing problem that has not been solved and there are many facets that still have to be understood. This thesis adds to the understanding of these nuances by identifying and characterizing new factors that contribute to cyanobacteria physiology, and distribution in lakes. Chapter 2 discusses the effect of small-scale turbulence on cultured *Microcystis* in controlled laboratory experiments with nutrient invariant conditions. In chapter 3, I discuss field observations using a newly developed research station in a

dimictic, eutrophic lake describing cyanobacteria biomass vertical heterogeneity in the water column using easily measurable physical lake parameters. Chapter 4 expands on this discussion by further describing biomass distribution above the thermocline to direct when, where, and how many samples to take in both a dimictic and polymictic eutrophic lake. Most importantly, this chapter links the biovolume and microcystin distributions to leverage the previously relationships with easily measurable conditions Finally, chapter 5 outlines the conclusions of this thesis and the recommendations for management and HAB monitoring developed from the results presented here.

Chapter 2

Effect of Small-Scale Turbulence on the Growth and Metabolism of *Microcystis aeruginosa*

Introduction

Cyanobacteria blooms are an ubiquitous nuisance in freshwater ecosystems throughout the world [23]. The cyanobacteria frequently dominate eutrophic lakes in summer months under high nutrient, warm, calm water conditions, where they can easily outcompete other aquatic microorganisms. Two unique adaptation strategies contribute to the dominance of cyanobacteria in these systems. First is the ability of individual cells to bond together into colonies. Second is the capability to regulate their buoyancy and thus their location with respect to the surface of the water column [24,25]. Cyanobacteria blooms are of such

interest not only because of the induced foul taste, odor and turbidity in lake water but also due to their contribution to hypoxia and subsequent fishery collapse [26]. Certain cyanobacteria, such as the *Microcystis aeruginosa*, produce a deadly liver toxin called microcystin. This compound has been regulated in drinking water by the World Health Organization (WHO), as it is known carcinogen, gastrointestinal irritant and is responsible for animal deaths when present in high concentration [26,27]. The production and utilization of microcystin by *Microcystis* has been widely studied, however evidence has not been entirely cohesive. Studies do point to the use of microcystin in competition with other organisms for dominance within aquatic system, for example: i) aiding in intracellular inorganic carbon (C_i) regulation under low environmental C_i conditions to sustain photosynthetic processes [28]; ii) inhibiting the metabolism of other microorganisms [29], and iii) maintaining colonies through promotion of polysaccharide production [30].

Microcystin production is only one of the competitive strategies that *Microcystis* can exhibit. *Microcystis* can persist in a broad range of environmental conditions where other microorganisms cannot, including cold temperatures [31], low C_i conditions [32], and in the presence of common herbicides [33]. Additionally, unlike many aquatic microorganisms, *Microcystis* remains photo-chemically active as they overwinter in the water column [31]. The authors reported that *Microcystis* react to environmental stressors, such as cold, dark water conditions, by reducing their metabolism. This behavior is known as a Type I stress response [34]. *Microcystis* have a photosynthetic metabolism and produces carbohydrates from C_i dissolved in the water and uses them for polysaccharide production, RNA and nucleic acid production. Any excess C_i is released during the dark

cycle during respiration. RNA and nucleic acids are primarily used in cell division, whereas polysaccharides are used in colony formation [35]. Thus, the availability of C_i is vital for the well-being of the *Microcystis* population. *Microcystis* can also adapt to varying levels of C_i within their environment through the utilization of a Carbon Concentrating Mechanism (CCM), which concentrates C_i on the primary CO_2 fixing enzyme, RuBisCO [8,36,37]. This adaptation is essential for survival in periods of high productivity when C_i concentrations are low. Conversely, when the C: N ratio gets too high, and the *Microcystis* become nitrogen limited; they can sink excess C_i into extracellular polysaccharides (EPS) [38,39]. For all these reasons, C_i concentration is a critical diagnostic variable when studying *Microcystis* growth and metabolism under different abiotic factors or environmental stresses.

Abiotic factors such as nutrient concentration, temperature, and photosynthetically active radiation (PAR) levels may define the necessary conditions for bloom initiation; however, hydrodynamics is recognized as a key controlling factor in the impact and extent of bloom persistence [40]. *Microcystis* are in fact exposed to a variety of fluid flow conditions, within their habitat, especially near the lake surface where they cluster during harmful algal bloom (HAB), and experience turbulent mixing effects by wind and waves [41]. Although many studies, discussed above, demonstrate *Microcystis'* ability to adapt to their dynamic environment, the influence of hydrodynamics has not been thoroughly investigated. It has been shown that different microscopic algae react in different ways to the variability of fluid flow conditions. For instance, Chengala et al. (2013)[42] demonstrated that fluid motion facilitates favorable nutrient uptake for a green alga,

Dunaliella primolecta, through the modification of the boundary layer around the cell. Kenis and Hoyt (1971) [43] and Jenkinson and Sun (2014)[44] showed that marine microalgae, planktonic algae, and bacteria produce EPS to increase drag reduction by locally modifying the viscosity of the ambient fluid.

Management and prediction of HAB formation and microcystin production require a comprehensive understanding of bloom mechanics and the response of microorganisms to the corresponding range of environmental conditions that occur in nature. Our particular objective is to investigate the metabolic and growth responses of *Microcystis aeruginosa* to different fluid flow conditions, consistent with observations in lacustrine environments. This is accomplished by evaluating the effect of turbulence based on careful monitoring of several physical and chemical variables including PAR, pH, alkalinity, dissolved oxygen (DO), and temperature while varying the hydrodynamic forcing. Experiments were performed in a bioreactor actuated by two underwater speakers, designed to maintain a quasi-homogeneous isotropic turbulent flow with limited mean flow and mean shear, which can be well described by the Taylor micro-scale Reynolds number (Re_λ). The fluid flow in the bioreactor was controlled to achieve comparable energy dissipation rates to those observed in the photic zone of Lake Minnetonka, Minneapolis, MN.

Materials and Methods

Speaker Reactor

The experimental setup, in Figure 2.1, is a submersible speaker bioreactor made from a 21.5 cm x 21.5 cm x 52 cm Plexiglas tank with two underwater speakers (AQ339 Aquasonic; Clark Synthesis, Littleton, CO, USA) positioned behind a mesh grid ($1cm^2$ mesh, 0.4 solidity) at each end. This experimental apparatus is also used in Chengala et al. (2013)[42]. The fluid motion in this setup is generated by the vibration of the speaker diaphragm, which pushes the fluid through the grid. The speakers were out of phase with each other by 180º (reverse polarity), therefore, when the left speaker contracted, the right speaker expanded, allowing for the continuous generation of eddies into the test section. The speakers can generate different flow conditions by actuating sinusoidal signals of varying prescribed frequencies (Hz) and amplitudes (V). A programmable Labview (National Instruments, Austin, TX, USA) function generator connected to an amplifier (Samson Servo 300, Samson Technologies, Hauppauge, New York, USA) generates the speaker signals. The bioreactor is completely enclosed and slightly pressurized. All instruments and adjustments are made *in situ*. A magnetic scraper (ProMag, Aqueon, Franklin, WI, USA) was employed before cell counts at the bottom of the tank to re-suspend settled cells and ensure proper cell concentration measurements.

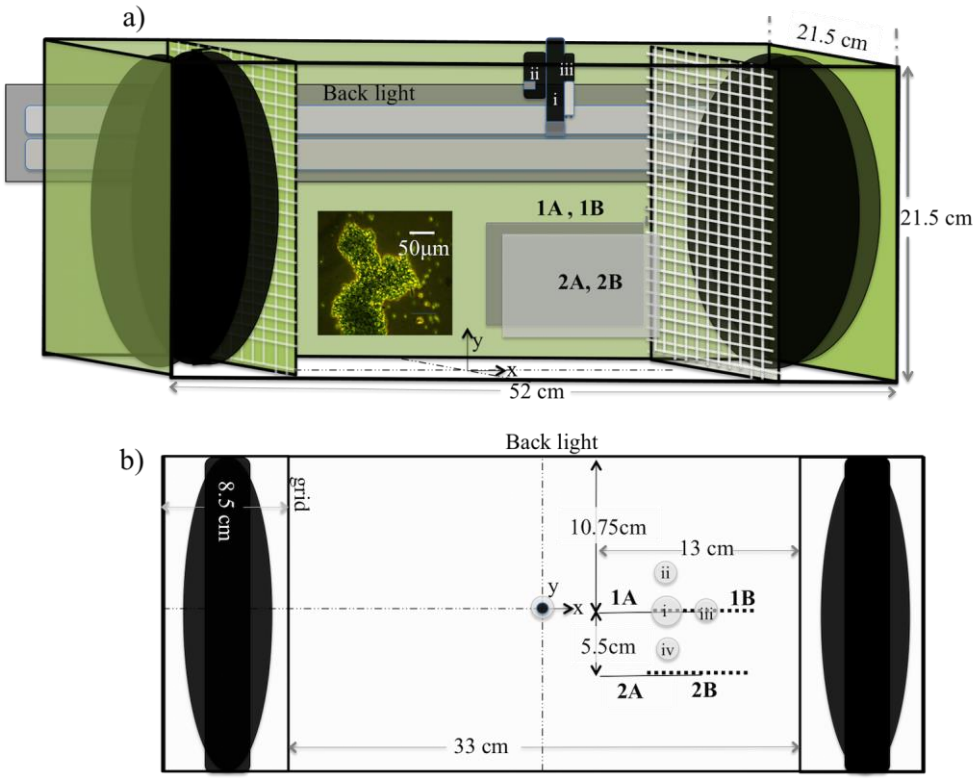

Figure 2.1: Schematic overview of the speaker reactor setup. a) Speaker reactor schematic detailing the positions of the PIV planes, the sampling location representing the positions of the instruments (i, chlorophyll probe, ii, DO probe, iii, pH meter), the origin and the orientation of the (x,y) reference system, the position of the back light, and orientation of the speakers with respect to the grid. b) Top view schematic showing the orientation of the PIV planes with respect to the instrument locations and the sampling hole (iv).

Initial experimental conditions

Each experiment used a 14:10 hour light-dark cycle from simulated solar fluorescent lights (Phillips Plant and Aquarium 20W, Phillips, Andover, MA, USA) positioned on each side of bioreactor parallel to the main aquarium axis and perpendicular to the speaker orientation to ensure uniform vertical light exposure, and prevent light dependent algal distribution. The PAR was measured near the tank every 5 minutes during the experiment by a spherical quantum sensor (LI-193 LICOR, Lincoln, NE, USA) yielding an average 58.3±4.4 (μmol/m^2 s) during the light cycle and 39.7±1.4 (μmol/m^2 s) during the dark period. The fluid temperature was monitored every five minutes in conjuncture with the DO measurements by an optical oxygen and temperature sensor (Optode 3835 Aanderaa Data Instruments AS, Bergen, Norway) yielding an average temperature of 23.03±1.86 °C.

Table 2.1: Comparison of average environmental conditions in the laboratory bioreactor and Lake Minnetonka, MN. The Lake Minnetonka data consist of time and depth-averaged values within the photic zone (0.5-1.5 m) at 10-10:30 am, see Appendix. The laboratory bioreactor data report time averaged values obtained during the maximum daily growth period (11 am-1pm) for all lab experiments, for all days.

	Environmental parameters		
	pH	DO_{sat}(%)	Light (μmol/m^2 s)
Lake Minnetonka	8.09	82.7	114.7-26.5
Laboratory bioreactor	6.8-7.4	55.7-132.9	58.3

After an equilibration period, the pH was adjusted (day 4-10) to 5.8-6.2, as shown in Figure 2.2, by bubbling industrial grade CO_2 gas (Matheson Gas, New Brighton, MN, USA) using a 23 in. air curtain diffuser (Elite Pet Supplies, Vineyard, NSW, Australia). The addition of CO_2 to the system increases the growth rate as compared to the estimated growth rate of samples without CO_2 adjustment (observed by Qiu and Gao, 2002[45] and confirmed in our preliminary experiments). On days 3-11, the DO saturation was reduced to 20-30% daily immediately following the pH adjustment, also shown in Figure 2.2, by bubbling industrial grade N_2 gas (Matheson Gas, New Brighton, MN, USA) through the same diffuser. Both environmental adjustments, pH and DO, had to be made because of the lack of gas exchange in the bioreactor, as it is a closed system. As discussed above, access to C_i is vital for the health of the population. The DO adjustment is made to prevent photo-oxidative death, in which too much oxygen and light can cause chlorophyll bleaching and premature population die off, especially in low C_i conditions [25,26].

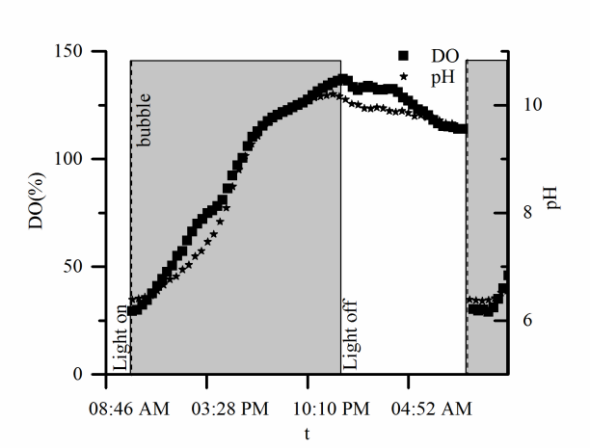

Figure 2.2: An example of daily light, DO and pH adjustments, the dashed line symbolizes when the CO_2 and N_2 gasses were bubbled, and the gray box represents the light cycle. As can be seen after the bubbling of N_2 and CO_2, the DO and pH are reduced to daily initial conditions (~9 am).

Flow Measurement Setup

The fluid motion within the bioreactor was quantified by non-intrusive two-dimensional (2D) Particle Image Velocimetry (PIV) in which small tracer particles are illuminated by a laser sheet and tracked through a series of high-speed images. The system comprised of a high speed camera (VC-4MC-M180E0 Viewworks, Anyang, Gyeonggi, Republic of Korea), fitted with Nikon AF 50mm lens (Nikon, Tokyo, Japan), with a resolution of 2048 x 2048 pixels, able to capture 1000 images at 30 frames per second within a field of view of 7 cm x 7 cm. The tracer particles were 8-12 μm hollow glass spheres (1.05 g cm^{-3}) and were illuminated by ND:YAG pulsed green laser (LPY 700 series Litron, Rugby England, UK). The laser and the camera were synchronized (TSI

LaserPulse, Shoreview, MN, USA) and controlled by Insight 4G software (TSI, MN) that processed the images to derive 2D velocity fields; u, and v, oriented according to Figure 1. The flow was measured in four planes without the presence of *Microcystis*, for two speaker settings (50 Hz frequency, at 0.2V amplitude and 30Hz at 0.2V). Based on symmetry considerations, flow statistics averaged over the four planes are considered representative of the full aquarium.

Fluid Flow Analysis

The experimental apparatus was designed to mimic environmental flows at laboratory scale under controlled and monitored conditions. Spatio-temporally resolved velocity fields were measured by PIV, see Figure 2.3, to adequately quantify turbulent characteristics in each experimental case, respectively identified by: the Reynolds number, $Re_\lambda=(u_{rms}\ \lambda)/\nu$ (where u_{rms} is the root mean square velocity, Taylor micro-scale (λ), and ν is the kinematic viscosity), the rate of energy dissipation (ε), and the Kolmogorov length scale (η). The Reynolds number based on the Taylor micro-scale is often used to describe homogeneous turbulence (e.g. [46]).

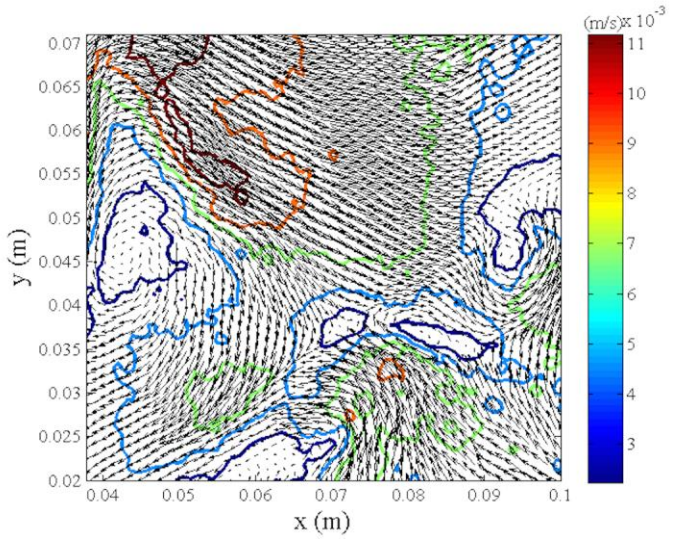

Figure 2.3: Sample instantaneous velocity vector field in the speaker reactor at Reλ =33. x and y are based on the origin shown in Figure 1. The contours represent the magnitude of the (u,v) velocity vectors (m/s).

The Taylor micro-scale, λ, is the intermediate length scale characterizing homogeneous and isotropic turbulence, in between the integral length scale ($L_{x,y}$) and the Kolmogorov length scale. Physically it defines the upper limit of the region where viscosity is still relevant to turbulent eddy formation. The Taylor micro-scale in this study was estimated in two ways: i) using Equation 2.1, requiring an estimate of ε (hence the notation λ_ε), ii) using the autocorrelation of fluctuating velocity components, u(x) or v(y), as shown in Figure 2.4, simply referred to as λ.

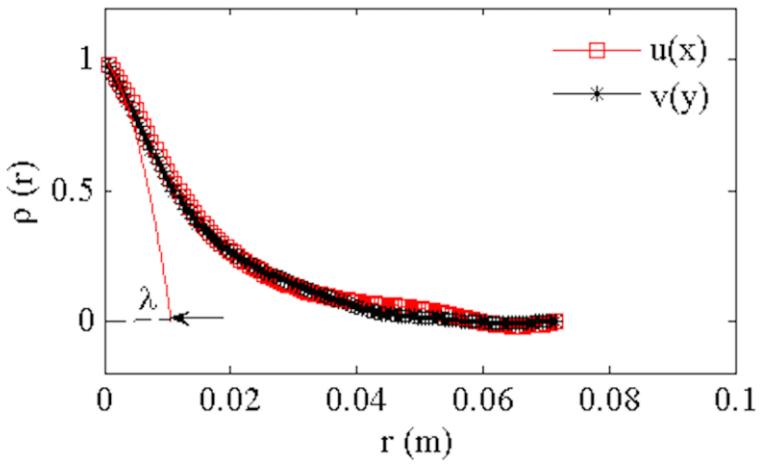

Figure 2.4: Spatial autocorrelation function of the horizontal and vertical velocity components along the vertical (y) and the transverse (x) directions of the bioreactor setup (Reλ =33) showing how the fit parabola yields the estimate of the Taylor micro-scale, λ, represented by the black arrow.

Here the autocorrelation function is defined for homogeneous isotropic turbulence as $\rho(r_\rho)=\langle u(x)u(x+r_\rho)\rangle/\langle u^2(x)\rangle$, where u(x) is the velocity fluctuation, r_ρ is the spatial lag, and the < > expression indicates spatial averaging along any x coordinate (e.g. [47]).

$$\lambda_\varepsilon = \sqrt{30\nu u_{rms}^2/\varepsilon} \tag{2.1}$$

where the rate of energy dissipation can be estimated using the two-dimensional (2D) spatial velocity derivatives [42,48,49]

$$\varepsilon(x,y) = 4\nu\left((\frac{\partial u}{\partial x})^2 + (\frac{\partial v}{\partial y})^2 + \frac{3}{4}(\frac{\partial u}{\partial y})^2 + \frac{3}{4}(\frac{\partial v}{\partial x})^2 + \frac{\partial u}{\partial x}\frac{\partial v}{\partial y} + \frac{3}{2}(\frac{\partial u}{\partial y}\frac{\partial v}{\partial x})\right) \tag{2.2}$$

A relevant turbulent length scale for phytoplankton growth and nutrient uptake in quasi-homogeneous turbulence is the Kolmogorov scale, $\eta=(\nu^3/\varepsilon)^{1/4}$ [42]. It represents the scale of the smallest eddies in the flow, where turbulent kinetic energy is eventually dissipated into heat and defines the lower limit of the inertial range.

Table 2.2: Flow characteristics in the speaker reactor and at the Lake Minnetonka measurement site. The values for u_{rms}, v_{rms} and ε are spatially averaged over the PIV planes (30Hz 1B,2A planes, 50Hz all planes), described in the fluid characterization section. A detailed description of Lake Minnetonka data analysis is in Appendix.

	Fluid parameters								
	Re_λ	$Re_{\lambda,\varepsilon}$	λ(m)	λ_ε(m)	u_{rms}(m/s)	u_{rms}/v_{rms}	$\varepsilon(m^2/s^3)$	η(m)	L_x/L_y
Laboratory bioreactor 30Hz0.2V	15	12	0.0112	9.1×10^{-3}	1.1×10^{-3}	1.33	3.7×10^{-7}	1.1×10^{-3}	0.93
Laboratory bioreactor 50Hz0.2V	33	26	$9.1x10^{-3}$	7.4×10^{-3}	3×10^{-3}	1.04	4.1×10^{-6}	6.2×10^{-4}	1.01
Lake Minnetonka	-	32	-	9.1×10^{-3}	3.2×10^{-3}	0.86	3.4×10^{-6}	6.9×10^{-4}	-

Agreement between λ_ε and λ, shown in Table 2.2, indicates consistency between the velocity autocorrelation and the estimation of $\varepsilon(x,y)$, based on spatial velocity derivatives, supporting both the quality of the flow measurements and the homogeneity of the flow. Although the Reynolds number is relatively small [46] there is strong agreement with the turbulence intensities observed in Lake Minnetonka in the presence of cyanobacteria near the surface of the water column (see Appendix).

Evidence of homogeneity and isotropy

As can be seen in Figure 2.5a, the energy dissipation rate is relatively uniform in the vertical profile with the exception of Re_λ =33, near the wall. This supports our effort to generate quasi-homogeneous turbulence within the bioreactor. Additionally, evidence of homogeneity can be seen in Figure 2.5b, as the autocorrelation curves obtained for different PIV planes are fairly consistent. Evidence of isotropic turbulence shown in Table 2.2 include: i) the ratio of velocity fluctuations $u_{rms}/v_{rms} \sim 1$, ii) the autocorrelation curves are illustrated in Figure 4 and the resulting estimates of the integral length scales are independent of the directions, u(x), v(y) along which statistics are computed: L_x / L_y = 1.01,0.93 for the Re_λ=33, and 15 respectively. Note that the integral length scales, L_x, L_y, calculated from the integral of the corresponding normalized autocorrelation curves, represent the largest, statistically significant, eddy in the turbulent flow.

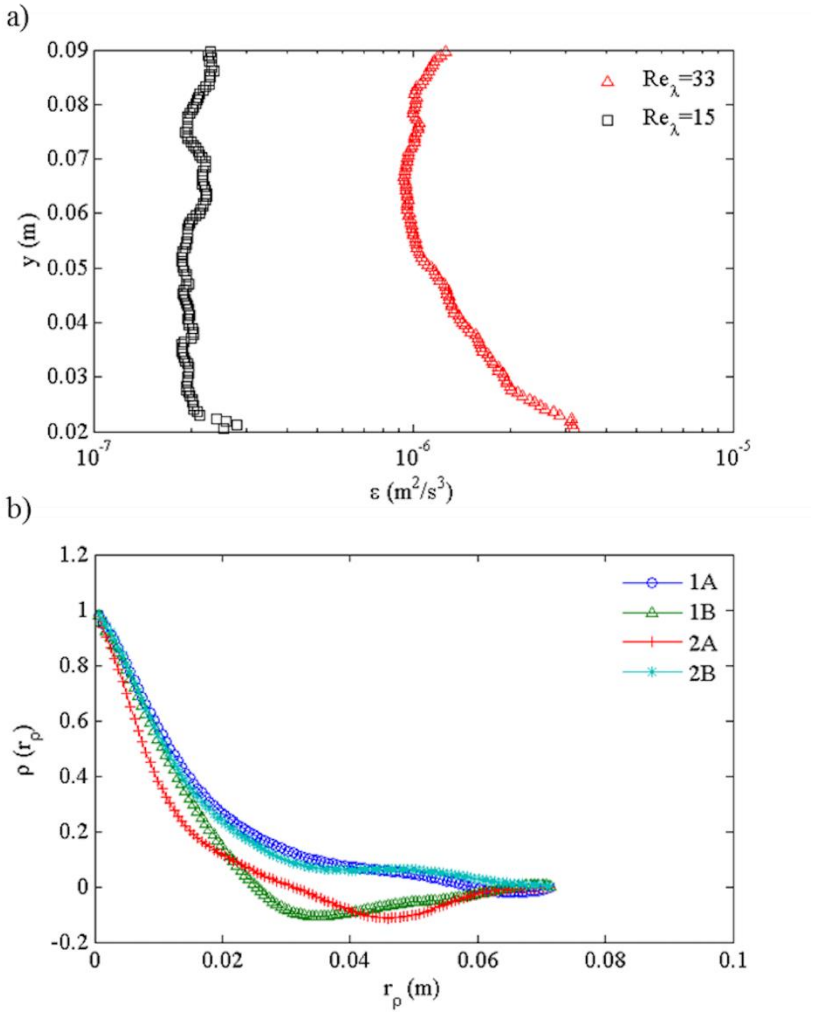

Figure 2.5: Evidence of isotropy in the speaker reactor a) Vertical Profile of energy dissipation rate, ε, (Re$_\lambda$ =33 and 15). The vertical profile of the energy dissipation rate is estimated by averaging along the x direction the median of the time historyε(x,y,t), determined from Equation 2.2 (Re$_\lambda$ =15 , planes 1B, 2A , and Re$_\lambda$ =33 all planes) . b) Normalized autocorrelation of u(x) estimated for all PIV planes at Re$_\lambda$ =33.

Microcystis culture and analysis

The *Microcystis aeruginosa* strain B3-R-7 was obtained by the Department of Fisheries and Allied Aquacultures, Auburn University, Alabama. The cultures were maintained in tanks in the presence of 1:50 BG-11 media dilution (Sigma-3061, Sigma-Aldrich, St Louis, MO, USA) and Mili-Q water (Millipore, Billerica, MA, USA) and exposed to natural light. Samples taken from this culture were diluted in fresh growth media, allowed to grow for 4-8 days, to ensure they were within the exponential growth phase. The speaker reactor was then inoculated with an initial concentration of 100,000 cells/mL from this culture. Three depth-averaged samples (9 mL) were taken from the top of the tank by inserting a plastic tube into the bioreactor, then blocking the top of the tube and extracting a sample. Samples were taken once per day (day 1-11), each morning after the pH and oxygen saturation were adjusted. The cell concentration was estimated using the average of triplicate cell counts using a hemocytometer. Statistical analysis of cell concentration data were analyzed using a two-way ANOVA with replication with factors (turbulence level and time) with an α =0.05 using Microsoft Office Excel 2010(Redmond, WA, USA).

Growth rate for the full experimental cycle can be estimated using the Verhulst logistic equation for population-limited growth, below [50,51]:

$$\frac{dN}{dt} = k_g N\left(1 - \frac{N}{K}\right) \tag{2.3}$$

where N is the cell concentration, t is time, k_g is the growth rate, and K is the carrying capacity.

A second method for assessing *Microcystis* concentration and growth is based on chlorophyll measurements. The fluorometer (Cyclops 7, Turner Designs, Sunnyvale, CA, USA) was employed to measure the chlorophyll *a* (Chla) within the tank, after a calibration procedure. From the fluorometer output (V), cell concentration data during the dark cycle can be obtained by the calibration curve (data not shown).

Dissolved Ci and DO Data

DO production, C_i, and DO uptake are indicators of photosynthetic activity and can reveal critical information on *Microcystis*' cellular metabolism [52]. The C_i can be calculated from Equation 2.4 by measuring the alkalinity and the pH within the speaker reactor. The pH of the system was taken in situ every five minutes with a pH meter (pHASE, SensorX, Garden Grove, CA, USA) connected to a transmitter (TX100pH/mV 2 wire, SensorX, Garden Grove ,CA, USA), which is logged by a Labview program. The alkalinity was measured twice per day (on days 4-10), once in the morning after pH and oxygen adjustment and again in the evening (6 hours later). The alkalinity measurements using 100mL depth averaged samples were titrated following the standard operating procedure (SOP) WQ/WC 202.1 (USDA/ARS-Stuttgart National Aquaculture Research Center, Almyra, AR, USA). The titrant used was a standardized 0.02N H_2SO_4, prepared according to the reagent preparation in the SOP, from carbon dioxide free water

and H_2SO_4 (ACS grade, BDH H3070, VWR, Radnor PA, USA). The pH and alkalinity measurements allow for C_i calculation through the carbonate cycle for a closed system.

$$[Alk] = \left(\frac{K_{a1}[H+] + 2K_{a1}K_{a2}}{[H+]^2 + K_{a1}[H+] + K_{a1}K_{a2}} \right) C_T + \frac{K_W}{[H+]} - [H+] \tag{2.4}$$

where [Alk] is the alkalinity, C_T is the total C_i, $[H+] = 10^{-pH}$, $K_{a1}=10^{-6.35}$, $K_{a2}=10^{-10.33}$, $K_w=10^{-14}$ at 25° C and 1 bar [53].

The flux of C_i, J_{Ci}, was calculated using the change in total C_i over the relevant daily growth period (~6 hours into the light cycle), using Equation 2.5:

$$\frac{dC_T}{dt} = J_{C_i} * SA_{cell} * N \tag{2.5}$$

where SA_{cell} is the cell surface area. The SA_{cell} was estimated based on measured cell equivalent radius [54].

Although both alkalinity and pH are necessary for C_i calculations in a closed system, pH time series data can give a qualitative measure of the C_i uptake during the light cycle (photosynthesis) and C_i production in the dark cycle (respiration). The lower the pH, the more C_i is present in the system due to the transformation of dissolved CO_2 gas to carbonic acid. Thus, when the *Microcystis* remove C_i from the water during photosynthesis, the pH increases as observed in Figure 2.6a. The CO_2 is not added until day 4 and the pH response is not as rapid as observed during the exponential growth period. This is due to the lower cell concentration in lag phase when the *Microcystis* population has not yet reached exponential growth. This trend is observed at both Re_λ.

As discussed above, CO_2 adjustments were enforced when the pH was above 5.8-6.2, ensuring that at the beginning of every day *Microcystis* were exposed to the same environmental conditions, pH, DO, and temperature.

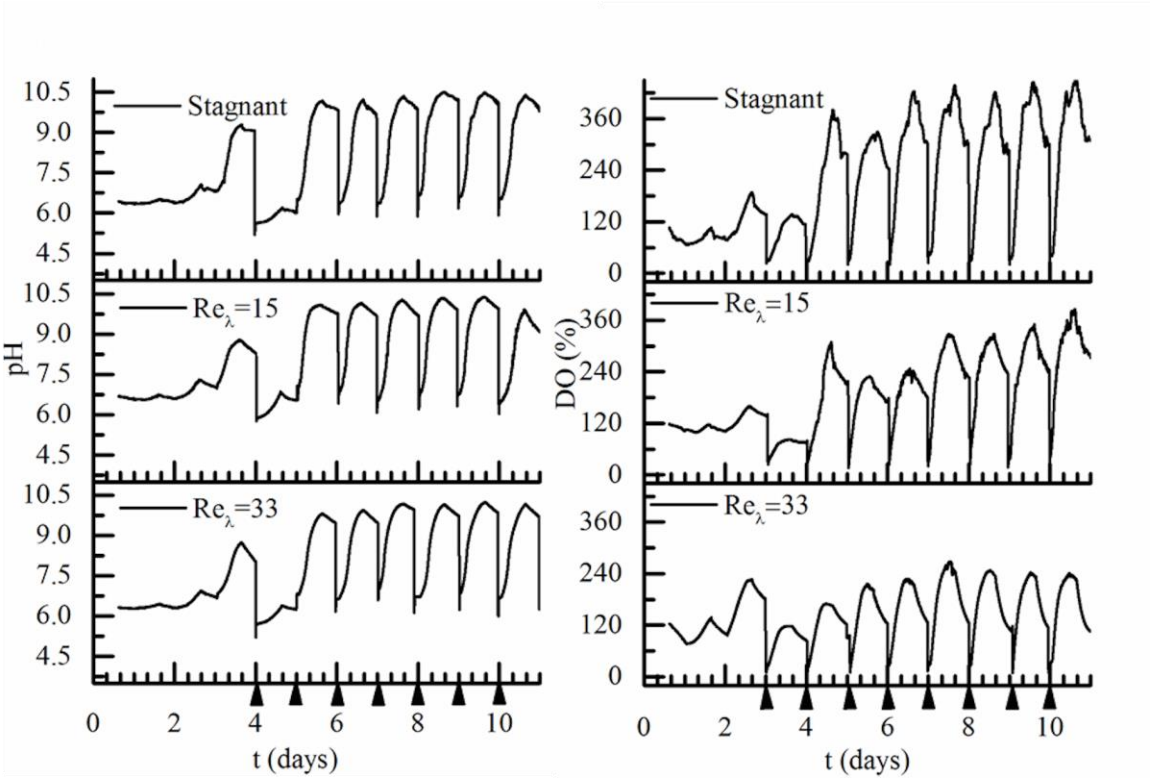

Figure 2.6: Example DO and pH time series for the three experimental conditions investigated (stagnant Reλ=33 and 15). The arrows indicate when the N2 and CO2 were bubbled to adjust the DO and pH in the bioreactor.

DO was measured, *in situ*, at 5 minutes increments using an optical oxygen and temperature sensor, as discussed above. The flux of oxygen, J_{DO}, was computed using the slope of the oxygen time series, (d(DO))/dt ((DO mol)/(L*min)), estimated in the

following time period: 5 hours after initial condition adjustment for net photosynthetic oxygen production, up to 5 hours prior to the adjustment for respiratory oxygen uptake.

$$\frac{d(DO)}{dt} = J_{DO} * SA_{cell} * N \qquad (2.6)$$

These fluxes represent the average net production of oxygen for each *Microcystis* cell during the day (J_{DOprod}) and the corresponding average uptake of DO during the night (J_{DOupt}). As shown in Figure 6b, diurnal oxygen production (net photosynthesis) and uptake (respiration) occurred throughout the exponential growth phase, which is to be expected with photosynthetic organisms. During the daily growth interval, the oxygen concentration reached super-saturation, thus requiring nitrogen bubbling to avoid damage to cell population.

Lake Minnetonka Data

Data were collected in August 2014 in Lake Minnetonka, MN from Halsted Bay, a site frequently reported to have HAB activity. The field measurements were performed using a SondTek MicroADV (acoustic-Doppler velocimetry) (SondTek ,San Diego, CA, USA) to measure u, v, and w velocity time series at 50Hz acquisition, and Hydrolab 4a Datasonde (Hach Company, Ames, IA, USA) to measure: temperature, pH, DO, specific conductivity, depth and PAR at full depth.

Velocity analysis

The ADV velocity data were taken within the photic zone at a 0.67 m depth, and were process by WinADV software (US Department of Interior Bureau of Reclamation). As

shown in Table 2, the averaged pH, DO and light (PAR) at 0.67 m depth are consistent with the initial conditions established in the laboratory speaker reactor experiments.

Energy dissipation rate estimation

The energy dissipation rate, ε, for the field data can be estimated by using the velocity time series from the ADV (see Figure 2.7) and the second order structure function (see Figure 2.8). First, velocity (u) data was aligned to the mean flow direction, $u_{aligned}$. Then the $u_{aligned}$ time series was filtered ($u_{filtered}$) to remove the effect of surface waves using a high pass filter with a cut off frequency (f_{cut}) of 1Hz.

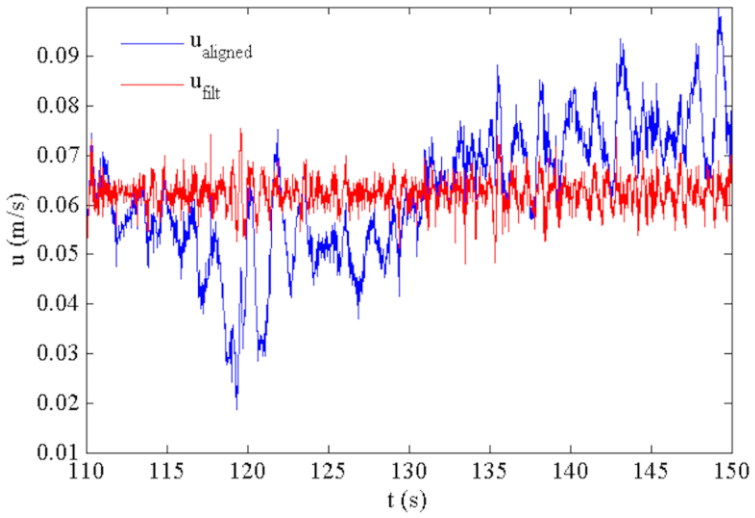

Figure 2.7: ualigned (m/s) compared to ufiltered (m/s).

We estimated the energy dissipation rate using the pre-multiplied second order structure function of $u_{filtered}$ in the inertial range [55] :

$$D_{11}(r) = \overline{[u_1(x_1 + r) - u_1(x_1)]^2} = C_2 \varepsilon^{2/3} r^{2/3} \tag{2.7}$$

$$\varepsilon(r) = \left(\frac{D_{11}}{C_2} \right)^{3/2} r \tag{2.8}$$

where C_2=2.

In Figure 2.8, the spatial lag, r, is obtained by converting the times series, reported in Figure 2.7, using the mean velocity, <u>=0.0625 m/s. The energy dissipation rate, reported in Table 2, is estimated by the plateau of the pre-multiplied second order structure function for r/η<20 Figure 2.8).

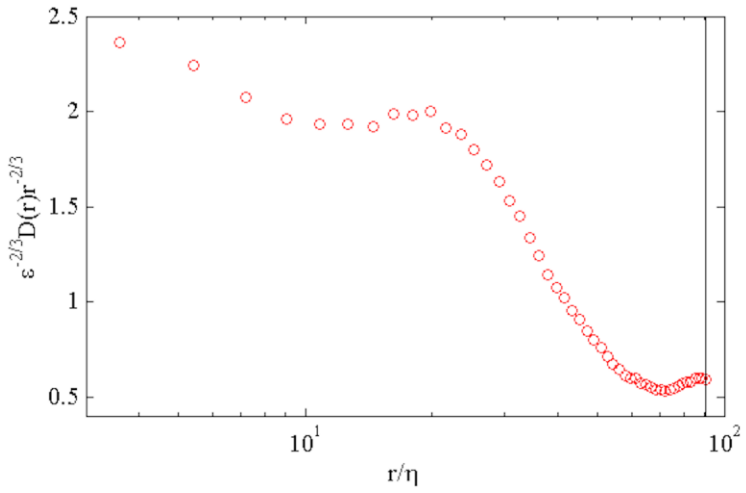

Figure 2.8: Normalized second order structure function of the ufiltered, the vertical black line represents the rcut=<u>/fcut

Results

Microcystis Population Data

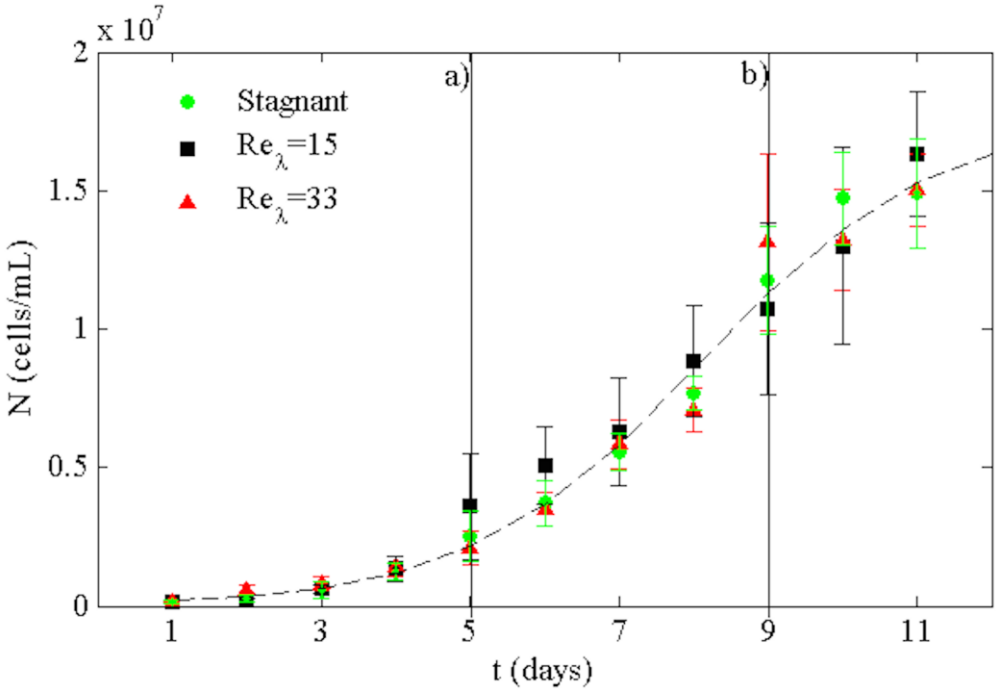

Figure 2.9: Population growth of Microcystis for stagnant, Reλ=15 and Reλ=33, sampled at the beginning of the light cycle. The mean cell concentrations are calculated from daily measurements (3 samples/day) of triplicate experiments, (n=9). The vertical bars represent standard deviation calculated from the nine data points per day. a) Denotes the beginning of the exponential growth phase b) denotes the start of the stationary phase, days 0-5. The dotted line represents the theoretical growth curve based on the Verhulst equation, Equation 3, fitted on all experimental growth measurements.

The population growth of *Microcystis* is shown in Figure 2.9. The range of cell concentration observed in this experiment was from 1×10^5 cells/mL to 17×10^6 cells/mL

and was well within the high-risk range for HAB established by the WHO [26]. From equation 2.3, the average estimated k_g were 0.62 (r^2=0.97), 0.59 (r^2=0.97), and 0.69 (r^2=0.97) (1/day) for stagnant, Re_λ=33, and Re_λ=15 respectively. The estimates indicate that the highest turbulence level, Re_λ=33, yielded the lowest growth rate by 5% compared to the stagnant condition, while the Re_λ=15 condition increased k_g by 11%. These results were corroborated by estimation of k_g using first order growth kinetics for the exponential growth phase days 1-9 and the same trend between the stagnant and turbulent experiments is observed.

From Figure 2.9, we can establish three growth phases within the 11-day experiments using the theoretical growth curve: lag phase (days 0-4), exponential phase (days 5-9) and the transition to the stationary phase (day 10-11). A two-way ANOVA was performed on the cell concentration times series considering turbulence regimes (factor A), and time (factor B). The cell counts for each day, (n=9 cell counts/day) represent the three replicate experiments. ANOVA analysis yielded a $P<0.05$ with $\alpha=0.05$ for the investigated cell concentration time series. The analysis indicates that with 95% confidence the difference in cell concentration among the stagnant and turbulent regimes (stagnant, Re_λ=33, and Re_λ =15) are statistically significant. However, the k_g values estimated from these cell concentration time series showed only marginal differences in population growth rate among the experimental conditions, as stated above.

A series of 24-hour cell concentration measurements were conducted to define the daily growth interval and the relevant time frame for the metabolic flux calculations. Figure 2.10 shows the daily evolution of cell growth for *Microcystis* during a 24-hour period at

the beginning of the exponential growth phase under different Re_λ. The *Microcystis* population experiences linear growth within the first 5 hours (9:00 am~2:00 pm) of the light cycle and then ceases growth, thereafter. The daily growth interval within the 24-hour period appears to be independent of the tested Re_λ.

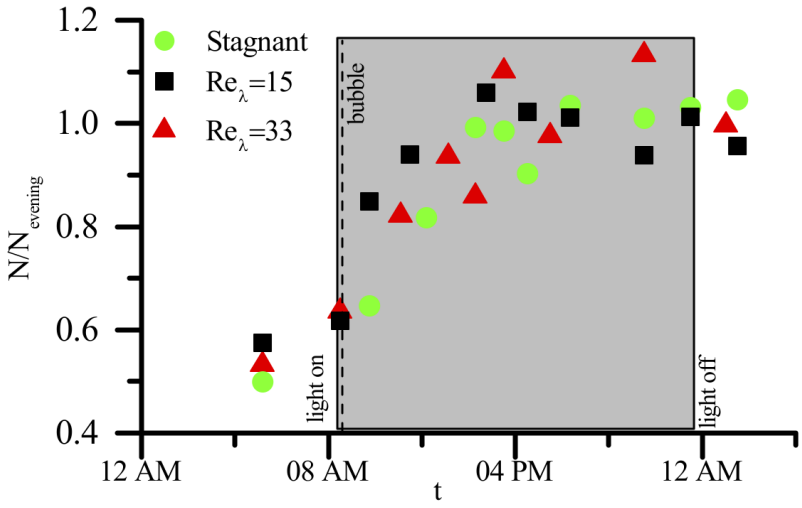

Figure 2.10: Cell concentration, N, measured at smaller time intervals within a 24 hour period at the start of the exponential growth phase (day 5) normalized by average cell concentration for the evening period of the constant cell population (4 pm-1am). The gray region represents the light cycle, and the dashed line represents the O2 saturation and pH adjustment is made.

Oxygen fluxes

The net DO production during photosynthesis is shown in Figure 2.11. The net DO production, J_{DOprod}, for the stagnant condition is consistently higher than that of turbulent cases (Re_λ=15, and 33). The results indicate a hindrance of photosynthesis due to environmental conditions induced by the fluid flow. The overall decline of net DO production in each case reflects the transition from the exponential growth phase to the stationary phase. However, all turbulent levels decline at similar slopes throughout the experiment. The DO uptake during respiration is shown in Figure 2.12. The stagnant condition shows consistently higher J_{DOupt} and has a steeper slope during the exponential growth phase (days 5-8), as compared to the turbulent conditions.

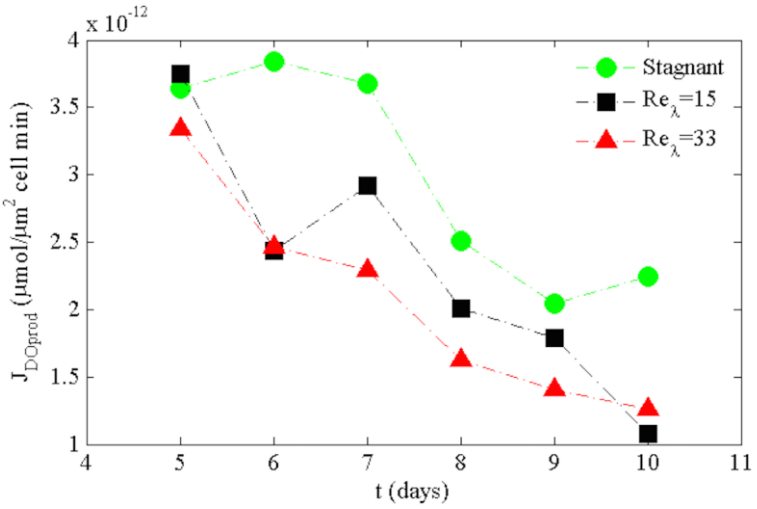

Figure 2.11: Oxygen production flux in the stagnant, Re_λ=15, and Re_λ=33 conditions. The data points represent an average of the triplicate experiments.

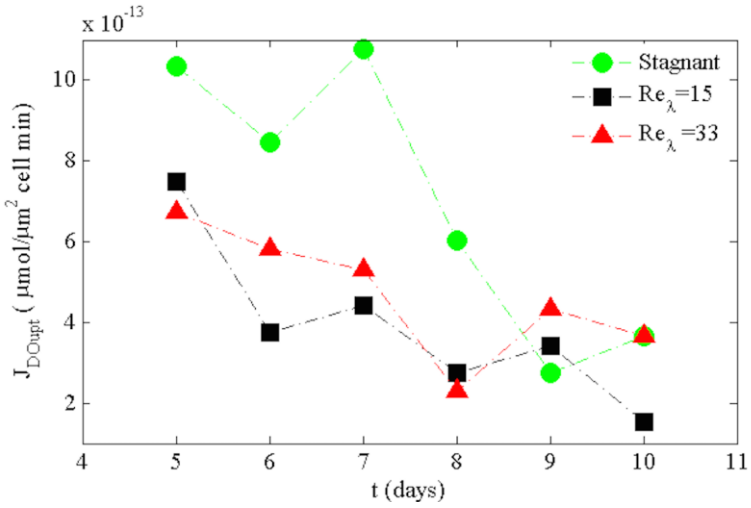

Figure 2.12: Oxygen uptake flux in stagnant, Reλ=15, and Reλ=33 conditions. The data points represent an average of triplicate experiments.

Inorganic Carbon fluxes

As seen in Figure 2.13, the stagnant and Re_λ=15 conditions appear to have a constant carbon uptake flux, whereas, the Re_λ=33 manifests a decreasing trend. Both turbulent cases are lower in comparison to the stagnant condition at the end of exponential growth and stationary growth phase (days 8-10). For days 8-10, the C_i uptake for the turbulent case (Re_λ=15 and Re_λ =33), on average, is 44.3%, 56.8% of the stagnant condition for Re_λ=33, 15, respectively. Qiu and Gao, (2002)[45] have reported a similar difference in photosynthesis for *Microcystis* due to various C_i and availability.

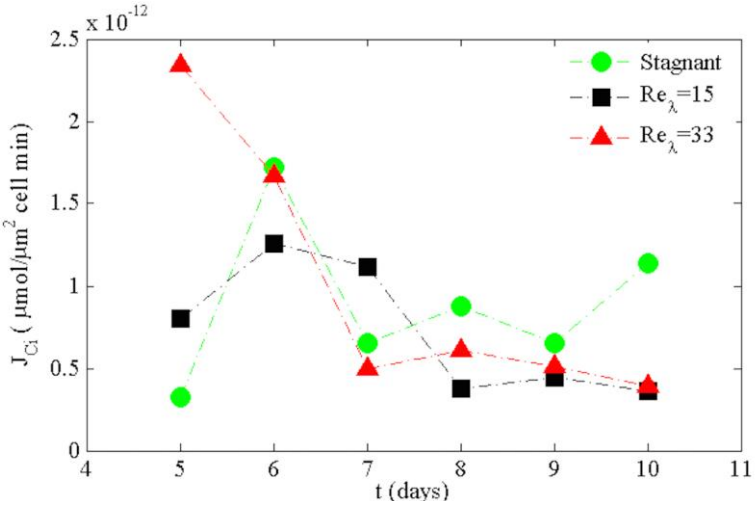

Figure 2.13: Comparison of dissolved inorganic carbon, Ci, uptake flux for stagnant, Reλ=33, and Reλ=15. The data points are obtained from Equations 2.4, 2.5 using averaged measurements of alkalinity and pH during one experiment for each Reλ.

Discussion

[56][56] suggested that cyanobacteria are relatively less sensitive to turbulence compared to other micro-algal groups. Additionally, the effect of small-scale turbulence has been shown to be less of a controlling factor on population growth, as compared to its contribution to turbulent mixing, such as entrainment of CO_2 from the atmosphere and the change in lighting conditions due to physical displacement of the *Microcystis* within the water column [24,40,57]. Although the population growth appears to be only marginally influenced by small-scale turbulent conditions, our study highlights an appreciable mediation of the photosynthetic metabolism by turbulence, independent of the influence of CO_2 entrainment into the water, DO or nutrients abundance, and changes in PAR

availability. The observed mediation of photosynthesis is a genuine stress response similar to *Microcystis*' response to cold and dark conditions, low environmental C_i concentrations, and other common environmental stressor experienced by *Microcystis* [24,10,38]. For example, [58] reported sodium chloride contamination inhibits photosynthesis in *Microcystis aeruginosa* by suppressing carbon assimilation. To facilitate the discussion of our findings in relation to different fluid flow conditions, we first highlight some relevant metabolic processes of *Microcystis*.

Microcystis are photosynthetic cyanobacteria, thus, they derive their carbohydrates from C_i dissolved in the water, which they use to produce several biochemical compounds, including microcystin and EPS. Thus, the C_i that has been taken up through photosynthesis but is not released during respiration is accumulated and utilized by the cell. Under stagnant fluid conditions, C_i uptake is the same for days 5-7 and higher for days 8-10, compared to the turbulent conditions. However, the respiration is higher at days 5-8 (~ exponential growth) and then the same for days 9-10 (~stationary phase) for the stagnant condition, again as compared to the turbulent conditions. This demonstrates a change from accumulation of C_i under turbulent condition in the exponential growth phase (where the cell is taking up the same C_i but respiring less compared to the stagnant condition) to the accumulation of C_i under stagnant condition (where the cell is taking up more C_i and respiring at the same rate compared to the turbulent) during the stationary phase. We hypothesize the difference in C_i accumulation during the exponential growth is due to EPS production, utilized to form a protective layer around the cell and reduce drag in the presence of the turbulence. Several studies have demonstrated that dilute polymer

solutions produced by microalgae act as drag reducers and are inferred to be a physiological response to mediate mechanical damage to the cell due to turbulence stress [43,44,59]. It is observed that there is a switch from C_i accumulation in the turbulent case exhibited during exponential growth phase to the C_i accumulation observed in the stagnant condition during stationary growth phase. As stated in the previous section, *Microcystis* use EPS as a sink for C_i to combat nitrogen deficiencies that would be present in the stationary growth phase, due to depleted nutrients. The marked increase in C_i uptake is supported by the observation that EPS production during nitrogen stress is 3-4 times greater than that produced to reduce drag [59]. The observed transient effect of C_i accumulation between the exponential growth phase and the stationary phase is further supported by the fact that, EPS structure and composition evolve throughout the growth cycle [60]. An additional explanation for the increased C_i uptake during the stationary phase could be that C_i is used for the production of microcystin. Presumably, the *Microcystis* produce additional microcystin as a self-defense mechanism during the nutrient limiting stationary phase [29].

The reduction in net DO production in the turbulent flow could be related to the way *Microcystis* uniquely respond to stress. Wu et al. [31] demonstrated that *Microcystis*, under such conditions, responded by reducing their metabolism, while maintaining their cell population, i.e. not growing exponentially. It could be that the *Microcystis* under turbulence-induced stress, not only can reduce their metabolism, as seen in Figure 9, but also grow exponentially. The incremental change in metabolic response to turbulence can be explained by the resilience of *Microcystis*, which have been shown to be more resistant to changes in their environment [40,57]. The effect of additional turbulent stress in

conjuncture with other environmental factors has not been investigated thoroughly, and it is possible that additional turbulent stress interrupts physiological processes.

Conclusion

Small-scale turbulence, in controlled laboratory experiments, has been observed to affect metabolic photosynthesis of *Microcystis*, by inducing a reduction in net oxygen production and uptake, and a moderation of the carbon uptake. These effects were observed at different growth phases of the *Microcystis*, even if the actual population growth rate estimated from the cell concentration was only slightly modulated by turbulence (-5% and 11% for Re_λ =33 and Re_λ =15, respectively, as compared to stagnant conditions). The reduced photosynthesis can be explained by the conjecture that *Microcystis* reduce their metabolism under different stress conditions. While the increased accumulation of C_i in the turbulent cases, during the exponential growth phase, provides evidence of *Microcystis'* ability to produce EPS, decrease drag and prevent cellular damage. Subsequently, the increased C_i uptake in the stationary phase in the stagnant condition may be attributed to the production of EPS to compensate for low nitrogen availability. The decreased C_i uptake in the stationary phase in the turbulent flow could be attributed to metabolic stress manifested by decreased net oxygen production (Figure 9).

Chapter 3

Investigating Abiotic Drivers for Vertical and Temporal Heterogeneities of Cyanobacteria Concentrations in Lakes Using a Seasonal *In situ* Monitoring Station

Introduction

Cyanobacteria blooms or Harmful Algal Blooms (HAB) are a ubiquitous nuisance to freshwater ecosystems across the planet. HAB are large accumulations of microscopic photosynthetic organisms, which populate freshwater environments, deteriorate water quality and pose a significant public health risk. Many cyanobacteria blooms are made up

of organisms, like the ones studied here, that are capable of producing toxins that are harmful to wildlife and humans [1,61]. Risk of exposure through recreational contact or drinking water is compounded by the fact that cyanobacteria blooms are spatially and temporarily transient and are difficult to predict. Cyanobacteria dominance in lakes is due to a combination of complex and codependent environmental factors rather than a single dominant variable [61–65]; many of which are driven directly and indirectly by temperature and local meteorological conditions (e.g. optimal water temperature for growth rates, temperature stratification, mixing, depth and strength of density gradients, access to hypolimnetic nutrients). Cyanobacteria achieve optimum growth rates at high temperatures allowing them to dominate freshwater ecosystems in summer, given sufficient nutrients [62,65]. However, high temperatures alone do not guarantee cyanobacteria blooms as *Cha et al.* (2014), *Wagner and Adrian* [17], and *Huber et al.* (2012) assert; warm temperatures and stable water stratification must be present for blooming to occur.

Beyond cyanobacterial dominance and blooming, vertical distribution is particularly challenging and interesting because of their ability to move throughout the water column and presumably seek favorable environmental conditions through cell density regulation of internal gas vesicles [67,68]. HAB can be composed of diverse genera with distinct ecotypes; reacting to environmental conditions differently in terms of buoyancy, metabolism and light affinity [61,62,69]. Buoyant cyanobacteria use lake stratification to maintain optimal growth conditions specific to their respective genus [70–72].Three dominant genera were observed in this study, *Microcystis*, *Planktothrix* and

Dolichospermum, all are capable of producing microcystin [1,61] and are classified as having different ecological traits and functional characteristics [4].

Highly buoyant genera of cyanobacteria, such as *Dolichospermum* and *Microcystis*, are bloom forming and are known to persist in calm stably stratified conditions [73], whereas *Planktothrix* have a low light affinity, and persist in colder more turbid conditions [4,69,72]. Additionally, these genera exhibit different tolerances for nutrient limitations. *Dolichospermum* and *Planktothrix* are capable of fixing atmospheric nitrogen and thus can grow with low inorganic nitrogen availability; whereas *Microcystis* cannot [4]. Regardless of these distinctions in eco-physiological traits, all three genera can benefit from warm temperatures and prolonged stratification because i) these conditions provide optimum temperature for growth, and ii) the weak mixing throughout the water column allows cyanobacteria to use buoyancy regulation to explore favorable environmental conditions [63]. Conversely, as mixing increases, cyanobacteria can become displaced throughout the water column, as they are no longer able regulate their buoyancy [5,74,75]. Additionally, physical forcing from the wind (e.g. shear induced turbulence) can i) modulate cyanobacteria metabolism including inorganic carbon uptake and dissolved oxygen production [76] ii) influence growth rate [77] and iii) disrupt cyanobacteria colonies [40].

Vertical heterogeneity of cyanobacteria biomass has been studied in freshwater ecosystems previously [70,71,73,78–81]. These studies show the relationship between cyanobacteria biomass and physical lake parameters; specifically, i) mixing and stratification conditions [73,79,80], ii) water temperature [71], iii) thermocline depth [71] and iv) light [70] through field observations and simulations. However, these studies have limited sampling frequencies, which constrains the ability to fully resolve both lacustrine

and cyanobacteria dynamics throughout the entire water column. Previous studies rely on data collected on a weekly, or monthly basis, with some studies supplementing that collection with only a few 24 hour sampling windows [81]. The scope of this study is more extensive, as it provides not only season-long monitoring but the ability to record full depth profiles every 2 hours with concurrent meteorological, temperature and water quality measurements. This extensive data set (1400 experimental profiles) captures disparate conditions in the lake stratification and water temperature. This dataset is then coupled with weekly water sample collection from the entire water column for nutrient and cyanobacteria identification.

The goal of this research is to document high-resolution seasonal monitoring of the vertical and temporal heterogeneity of cyanobacteria biomass in a eutrophic lake. Concurrent high resolution seasonal meteorological, temperature and water quality data are expected to elucidate which of the competing abiotic lake and meteorological parameters drive changes in cyanobacteria accumulation and distribution in eutrophic systems. The framework described here develops a predictive relationship for spatial heterogeneities in cyanobacterial biomass based on easily measurable lake parameters; such as temperature, wind, and stratification conditions in eutrophic lakes.

Materials and Methods

Site Description

Madison Lake is a residential and recreational lake located in a primarily agricultural watershed in south central Minnesota (Figure 3.1a). It has an area of 5.4 km^2 and a maximum depth of 18 m with a mean depth of 3.4 m. The lake was chosen as the

study site because of its eutrophic classification, long water quality monitoring record, and history of frequent toxic algal blooms throughout the summer [19]. Because of the high nutrient inputs from its surrounding agricultural watershed, Madison Lake is classified as eutrophic bordering on hyper-eutrophic and was placed on the 2010 impaired waters list [82]. The lake has a long water quality monitoring history with records back to 1947 including a large algal toxin study investigating microcystin concentration in lakes in Minnesota, performed by the Minnesota Pollution Control Agency (MPCA) in 2006. In Madison Lake in June-September 2006, the total microcystin concentrations were detectable at the pelagic sampling location (up to 3.3 ppb) and near shore sites (up to 2,200 ppb) and provided the second highest microcystin concentration that was recorded during the survey [19].

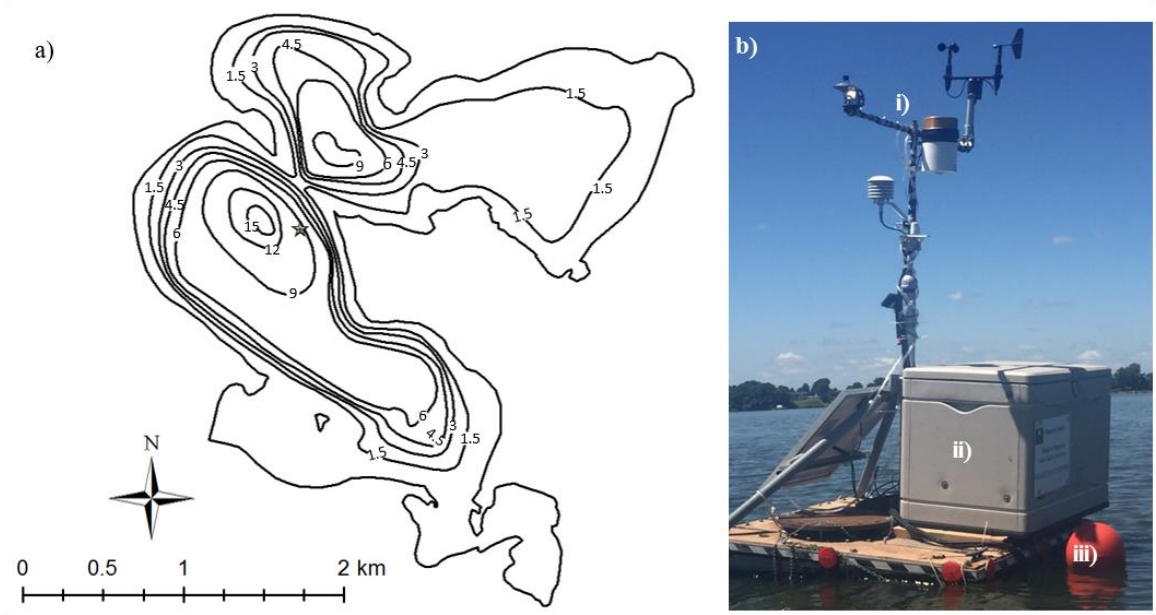

Figure 3.1: a) Bathymetry of Madison Lake, MN (contour lines marked in meters). The star marks the location of floating research station (44.19056,-93.80861) during summer 2016 (June-October). The local depth was 9.2 m. b) Photograph of the research station equipped with: i) a meteorological station housed on a 1.5 m mast recording: wind speed and direction, air temperature, relative humidity, precipitation, and ambient PAR, ii) a water quality probe profiling the water column from 1m to 8.5 m depth, every 2 hours, and measuring every 0.5 m, iii) an anchored thermistor chain with temperature probes at 0.5 m increments from 0.1-2.5 m and every 1m from 2.5 - 8.5 m

Research Station

The research station consisted of a floating platform with three synchronized measuring systems, Figure 3.1b. For local weather conditions, a 1.5 m high meteorological station enabled simultaneous measurements of wind speed, wind direction, ambient PAR, air temperature, and relative humidity. These measurements, sampled at 1Hz, 60 samples per minute, were connected to a data logger (Cambell Scientific, UT, USA). The data logger outputs five-minute average for all meteorological station data. The second

measuring component is a water quality profiler measuring every 0.5 m, in a range of 1-8.5 m depths, profiling every two hours. The specific multi-probe was a Hydrolab DS5 Water Quality Multiprobe (Hach Environmental CO, USA) which was equipped with pH, dissolved oxygen (DO), temperature, PAR, specific conductivity, and phycocyanin fluorometry (Turner Designs, CA, USA) sensors. The probe was suspended in the water at 1 meter until it was triggered to profile on every even hour. For every profile, (12/day) the probe was lowered by a motorized reel (Hannay Reels, NY, USA) at 0.5 m increments and acquired measurements from each sensor at that depth for 2 minutes. The third measuring system was an anchored thermistor chain with 12 stainless-steel temperature probes (Cambell Scientific, UT, USA) placed every 0.5 m (in the range 0-2.5m), and every meter (in the range of 2.5-8.5m). The data logger outputs five-minute average temperature data at all depths. All the Hydrolab, meteorological station and thermistor chain data were transferred to the main data logger (Cambell Scientific, UT, USA), which had wireless data transfer to a server, allowing real-time data assessment.

Water Sample Analysis

Sample Collection

All measurements from the floating research station were complemented with *in situ*, water samples, taken in the proximity of the research station, on a weekly basis from mid-June to mid-October, 2016, at one-meter increments in the 0-9 m depth, using a Van Dorn sampler. In the laboratory, the samples were used for phytoplankton cell enumeration and identification, nutrient and phycocyanin concentrations. Water samples were collected near the research station at concurrent depth and time of probe measurements.

Phytoplankton Identification

Phytoplankton species were identified and enumerated using microscopy, Figure 3.2a, and a gridded Sedgewick-Rafter counter (Wildlife Supply Co, FL, USA) at 10x magnification; further identification of *Planktothrix* spp was done using a hemacytometer at 40x magnification. The whole water samples for cell identification and enumeration were preserved with Lugol's iodine and stored in 2 °C upon returning from the lake (approximately 2 hours after sampling). There were three dominate genera of cyanobacteria, making up 95% of the total biovolume (μm^3/mL), identified and enumerated throughout the summer; *Microcystis* spp., *Dolichospermum* spp. and *Planktothrix* spp., all microcystin producers [61,83]. Cell concentrations for *Microcystis* spp., N_{mic}, *Dolichospermum* spp., N_{ana}, and *Planktothrix* spp., N_{plk} were counted using 12 (50 µm), 12 (50 µm) and 25 (1 µL) entire subsamples, respectively. The cell counts per subsamples ranged from: 0-3 (colony/subsample), 40-1300 (cell/subsample) and 2-15 (filaments/subsample) for *Microcystis* spp., *Dolichospermum* spp., and *Planktothrix* spp., respectively. Figure 3.2b shows the temporal evolution of the cyanobacteria community represented by the depth averaged cell concentrations amongst the above cyanobacteria constituents.

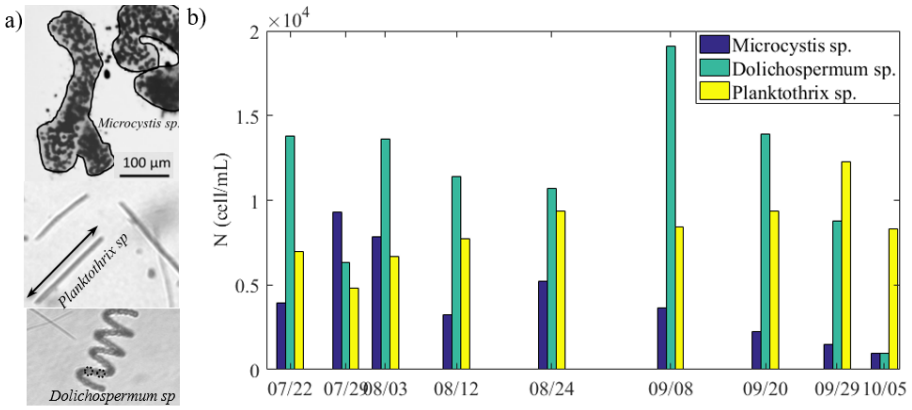

Figure 3.2: Cyanobacteria genera from Madison Lake. a) Schematic of cyanobacteria identification and biovolume estimation, where the black curves represent the estimated surface area of the *Microcysits* spp. colony, the arrow represents the estimated length of the *Planktothrix* spp. filament and the circles represent estimation of the *Dolichospermum* spp. cell area. The image is taken the water sample from August 3, 2016 at 2 m depth. b) Time series of depth averaged cell concentrations of *Dolichospermum* spp. (green), *Microcystis* spp. (blue), *Planktothrix* spp. (yellow) from discrete water samples collected on the corresponding dates.

Cyanobacteria Enumeration

A relatively low correlation (R^2 = 0.36) was obtained by analyzing the cell concentration (cell/mL) versus phycocyanin measured by the probe. Similar findings have been reported in other studies, as well, which prompted the need for conversion of cell concentrations into biovolume (μm^3/mL) as a more representative quantification of cyanobacteria biomass in diverse populations [84–86].

$$BV\left(\frac{\mu m^3}{mL}\right)=BV_{dol}\left(\frac{\mu m^3}{cell}\right)N_{dol}\left(\frac{cell}{mL}\right)+BV_{mic}\left(\frac{\mu m^3}{colony}\right)N_{mic}\left(\frac{colony}{mL}\right)+BV_{plk}\left(\frac{\mu m^3}{filament}\right)N_{plk}\left(\frac{filament}{mL}\right) \quad (3.1)$$

where BV is the total biovolume measured from the sample; BV_{dol} is the average biovolume per cell of *Dolichospermum* spp., N_{dol} is the cell concentration of *Dolichospermum* spp., BV_{mic} is the average biovolume per colony of *Microcystis* spp., N_{mic} is the colony concentration of *Microcystis;* BV_{plk} is the average biovolume per filament of *Planktothrix* spp., N_{plk} is the filament concentration of *Planktothrix* spp.. The biovolume of each genus of cyanobacteria was determined by measuring the average volume for each cell, colony or filament (μm^3/cell), e.g., Figure 3.2a, and then multiplying by the cell or colony number density (cell/mL), equation 3.1. The average biovolumes were determined using standard geometry body approximations detailed in *Hillebrand et al.* (1999). Specifically, *Dolichospermum* spp. and *Microcystis* spp. cells were approximated as spheres and *Planktothrix* spp. filaments were approximated as cylinders. The average cellular volume for *Dolichospermum* spp. was estimated by analyzing micrographs using ImageJ from up to 10 sub-samples from 3 representative depths for each sampling week, n=58, yielding an average 113 (±17.7) (μm^3/cell). The total biovolume concentration for *Microcystis* spp. was computed by multiplying the average colony volume BV_{mic} (μm^3/colony) and the colony density, N_{mic} (colony/mL). The average colony volume was estimated by multiplying the colony area, estimated at each cell layer forming the colony (measured using ImageJ) by the average depth of the selected colonies using microscopy, n=22, yielding 5.15×10^5 ($\pm 4.58 \times 10^5$) (μm^3/colony). The *Planktothrix* spp. biovolume concentration was determined by multiplying the average filament volume BV_{plk} (μm^3/filament) by the filament density, N_{plk} (filament/mL). The *Planktothrix* spp. average filament biovolume was determined by measuring the major and minor axis of *Planktothrix*

spp. filaments analyzed from micrographs from 25 sub-samples (1µL) of each water sample using ImageJ and MatLab, n=1225, $7.5x10^3$ ($\pm 6.5x10^3$) (μm^3/filament). The results for the measured biovolume parameters are comparable to those reported in the literature (Table 3.1).

Table 3.1: Comparison of measured and reported biovolumes for the dominant cyanobacteria genera. Measured cellular biovolume (μm^3/cell) for *Microcystis* spp. and *Dolichospermum* spp. are described as the average cellular biovolume (± standard deviation) while the reported cellular biovolume is described as ranges of recorded in the cited literature. The biovolume measured and reported for *Planktothrix* spp. is filament length (µm) and is described as averaged filament lengths (± standard deviation) while the reported filament lengths are described as ranges of recorded in the cited literature.

	Genus	Measured	Reported	Citation
BV_{mic} (μm^3/cell)	*Microcystis* spp.	147 (±1.84)	25.8-65.4	Torres et al., 2016
			54-343	Yamamoto et al.,
(μm^3/colony)		$5.15x10^5$ ($\pm 4.58x10^5$)	-	2009 -
BV_{dol}(μm^3/cell)	*Dolichospermum* spp.	113 (±17.7)	47.683	Kong et al., 2014
			70-300	Yamamoto et al., 2009
Filament length (µm)	*Planktothrix* spp.	253 (± 219)	77-594	Torres et al., 2016
			30-400	Yamamoto et al.,
		$7.5x10^3$	-	2009
BV_{plk} (μm^3/filament)		($\pm 6.5x10^3$).		-

Phycocyanin Extraction

Extracted phycocyanin concentrations, taken from the water samples, were measured by a laboratory bench-top fluorometer (Trilogy, Turner Designs, CA, USA) augmented with an orange module (#7200-044, Turner Designs CA USA) that

accommodated a four-sided, clear 10 mm, glass square cuvette [85]. The water samples were vacuum filtered with GF/F filters (Whatman, Maidstone, UK) and stored at 2 °C until analyzed with storage time ranging from 5-21 days. Five hours prior to measurement, the filters were ground in 10 mL of 50 mM phosphate buffer (40 mL of concentrated phosphate buffer (D1253 Ricca Chem Co IN, USA) in 960 mL Mili-Q water (Millipore, MA, USA) under reduced light using a smooth Teflon grinder in a centrifuge tube for 1 minute. Another 10 mL of phosphate buffer was used to rinse the grinder into the centrifuge tube, bringing the total extract volume to 20 mL. The samples were stored in the dark at 4 °C for 2 hours and then placed in a dark laminar flow hood for another 6 hours to warm to room temperature (21 °C) yielding a total extraction time of 8 hours. After extraction, the samples were centrifuged at 15,000 rpm for 20 minutes. The supernatant was analyzed for phycocyanin concentration using a Turner Designs Trilogy fluorometer fitted with an orange module, which yielded raw fluorescence units (RFU). RFU measured by the bench-top fluorometer were converted to phycocyanin concentration (µg/L) using a standard curve. The fluorometer is calibrated using a stock solution of phycocyanin partially purified from Spirulina (Sigma-Aldrich MO, USA) dissolved in phosphate buffer immediately before each set of measurements.

Cyanobacteria Biovolume Calibration

The relationship between the total cyanobacteria biovolume, BV (estimated from water samples taken at concurrent depth and time as the *in situ* measurements, equation 3.1) and phycocyanin concentrations provided data for the calibration curves, Figure 3.3. There are two different types of phycocyanin measurements: P_F, which represents the phycocyanin measured by the probe in the field and, P_L, which represents phycocyanin

measured in the laboratory from the extracted phycocyanin from the water samples. To convert phycocyanin concentrations measured in the field, P_F (V) to cyanobacteria biomass, specifically to the biovolume BV ($\mu m^3/mL$), the following functional relationship is used based on the data presented in Figure 3.3a.

$$BV=1.6\times10^{9}P_F \tag{3.2}$$

The calibration data represented in Figure 3.3 are log transformed because of the wide range of cyanobacteria biovolume and phycocyanin concentrations across different depths and at different times in the summer. A measure of the BV variability is provided through the standard deviation of the unit biovolume (cell or colony) estimated for each water sample corresponding to a specific day and depth. The standard deviation for the biovolume of each genus was calculated as the standard deviation of the cell density, σ_N, multiplied by the respective average biovolume, $\overline{BV}$, as in Table 3.1; i.e. $\sigma_{mic,dol,plk} = \sigma_N \times \overline{BV}$. The total standard deviation for the BV used the standard error propagation of addition for each genera standard deviation,$\sigma_{total} = \left(\sigma_{mic}^2 + \sigma_{dol}^2 + \sigma_{plk}^2\right)^{1/2}$ illustrated by the vertical bars in Figure 3.3. We acknowledge that variability in both the phycocyanin production/cell and the biovolume of individual cyanobacteria throughout the season, could locally affect the proposed calibration. Despite this variability, an acceptable calibration was achieved because of the use of samples ranging in dates July-September and depths from 1-9 m, which accounts for known variability in BV to fluorometry relationships as demonstrated in Hodges et al [6].

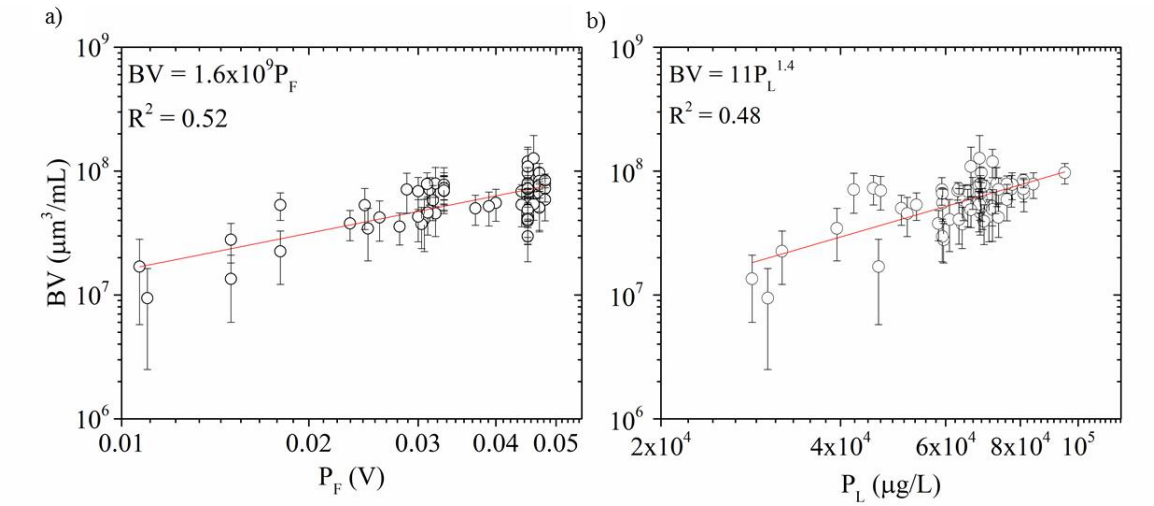

Figure 3.3: Calibration curves relating the measured BV (µm^3/mL) of cyanobacteria from the water samples to *in situ* phycocyanin measured by the field probe, P_F, and extracted from the water samples, P_L. a) Cyanobacterial biovolume (µm^3/mL) versus P_F (V). b) Cyanobacterial biovolume (µm^3/mL) versus phycocyanin concentrations extracted from water samples measured by the laboratory fluorometer, P_L (µg/L). The data points represent total biovolume concentrations and the error bars represent, σ_{total}.

Nutrient Analysis

To determine the availability of abundance and vertical distribution of macronutrients throughout the summer, phosphate and nitrate concentrations were analyzed from the discrete water samples. The water samples were first filtered through GF/F filters (Whatman, Maidstone, UK) and stored at 2 °C until analyzed. The filtered water samples were measured by a laboratory bench-top fluorometer (Trilogy, Turner Designs, CA, USA P/N:7200-0000). For phosphate concentration, the bench-top fluorometer is augmented with a phosphate absorbance module (Trilogy, Turner Designs, CA, USA P/N:7200-070) that accommodated a four-sided, clear 10 mm, glass square cuvette. The phosphate concentrations, [PO_4], were measured according to *Strickland and*

Parsons (1972) and *Parson et al.* (1984). A calibration curve was constructed using a serial dilution of potassium dihydrogen phosphate standards with concentrations ranging from 8.9-1,138 µg/L. For the nitrate concentration, the bench-top fluorometer is augmented with a nitrate absorbance module (Trilogy, Turner Designs, CA, USA (P/N: 7200-074) that accommodated a four-sided, clear 10 mm, glass square cuvette. The LaMotte nitrate test kit method using the Nitrate-Nitrogen Model NCR (LaMotte, Chestertown, MD, USA Cat. No. 77101). A calibration curve was constructed using a serial dilution of nitrate standard (Ricca Chemical Company, Arlington, MD, USA Cat. No.5307-16) ranging from 0.15-8 mg/L. Additionally, nitrate+nitrite concentrations measured by the Minnesota Pollution Control Agency in the same lake measured in the top 2 m of the water column were used to supplement our data collection.

Stratification and Meteorological Conditions

All the data taken from the research station were analyzed using Matlab (Mathworks). The water temperature in the diurnal surface layer, T_s, was determined as the average temperature in the diurnal surface layer, h_{SL}. h_{SL} is defined as the depth where the temperature difference from the surface is less than 0.3 °C, based on the resolution of the thermistor chain. The thermocline depth, z_T, is estimated from the temperature profiles by determining the first moment of the density gradient, equation 3.3, which has been shown to correspond to the maximum density gradient [90,91].

$$z_T = \frac{\int_0^{z_M} z \frac{d\rho(z)}{dz} dz}{\int_0^{z_M} \frac{d\rho(z)}{dz} dz} \tag{3.3}$$

where ρ is the water density estimated from temperature measured at specific depths, z, and times, t.

The measured water temperatures were averaged over the period of internal seiche for the estimation of ρ. The vertical one mode seiche period was used to provide a relevant time scale for BV vertical heterogeneity to average local meteorological and temperature data. We do not describe the internal wave field or estimate higher seiche modes. The period of the first vertical mode of internal seiche was estimated by the equation 3.4.

$$t_1 = \frac{2L_T}{\sqrt{\frac{g' z_T (z_M - z_T)}{z_M}}} \qquad (3.4)$$

where L_T is the basin length at the thermocline depth, z_T, along the prevailing wind direction, g' is the reduced gravity due to change in density between the hypolimnion, ρ_h, and the epilimnion, ρ_e, $g' = g\Delta\rho/\rho_h$, and z_M is maximum depth. The seasonal seiche period, t_1, of approximately three hours, was determined by taking the average seiche period computed using L_T from the two prevailing wind directions; 153º and 0º from North, assuming z_T as the seasonal average. All the meteorological and temperature data used and plotted hereinafter are averaged over the three hours seasonal seiche period centered around of each probe profile, to capture the seiche variability. To quantify the strength of thermal stratification, the Schmidt stability, St, was estimated by equation 3.5 using the seiche average temperature profiles. St describes the resistance to mechanical mixing due to the potential energy of the density stratification in the water column [92,93]. It is a measure of the amount of work per unit surface area needed to mix the water column to a uniform temperature. St is an ecologically relevant parameter because it is an indicator of

the presence of a persistent warm surface mixed layer and has been shown to be a driver of cyanobacteria biomass [63,73,94] St is defined as:

$$St = \frac{g}{A_s}\int_0^{z_M}(z - z_V)\rho_z A_z dz \quad (3.5)$$

where A_s is the surface area of the lake, z_v is the depth at the center of volume, ρ_z is the density at depth z and A_z is the basin area at z. St is purely dependent on the lake geometry and on the temperature structure in the water column and thus does not describe dynamic stability or the extent of mixing in the water column, as it does not include the wind, i.e. the forcing on the system. To incorporate the contribution of wind to internal mixing processes, the Lake Number (LN) is calculated. LN represents the ratio of the moment of stabilizing density stratification force due to gravity, to the moment of destabilizing forces due to the wind, about the center of volume [95]. For Lake Number less than 1.0, stratification is weak and intermittent. LN is defined as

$$LN = \frac{St\ z_T}{\rho_h u_*^2 A_s^{1/2} z_V} \quad (3.6)$$

where u_* is the shear velocity , $u_* = (\tau_w/\rho_e)^{1/2}$, $\tau_w = C_D \rho_{air} U^2$ is the wind shear at the water surface, ρ_{air} is the density of the air, C_D is the coefficient of drag (assumed to be $1x10^{-3}$ for U <5 m/s and $1.5x10^{-3}$ for U >5 m/s [96]) and U is the wind speed at 10 m approximated by $U = U[1-(C_D^{0.5}/\kappa)\ln(10/H)]$; H=1.5 m is the height of the wind sensor at the research station, U is the measured wind speed, and κ is the von Karman's constant, 0.4.

The photic depth, z_p, is defined as the depth consistent with 0.01of the incident PAR at the lake surface (I_0), and I(z) is the PAR at water depth z. Thus z_p is computed as, z_p=-

ln(0.01)/ μ, where the attenuation coefficient, μ, is estimated by fitting equation 3.7 to the PAR depth profiles collected from the research station [97].

$$I(z)=I_0 e^{-\mu z} \quad (3.7)$$

Results

Thermal Stratification: Temporal and Vertical Variability

The meteorological and thermal conditions were monitored at the research site over the season, July-October, Figure 3.4. The wind speed time series exhibits a fairly cyclic pattern observed at the field site, characterized by mostly diurnal oscillation ranging from 0.25 to 10.3 m/s with a mean wind speed at 3.7 m/s (Figure 3.4a). The time series of LN shows a stable stratification with LN >1 before August 19 when the time averaged LN, $\overline{LN}$, is 6.7, Figure 3.4b. Under such persistent thermal stratification, a distinct thermocline is observed with an average depth during the strongly stratified period of 5.12 m. Conversely, LN<1 represents a period of weak stratification when the wind easily mixes the entire water as observed after August 18 (where $\overline{LN}$ =0.37). These two distinct dynamic stratification conditions observed during the sampling time are also supported by the temperature depth contours which shows stable thermal stratification when $\overline{LN} > 1$ and weakly stratified tending toward uniform temperatures observed for $\overline{LN} < 1$ (Figure 3.4c).

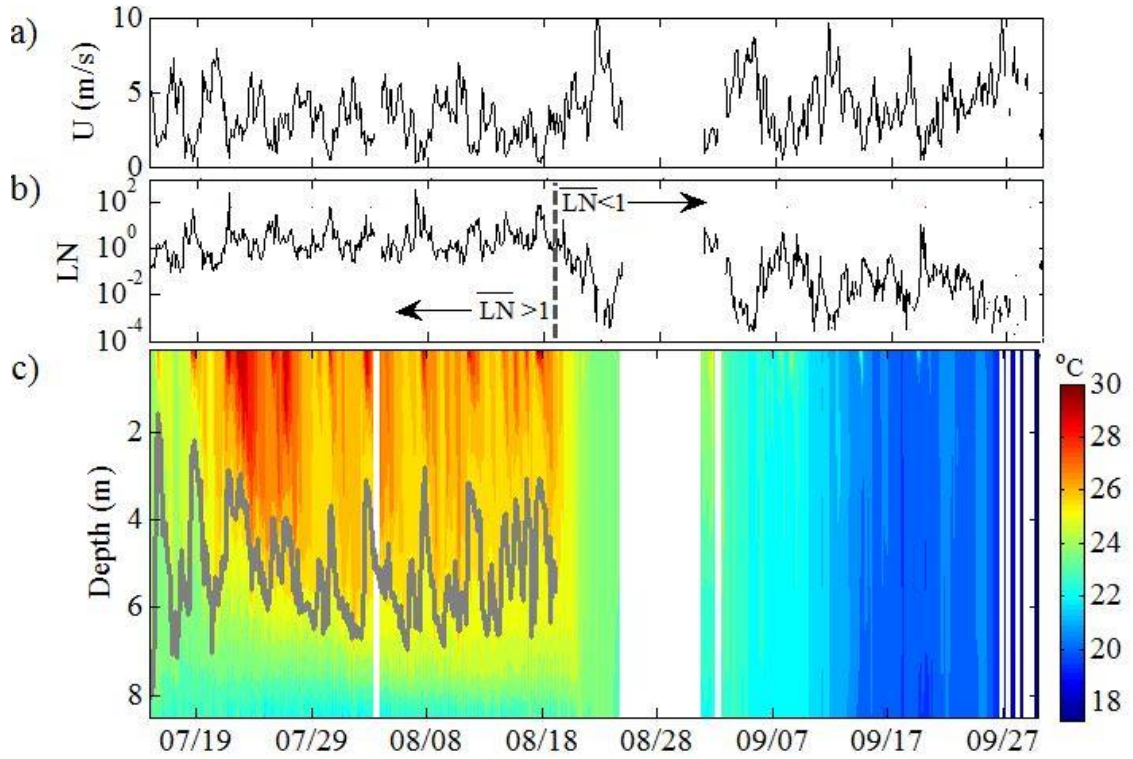

Figure 3.4: a) Time series of wind speed averaged over a 3-hour lake seiche period. b) Time series of the Lake Number (LN), the dotted line represents the division between two defined stratification conditions observed during the season during the July 15-August 19 period, $\overline{LN}$ is 6.7 and during the August 18-October 1 period, $\overline{LN}$ is 0.37. c) Depth contour of temperature time series averaged over 3 hour seiche period. The gray line represents the depth of the thermocline. The white blocks represent data outages.

Nutrient Variability

[PO4] were measured from discrete water samples from the epilimnion and hypolimnion throughout the season (Figure 3.5a). The data represents the maximum phosphate concentration measured above the thermocline, $[PO4]_e$, and the maximum concentration below the thermocline $[PO4]_h$, ranging from 71-207 µg/L and 39-281 µg/L, respectively. These concentrations are consistent with those recorded in the pelagic zone in Madison Lake during the summer of 2006 when high microcystin concentrations

persisted throughout the summer [19]. During stable stratification, $\overline{LN}$> 1, $[PO4]_e$ are above the threshold of 100 µg/L, proposed by Huber et al., (2012) for the initiation of cyanobacteria blooms. High $[PO4]_h$ when LN>1 is consistent with the phosphate release from the sediment during anoxic conditions observed from July 18, 2016 to August 18 ,2016. Subsequently, during the weak stratification, we observed a decrease in $[PO4]_h$ as nutrients and oxygenated water are mixed throughout the water column (data not shown). Nitrate concentrations have been measured at the same depths as the phosphate concentrations. All of samples were under the detection limit <0.15mg/L. These measurements have been corroborated with samples taken by the MPCA just 100 m from our sample site (Figure 3.5b). The nitrate+nitrite concentration measured in the top 2 m of the water column are all concentrations <0.15 mg/L. The nitrate+nitrite concentration exponentially decreases from 0.12 mg/L in May to <0.05 mg/L during the observation period, July-October 2016. These low concentrations are typical of Minnesota Lakes,[19]. Overall, there are no trends in either phosphate or nitrate+nitrite during the observation period that would be able to described vertical or temporal heterogeneity in cyanobacteria BV.

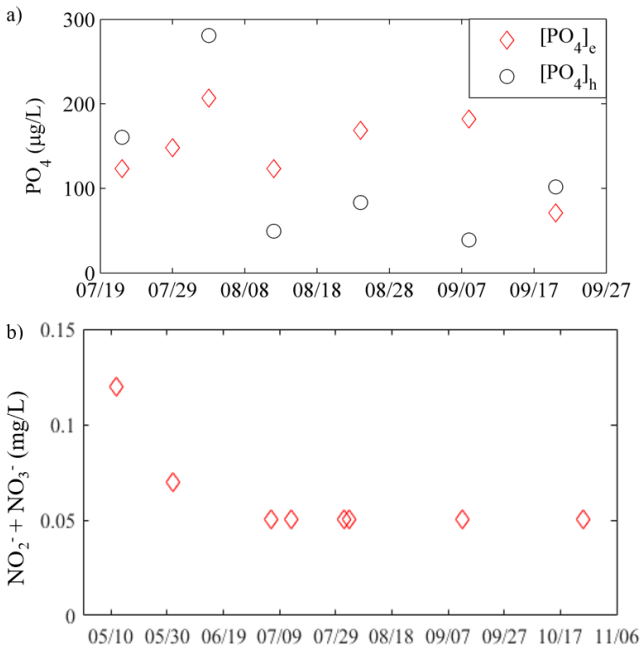

Figure 3.5: a) Time series of maximum PO4 concentrations measured in the epilimnion, $[PO4]_e$, and in the hypolimnion, $[PO4]_h$. b) Nitrate+ nitrite concentrations measured in the top 2m of the water column. Note that the time series extends to prior to the start of the BV measurements.

Cyanobacteria Temporal Variability

Phycocyanin profiles, converted to BV, were collected every two hours throughout the summer to capture both the cyanobacteria vertical and temporal variability, and associated physical lake processes monitored by the research station, Figure 3.6a-c. The BV increases as the summer progresses from mid-July (BV 3.14 x 10^7 (μm^3/mL) at 1 m) to mid-August (BV 8.58 x 10^7 (μm^3/mL) at 1 m); with the BV systematically concentrating above the thermocline during this period. After August 19, following strong wind events and decreasing air temperature overturning the lake stratification ($\overline{LN} < 1$), the BV remains nearly uniformly distributed throughout the water column with depth average concentration at 7.3 x 10^7 (μm^3/mL), from early September to early October. Based on the

time series, the increase in biomass in mid-July might be attributed to: i) the increase of temperature up to 30 ºC, with an average of 27 ºC which is optimal for cyanobacteria growth, Figure 3.6a [65], ii) stably stratified conditions for an extended period of time (1 month), Figure 3.6b and iii) access to a monthly average phosphate concentration of 150 μg/L in the epilimnion [17,63,73].

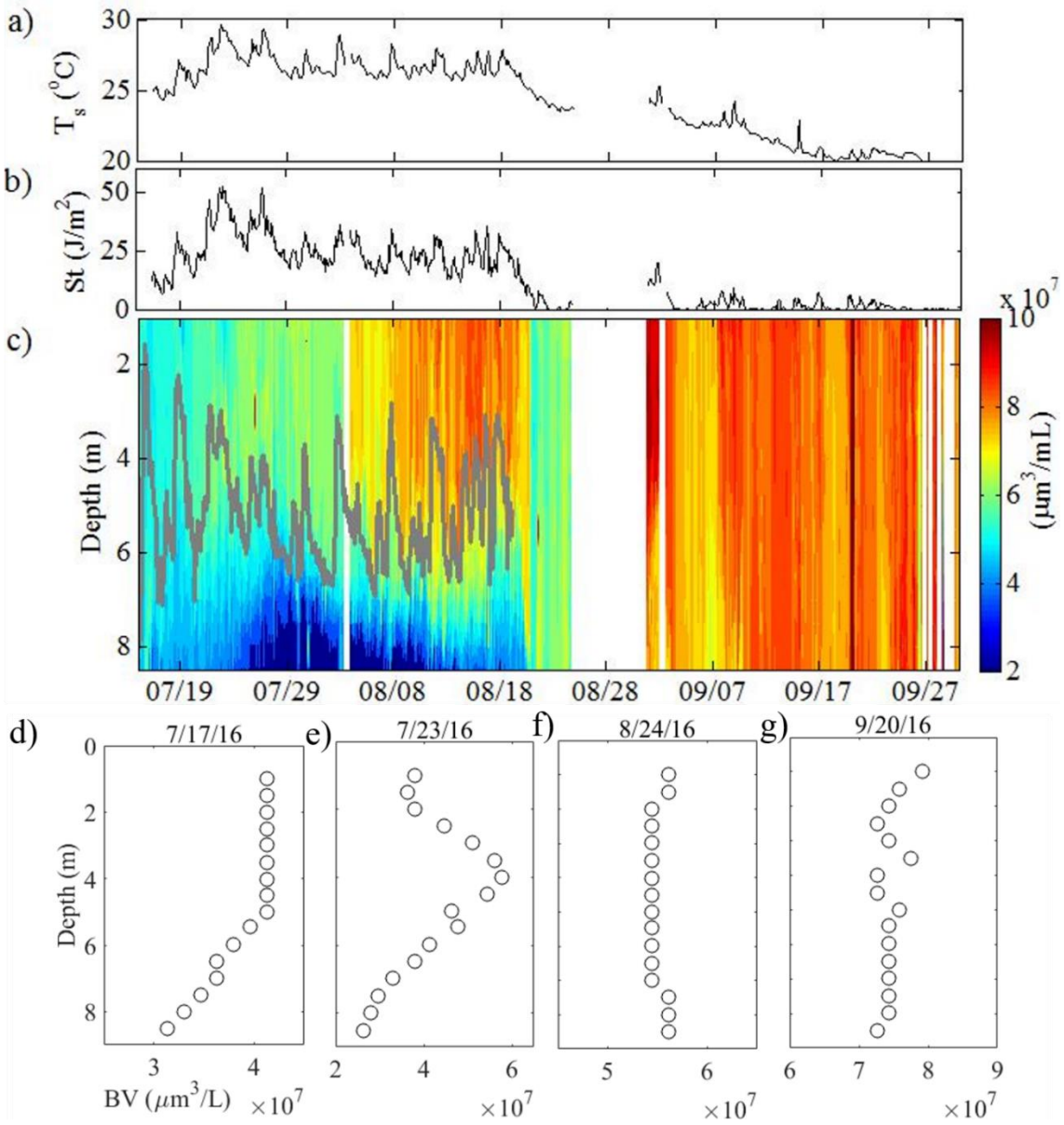

Figure 3.6: a) Time series of the seiche-averaged water temperature in the diurnal surface layer, T_s. b) Time series of St. c) Depth contour of BV time series, the gray line represents the depth of the thermocline. The white blocks represent periods when the research station was out of order. d) Selected BV profiles from both the strong and weakly stratified condition, the black circles represent data points measured by the probe and converted to BV.

Cyanobacteria Stratification

In addition to the seasonal variability, the cyanobacteria concentration shows significant vertical heterogeneities as demonstrated by the BV contour plot and by the selected profiles in Figure 3.6c-g. The ratio of BV_{max}, the maximum BV measured for each profile, to BV_{ave} , the depth average BV for each profile, describes the BV heterogeneities across the water column. We investigated statistical signatures relating the BV ratio time history with other quantities measured by the station or derived as lake parameters to elucidate possible drivers of BV variability throughout the season. A matrix of Pearson-R correlation coefficients (Matlab, Mathworks) identified which quantities are expected to grow/decay simultaneously with the BV ratio. This is a normalized cross correlation with zero temporal lags: although it does not quantify any delay between growth or decay processes, it is very important to highlight which variables should be included in a real-time model for cyanobacteria growth and distribution informed by *in situ* measurements. Table 3.2 summarizes Pearson-R coefficients of cyanobacteria BV (column 1) versus stratification and meteorological parameter quantifying positive (in phase) and negative (out of phase) correlations. Note we did not list ambient PAR, precipitation, and relative humidity because those quantities exhibited low correlation coefficients. These are the parameters that have been identified as significant for cyanobacteria accumulation and distribution, consistent with findings by *Chung et al.* [73], *Huber et al.* [63], *Cha et al.* [66] and *Kerimoglu and Rinke* [64]. Overall, there are no strong correlations among BV_{ave} or BV_{max} and other lake quantities likely because the temporal variation of depth-averaged biomass depends on the spatial (horizontal) heterogeneity of biomass distribution in the lake as wind and/or currents advect biomass at the research station location [71]. The

temporal variability of BV_{ave} is indeed inferred to be related to the large scale seasonal trends, discussed above.

Table 3.2: Pearson-R correlation coefficients among BV-related quantities and physical lake parameters and varaibles; including: the diurnal surface layer water temperature, T_s, Schmidt stability, St, wind speed U, Lake number, LN, thermocline depth, z_T and the temperature at the thermocline T_{zT}, for $\overline{LN} > 1$ (July -August 18) and $\overline{LN} < 1$ periods (August 19-October 1). There is no data for z_T nor T_{zT} in the $\overline{LN} < 1$ period because there is no significant thermocline during this time period.

$\overline{LN} > 1$ (July 15- August 19)						
	T_s (^{o}C)	St (J/m^2)	U (m/s)	LN	z_T (m)	T_{zT} (oC)
BV_{ave}(μm^3/mL)	0.05	-0.18	-0.2	0.07	0.12	0.27
BV_{max}(μm^3/mL)	0.2	-0.04	-0.24	0.07	0.03	0.4
BV_{max}/ BV_{ave}	0.5	0.38	-0.2	0.03	-0.18	0.54
$\overline{LN} < 1$ (August 19-October 1)						
BV_{ave}(μm^3/mL)	-0.12	-0.04	-0.2	0.04	-	-
BV_{max}(μm^3/mL)	0.03	0.29	-0.33	0.13	-	-
BV_{max}/ BV_{ave}	0.35	0.81	-0.33	0.22	-	-

The analyses of vertical heterogeneities is more interesting as it reveals high correlations among the BV ratio, the water temperature in the diurnal surface layer, T_s, and Schmidt Stability, St, for both stratification conditions (R=0.5,0.38 for $\overline{LN} > 1$, and R=0.35,0.81 for $\overline{LN} < 1$). This indicates that both strong and weak vertical heterogeneities, defined by the BV ratio, are enhanced by increasing T_s and St. The correlation coefficient between the BV ratio and St in the $\overline{LN} < 1$ is particularly high, R=0.81, which is notable because it shows the cyanobacteria stratification is especially sensitive to the thermal stratification stability, when the thermal stratification is weak. Also, negative correlation coefficients (R=-0.2 and -0.33) with U suggest that weak wind also contribute to increase

vertical heterogeneities. From a physical perspective, these values suggest that increased stratification, facilitated by high surface water temperature and low wind, and reflected in high St, leads to a vertically heterogeneous distribution of the biomass in the water column.

We confirm that the BV ratio is high, with a seasonal average BV ratio of 1.26, during periods of stable stratification (Figure 3.7a). The BV ratio then declines as the water column mixes due to weak stratification, $\overline{LN} < 1$. Based on the correlation matrix shown in Table 3.2, we identify the two parameters with the highest correlation coefficient, St and T_s, which can be used to explain biomass vertical heterogeneities in both stratification conditions. Obviously these two parameters are also well correlated among each other, as high surface temperature is a driver for stable stratification. The cyanobacteria vertical heterogeneity and the BV ratio are significantly correlated with these two lake parameters, $R^2=0.62$, across a wide range of stratification conditions, as seen in Figure 3.7b. The proposed relationship can give predictive information of cyanobacteria stratification based solely on water temperature measurements (Figure 3.7b)

$$\frac{BV_{max}}{BV_{ave}} = 1.3\times10^{-4}(Stc_pT_s)^{1/2}+1 \qquad (3.8)$$

where c_p is the specific heat of water. The proposed functional dependence demonstrates a decay of BV heterogeneity with the decrease in thermal stratification stability and surface water temperature (see also the Appendix). To incorporate the wind, we tested a similar functional relationship using the Lake Number, LN, Figure 3.7c, $R^2=0.45$. This relationship shows a decay of BV vertical heterogeneity with weakening dynamic stratification conditions.

$$\frac{BV_{max}}{BV_{ave}} = 0.17(LN)^{1/4} + 1 \qquad (3.9)$$

The lower R^2-value may be due to the periodic diurnal nature of the wind, which introduces variability in LN without necessarily inducing an equivalent variability in the BV ratio, suggesting that cyanobacteria vertical layering likely does not respond to wind events within short time scales. This is expected because correlations, as well as scatter plots do not account for any time lags between the increase in wind and the vertical adjustments of the lake temperature and, in particular, of BV vertical distributions.

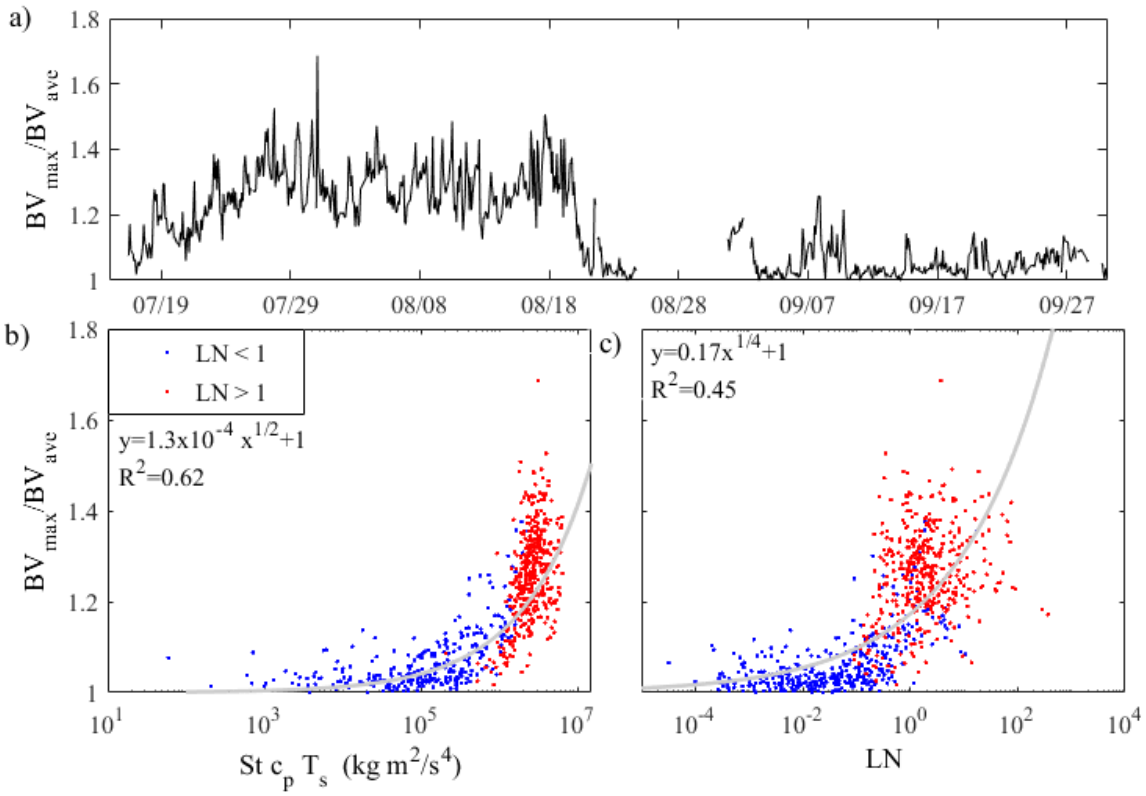

Figure 3.7: a) Time series of BV ratio throughout the summer b) BV ratio vs physical parameters driving cyanobacteria biomass, St and T_s. The red circles represent the data

points observed in the $\overline{LN} > 1$ and the blue circles represent data during the $\overline{LN} < 1$. The gray line represents the best regression function described by the following equation $y=1.3\times 10^{-4}(St\, c_p\, T_s)^{1/2}+1$ and yields a $R^2=0.62$. c) BV ratio vs LN. The red circles represent the data points observed in the $\overline{LN} > 1$and the blue circles represent data during the $\overline{LN} < 1$. The gray line represents the regression line described by the following equation $y=0.17(LN)^{1/4}+1$ and yields a $R^2=0.45$.

Local Cyanobacteria Maxima

Since the vertical biovolume heterogeneity can be quantified as a function of easily monitored parameters, we can further explore the nature of these heterogeneities by investigating how the shape of the BV distribution throughout the water column changes with the lake thermal structure and the local physical conditions (Figure 3.8). We defined two cases that describe BV distribution during stable stratification: i) uniform BV distribution in the surface mixed layer (i.e. Figure 3.6d); and ii) evident peak in the BV distribution (i.e. Figure 3.6e). In the uniform case, we have defined two variables to quantify the relevant depths of BV accumulation in the water column, specifically h_{BV} and $z_{BVuniform}$. h_{BV} is the depth of the uniform BV distribution in the surface layer, and $z_{BVuniform}$ is the average depth of the uniform BV distribution in the surface layer ($h_{BV}/2$). For peak distributions the relevant parameter is z_{BVmax}, i.e. the depth of the maximum BV for each profile (at each time). Uniform profiles represent 64% of the profiles in the LN>1 period (n=257), and profiles with peaks represent the remaining 36% of the profiles (n=146). The evolution of z_{BV} (including both $z_{BVuniform}$ and z_{BVmax}) is variable but it is consistently above the thermocline, (Figure 3.8).

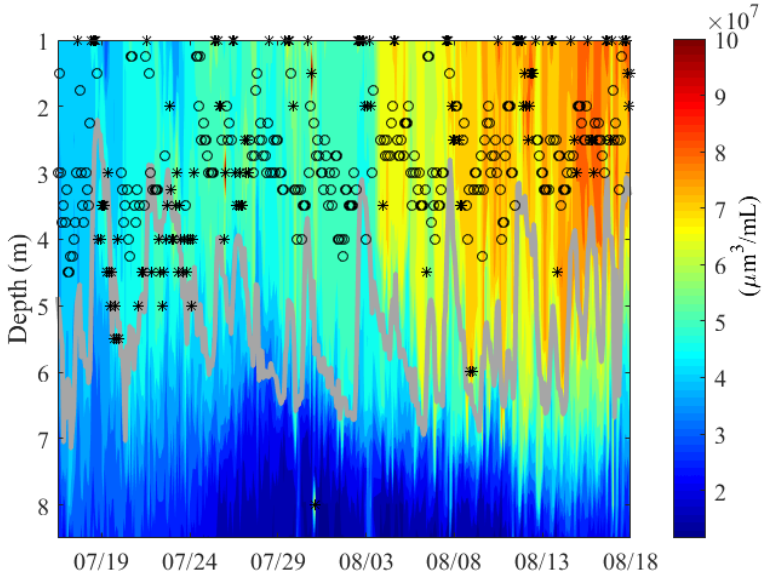

Figure 3.8: Depth contour of BV time series during the stable stratified period ($\overline{LN}$>1). The gray line is the depth of the thermocline, the black diamonds are the depth at $z_{BVuniform}$, the black stars represent the depth at z_{BVmax}.

It is of great interest to examine the physical conditions associated with the different distribution types to identify potential drivers. We observe that the average wind shear velocity, u_*, concurrent with uniform BV profiles was higher than the average wind shear velocity concurrent with profiles with BV peaks, specifically, $\overline{u*_{\text{uniform}}}$=0.005, while $\overline{u*_{\text{peak}}}$=0.003 (P-value < 0.05). Therefore, the uniform BV profiles are likely the result of mechanical mixing by wind, during which cyanobacteria behave more similarly to passive tracers advected throughout the surface layer. Conversely, under low wind shear velocity, cyanobacteria can form local BV maxima in response to other physiological drivers. There are two types of peak distributions observed, i) surface peaks with BV maxima at 1 m (n=47, shallowest sampling location) and ii) peaks at depths larger than1 m (n=99). The locations of local maxima are theorized to be, at least partially, driven by light. Specifically, peaks below the surface happened to coincide with specific PAR values measured, ~10

µE/m^{2}s, except for five data points corresponding to twilight hours, see Figure 3.9. Observed peaks at 1 m are excluded because they are not distinguishable between local maxima (z_{BVmax} = 1m) and uniform (h_{BV} = 1m) because the vertical limitations of the measurements.

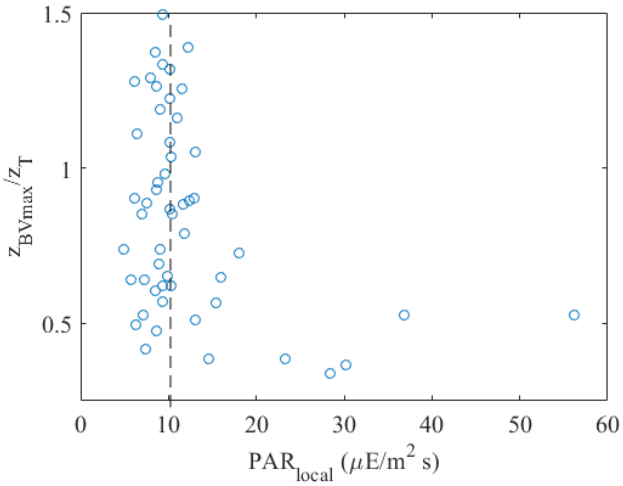

Figure 3.9: z_{BVmax} normalized by the thermocline depth vs PAR measured at z_{BVmax}. The black dots represent the data points measured during the day, PAR_{air} >20 (µE/m^{2}s), The dashed line represents PAR_{local} =10 (µE/m^{2}s). The data presented, here include all points when z_{BVmax} > 1m.

Overall, we have determined that BV heterogeneities can be described by thermal structure, mixing in the surface layer due to wind, and light conditions in the water column. As wind, light and surface air temperature change during the day, we computed averages of biovolume depth $\overline{z_{BV}}$, thermocline depth ($\overline{z_T}$) and photic depth ($\overline{z_p}$) over the whole stably stratified period, conditioned by the hour of the day. Although there is variability in the diurnal behavior of z_{BV}, which is demonstrated by the large standard deviations, on average z_{BV} is observed at shallower depths during the middle of the day, moving deeper into the water column in the twilight/dawn and night hours (Figure 3.10a). Despite the variability

in the $\overline{z_{BV}}$, the depth of relevant BV accumulation is consistently above the thermocline and within the photic zone, Figure 3.10. Qualitatively the diurnal trend in z_{BV} is consistent with the diurnal trends in z_T, confirming the confining effect by the thermocline as it adjusts with the surface temperature and the wind (typically in the late afternoon-evening) during the day.

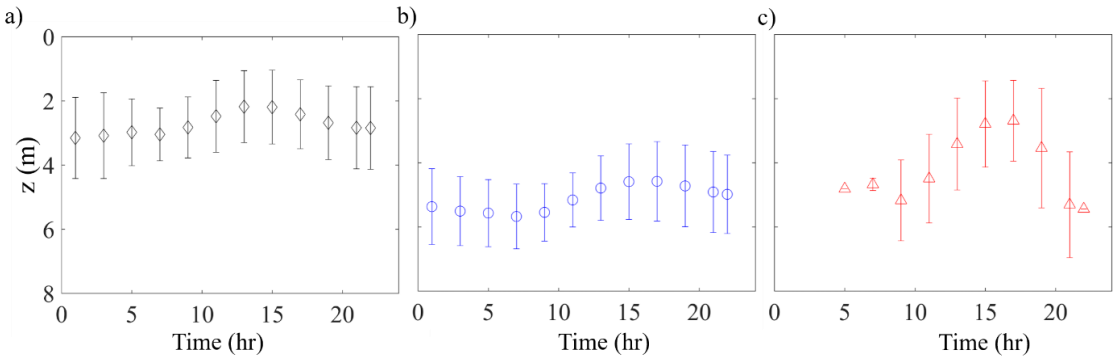

Figure 3.10:Observations are conditioned on the hour of the day for (a) biovolume depth ($\overline{z_{BV}}$, diamond), (b) thermoclinde depth ($\overline{z_T}$, circle), and (c) photic depth ($\overline{z_p}$, triangle) under stable stratification ($\overline{LN}$>1). The vertical bars represent one standard deviation of the conditional averaged values.

Discussion

Temporal Heterogeneity

High biovolume concentrations, BV, progressively increased from mid-July to mid-August in the surface mixing layer, confined by the thermocline, z_T. When stratification weakened the high BV persisted until late September and was uniformly distributed throughout the water column. This trend, reflected in the correlation matrix in Table 3.2, suggested that the accumulation of BV is consistent with prolonged high Schmidt stability index, St, on the order of 1 month, high water temperatures and high

epilimnetic concentrations of PO_4 (Figure 3.3). Wagner and Adrian [17] similarly demonstrated that cyanobacteria dominated inland lakes when stable stratification lasts longer than three weeks in the presence of sufficient phosphorous availability. Although nutrient dynamics can be a driver for cyanobacteria blooms, neither the nitrate+nitrite nor the phosphate concentration temporal evolution can describe the temporal heterogeneity of cyanobacteria BV (Figure 3.5). Instead, cyanobacteria BV heterogeneity was governed by lake dynamics, thermal structure, and seasonal temperature variation.

Vertical Heterogeneity

As there was a persistent and high concentration of phosphate in the epilimnion throughout the summer (Figure 3.5a), the nutrient upwelling and entrainment from the hypolimnion can be eliminated as a driving force for vertical heterogeneity observed in the cyanobacteria biovolume profiles. This investigation and results were therefore primarily focused on physical lake processes governed by wind, and water temperature structure, as they were shown to be highly correlated with BV heterogeneity (Table 3.2). Increasing air temperature promotes warmer surface water temperature and more stable stratification for extended time periods [63,65]. Both observations are consistent with vertical BV heterogeneity as demonstrated Table 3.2 and Figure 3.7. High BV was observed to persist after stratification weakened, i.e. when the BV concentrated layers were no longer confined by the thermocline and became more homogeneous throughout the water column. During this period, high concentrations (BV=8.58 x 10^7 $\mu m^3/mL$) of potentially toxic cyanobacteria were observed throughout the water column (Figure 3.6c). This is important since the cyanobacteria biomass has the potential to be undetected by conventional water quality monitoring methods utilizing depth integrated samples in the photic zone [19].

Additionally, large scale monitoring and prediction models are currently based on remote sensing technology [98], however as outlined in *Kutser et al.* [7] vertical distribution of cyanobacteria below the surface affects the spectral signature observed by remote sensing. Thus, the high BV recorded throughout the water column in this study can be easily undetected and have the potential to increase the risk of contamination of drinking water. For this reason, it is crucial to improve not only the prediction of cyanobacteria blooms in time but also their distribution in the water column.

Although vertical distribution of cyanobacteria has been investigated previously [70,71,73,79,80], this study is the first to establish quantitative relationships, as equations 8 and 9, for cyanobacteria BV stratification with water column thermal stratification conditions, St, surface layer temperature, (Ts), and lake number (LN) on a seasonal scale (Figure 3.7b and Figure 3.7c). The proposed scaling relationship, equation 3.8, has been verified using the additional data collected from South Center Lake (3.4 km^2) in the summer of 2017 (please see Appendix and Figure 12). The scaling relationship is effective in both dimictic and polymictic lakes, for more than an order of magnitude of total BV, and 5 orders of magnitude of Stc_pT_s. Even though the data were collected during two different years and in two different lakes with different i) nutrient and stratification conditions, ii) cyanobacteria composition distributions, and iii) meteorological conditions. Additionally, the proposed scaling relationship is not species-specific because the phycocyanin (voltage) to BV calibration remains linear while incorporating a range of different ecotypes of cyanobacteria and different dominance throughout the summer.

This proposed scaling relationship is relevant to sampling protocols of cyanobacteria blooms in lakes (i.e. remote sensing, photic zone sampling and fixed point

samples) as it informs if the sample depth is representative of the entire water column; guiding the extrapolation of single point monitoring. During weak stratification based on Schmidt stability index and the temperature of water in the diurnal surface layer, the BV measured at any depth is representative of the entire water column because the BV is uniformly distributed throughout. Conversely, during strong stratification, z_{BV} is above the thermocline depth (z_T) in the photic zone, and exhibits high BV heterogeneity, implying single point measurements will not be representative of the entire water column. Thus, measurements at multiple depths above the thermocline are recommended to capture cyanobacteria BV in the water column. Recent climate trends suggest that both St and T_s will increase season to season [63,65] indicating that BV heterogeneity will also increase, making the conventional single point measurement protocol less informative for cyanobacteria monitoring.

The broad range of time-scales (seasonal, wind-driven, diurnal) and abiotic factors involved in the variability of cyanobacteria biovolume suggests that the next step in accurate modeling might require temporal delays accounting for i) the adjustments of the water thermal structure, z_T, by the wind and for ii) the vertical movements of cyanobacteria within the water column. Nevertheless, despite the large variability imposed by cyanobacteria composition and meteorological and physical lake conditions, these relationships can quantitatively describe cyanobacteria heterogeneities on a seasonal scale in eutrophic lakes.

Local Drivers for Biovolume Maxima

Our observations show that BV accumulation is above the thermocline and exhibits different distribution behaviors in the surface layer which can be distinguished by wind

shear. Different cyanobacteria taxa have specific drivers to actively regulate buoyancy, e.g. access to light [72], temperature [71], nutrients [70] or any favorable mixture of these parameters [79,99]. Overall, we observed a tendency to form local maxima below 1 m consistently at depths with local PAR=10 $\mu E/m^2s$. This may be a consequence of the presence of *Planktothrix,* which has been shown to be a driven by affinity for low light [69,72]. We show that z_{BV} is above the thermocline and in the photic zone and qualitatively follows the behavior of z_T. This is a similar trend to that reported in *Cantin et al.* [70] which showed the location of the highest concentration of cyanobacteria BV deepens as the thermocline deepens (Figure 3.10).

Conclusions

Our objective was to investigate how the abiotic physical and meteorological conditions influence the temporal and vertical heterogeneities of total cyanobacteria Biovolume (BV) using high frequency and high-resolution seasonal monitoring observations in a stratified lake, under eutrophic conditions. While other studies relied on weekly or monthly monitoring [70,71,73,79], this study was the first to capture the hourly dynamics of cyanobacteria biovolume (BV) throughout the water column over the course of the season. The observations revealed the effects of local meteorological and water stratification conditions on the vertical and temporal heterogeneity of cyanobacteria in a eutrophic lake, where nitrate or phosphate concentration did not seem to play a key role. High BV recorded in the epilimnion in mid-July was attributed to prolonged, strong stratification within the water column, high surface water temperatures, and high phosphate concentrations in the epilimnion. When the stratification weakened, the thermocline no longer confined cyanobacteria-rich layers, and cyanobacteria vertical heterogeneities

decayed, with high BV expanding well below the photic depth. The analyses of BV vertical heterogeneity demonstrated high correlations among BV stratification, surface water temperature, and stratification stability, the latter depending on the thermal structure in the water column. A quantitative scaling relationship was developed, posing the relationship between BV heterogeneity and thermal stratification stability and surface water temperature. This model was verified in a dimictic lake the following year. To incorporate dynamic mixing effects of the wind, a quantitative relationship among the LN and BV ratio was also provided, but it was less effective, likely due to the slow response of the thermocline to wind variability. Predicting vertical heterogeneity is relevant to sampling protocols of cyanobacteria blooms in lakes (i.e. remote sensing, photic zone integrated sampling and fixed point samples) as it informs if the sample depth is representative of the entire water column, thus guiding the extrapolation of single point monitoring.

To expand on the results of BV vertical heterogeneity, BV distributions were further characterized as i) uniform BV distribution in the surface layer and ii) BV with local maxima. When the BV is not uniformly distributed in the epilimnion by wind forcing and mixing, the location of BV accumulation was observed to be driven by light penetration conditions. The maximum concentrations of BV at deeper levels of the lake (i.e. not at the surface, thus for $z > 1$ m) were located at varying depths, but consistently defined by $PAR_{local} \sim 10\ \mu E/m^2s$. Overall BV accumulation in the surface layer is above the thermocline and in the photic zone. The observations suggest that cyanobacteria tend to move and accumulate in specific warm water layers, confined by the thermocline and characterized by well-defined light conditions.

Although nutrient distribution can be a driver for cyanobacteria blooms, our observations show that the temporal variability of cyanobacteria BV is not explained by the nutrient evolution and thus, rather governed by lake dynamics, thermal structure, seasonal temperature variation, and light availability. The analyses of temporal and spatial heterogeneities of cyanobacteria BV are important to mitigate risks of contamination of drinking water, as well as evoke public awareness and concerns to harmful algal blooms. The mitigation and water management strategies of harmful algal blooms are largely based on watershed nutrient input management. However, under nutrients invariant conditions, as investigated in this work, predictive tools should include the local meteorological and physical lake conditions as drivers of BV temporal and vertical heterogeneities.

Model Validation in Dimictic Lake

The research station was deployed in a eutrophic dimictic lake in central Minnesota, (South Center lake; 45.3716170, -92.8275500), and was anchored from mid-May to early August 2017 at 16.7 m depth. The phycocyanin probe (V), calibrated using the methods described above, resulted in a linear relationship between cyanobacteria BV and the probe (not shown). Both Madison lake (5.4 km^2) and South Center lake (3.4 km^2) are considered eutrophic lakes, but have low nitrate concentrations (<0.15 mg/L) during the study periods. There are several differences between Madison Lake and South Center Lake i) the phosphate concentrations were lower ($[PO4]_e$=39.8 µg/L) in South Center Lake but similarly invariant throughout the sampling period ii) St is persistently higher in South Center lake (Figure 3.11ab) iii) the cyanobacteria species distributions were different, but the same dominant species were present and iv) the BV concentration in South Center Lake is lower than that in Madison Lake (Figure 3.11c). Despite these differences, the scaling

relationship developed in Madison Lake still describes the combined data sets while covering a broader range of physical conditions (Stc_pT_s) and BV ratios, up to 2.2 (Figure 3.12).

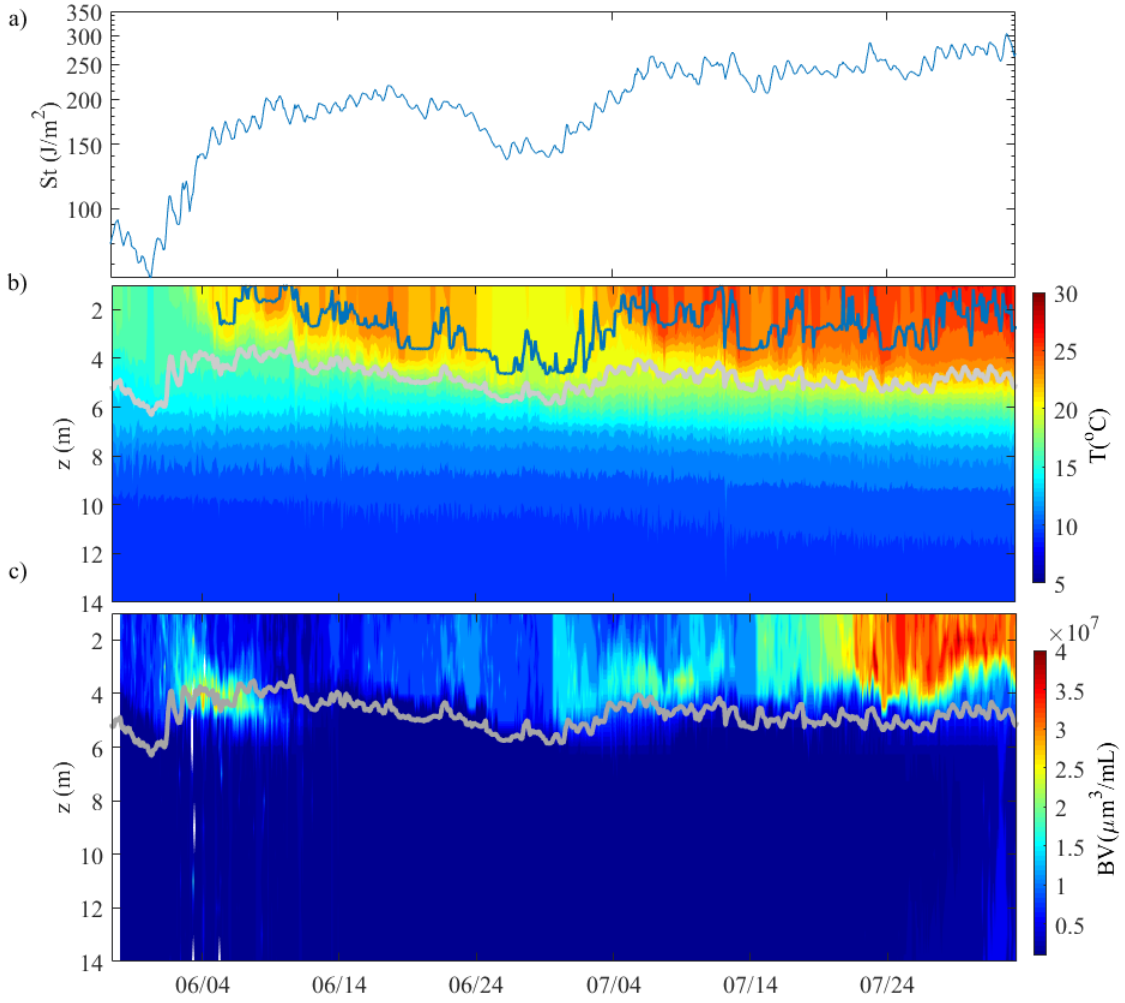

Figure 3.11: Physical lake conditions for South Center Lake. a) Time series of Schmidt stability index, St. b) Temperature depth contour measured by the thermistor chain and averaged with the seiche period. The gray line represents the depth of the thermocline, z_T,

and the blue line represents the depth of the surface layer, h_{SL}. c) Time series of BV contour where the gray line is the thermocline depth.

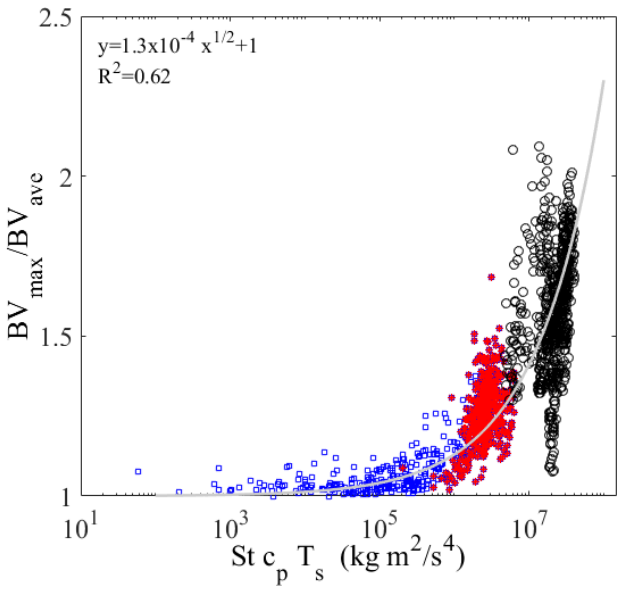

Figure 3.12: BV ratio vs St $c_p T_s$, for Madison Lake (red-stratified, $\overline{LN} > 1$, and blue-weakly stratified, $\overline{LN} < 1$) and S. Center Lake (black). The gray line represents the fit model (Equation 3.8).

Chapter 4

Investigating Vertical Heterogeneities of Cyanobacteria and Microcystin Concentrations in Lakes Using a Seasonal *In situ* Monitoring Station

Introduction

Cyanobacteria blooms are accumulations of photosynthetic microorganisms, which represent a ubiquitous nuisance in freshwater ecosystems across the world. Most studies have been focused on the large, well-known water bodies suffering from seasonal blooms including Lake Erie in North America, Lake Taihu in China, and Lake Victoria in Africa [100]. However, smaller lakes are an integral part of the fresh surface water, especially in central North America [101]. Dynamics of blooms in small to medium lakes across the

globe are changing more rapidly due to changes in temperature regimes including warming surface water and strong stratification [102]. Additionally, smaller lakes experience a broader range of stratification conditions throughout a season, as quantified by the Lake Number or Schmidt Stability index (St) ([101,102].

Although nutrient dynamics are essential for cyanobacteria growth and have been targeted as a management strategy to control these blooms, they are not the sole contributor to describe the global trends in cyanobacteria bloom dynamics, particularly to explain the frequency and spatial variability of cyanobacterial concentrations [15,102–105]. To more fully understand and predict the spatial variability of cyanobacteria blooms, filed investigations should include observations of local meteorological conditions in addition to nutrients and water temperature [70,100]. Vertical variability of cyanobacteria blooms is much higher than that of horizontal variability across the lake surface [102,104]. This vertical variability is very important for risk management of public drinking water intake and must be considered for both bloom sampling and remote sensing efforts [71].

A critical aspect of cyanobacteria blooms is their potential to produce a wide range of cyanotoxins, including microcystin, which is produced by several cyanobacteria genera like the ones observed in this study. Understanding the distribution for the toxin concentrations is important for mitigation of potential contamination of drinking water, recreational exposure, and overall ecosystem health [1]. Toxin production of cyanobacteria in lakes has been recently shown to be driven by a combination of environmental factors including nutrients [70], light [72], and temperature [68,71], which all vary with depth [106]. More importantly, recent studies have shown the interplay amongst vertical lake

structure and the combination of these parameters to drive cyanobacteria distribution and toxicity [15,104,107]. It is therefore important to consider the vertical variability of both the cyanobacteria concentrations and the toxins produced.

Chapter 3 used a high frequency, high resolution, research station to observe, the effects of physical lake parameters, water temperature and water column stratification) on the vertical distributions of cyanobacteria biovolume (BV) in the water column, during the summer months. Using the same high frequency, high resolution, research station, we explored the following objectives in the current work: 1) identify the physical drivers associated with the BV vertical distribution above the thermocline, 2) describe the vertical variability of microcystin in relation to BV and physical lake conditions, and 3) identify the temporal lag between microcystin production and BV accumulation. The results presented here shed new light on the complexity of BV and microcystin distributions and have important implications for future water quality management, sensing, and sampling strategies.

Methods

Research Station

The long-term, high frequency, and high resolution vertically profiling research station used in this study is described in detail in Chapter 3. The station was anchored in Madison Lake from July to mid-August 2016 at a location with 9.2 m depth, and in South Center Lake from May to mid-August 2017 at a location with 16.7 m depth. The two lakes are described in the following sub-sections. The research station collects measurements in

three forms: 1) 5 minute average local meteorological data for the wind speed, wind direction, ambient photosynthetically active radiation (PAR), precipitation, air temperature, and relative humidity; 2) *in situ* temperature data; 3) a vertical profile of water quality parameters every 2 hours every one meter of depth. The water quality parameters, measured by a Hydrolab DS5 Water Quality Multiprobe (Hach Environmental CO, USA), include the water temperature, pH, dissolved oxygen (DO), PAR, specific conductivity, and phycocyanin (a proxy for cyanobacteria BV). All data were recorded with a sampling interval of 5s over a sampling time of 1 min at each depth. Therefore, each water quality data point is an average of 12 replicate measurements. All data were available in real-time via a wireless connection to allow for rapid detection and response to BV accumulation for discrete sampling.

Madison Lake

Madison Lake (coordinate 44.19056°,-93.80861°) is a residential and recreational lake located in a primarily agricultural watershed in south-central Minnesota, Figure 3.1a. It is a polymictic lake with an area of 5.4 km^2, a maximum depth of 18 m, and a mean depth of 3.4 m. Because of the high nutrient inputs from its surrounding agricultural watershed, Madison Lake is classified as eutrophic [82]. The lake was chosen as the study site because of its eutrophic classification, long water quality monitoring record, and history of frequent toxic algal blooms throughout the summer [19].

South Center Lake

South Center Lake (coordinate 45.3716170°, -92.8275500°) is a 3.4 km^2 dimictic, eutrophic lake with a maximum depth of 36 m and a mean depth of 5.7 m. This lake has a

long history of water quality monitoring and is classified by the Minnesota Pollution Control Agency (MPCA) as a eutrophic Sentinel Lake [82].. South Center Lake serves as a recreational lake with high summer boat traffic and high fishing pressure throughout the year. Note that longer records of BV, water temperatures and meteorological data are available for South Center Lake, because the research station was deployed earlier in the year.

Discrete samples

To supplement the research station measurements, discrete water samples were taken weekly with a Van Dorn sampler at the research station. Samples were collected for every meter of depth, concurrent with the profiles collected by the research station. These samples were used to evaluate local total microcystin concentration, MC, dissolved nitrate and phosphate concentrations, phycocyanin concentrations, and cyanobacteria BV and composition. To determine the vertical distribution of macronutrients throughout the summer, phosphate and inorganic nitrogen concentrations were analyzed from the discrete water samples. The water samples were first filtered through GF/F filters (Whatman, Maidstone, UK) and stored at 2 °C until analyzed. The filtered water samples were measured by a laboratory bench-top fluorometer (Trilogy, Turner Designs, CA, USA P/N: 7200-0000). For phosphate concentration the bench-top fluorometer was augmented with a phosphate absorbance module (Trilogy, Turner Designs, CA, USA P/N: 7200-070) that accommodated a four-sided, clear 10 mm, glass square cuvette. The phosphate concentrations, [PO4], were measured according to [89]. A calibration curve was constructed using a serial dilution of potassium dihydrogen phosphate standards with

concentrations ranging from 8.9 - 1,138 µg/L. For the nitrate concentration, the bench-top fluorometer was similarly augmented with a nitrate absorbance module (Trilogy, Turner Designs, CA, USA (P/N: 7200-074) that accommodated the same glass square cuvette. The LaMotte nitrate test kit method using the Nitrate-Nitrogen Model NCR (LaMotte, Chestertown, MD, USA Cat. No. 77101). A calibration curve was constructed using a serial dilution of nitrate standard (Ricca Chemical Company, Arlington, MD, USA Cat. No. 5307-16) ranging from 0.15 - 8 mg/L. The nitrate concentrations were corroborated with nitrate+nitrite concentrations collected by the MPCA during the observation periods.

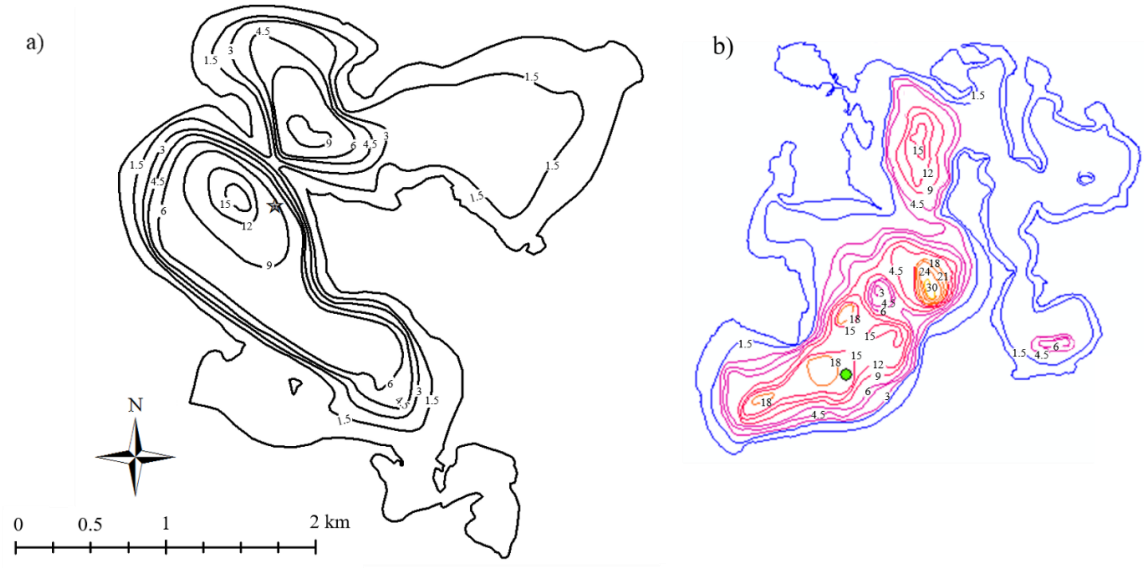

Figure 4.1: a) Contour map of Madison Lake, MN (contour lines marked in meters). The star marks the location of the floating research station during summer 2016 .The depth at this location is 9.2 m. b) Contour map of South Center Lake. The circle represents the location of the research station during the summer of 2017 (local depth is ~14m).

BV and Identification

The phytoplankton sample identification and BV were measured from the discrete water samples, preserved using 1:100 ratio of Lugols Iodine and stored in 4 °C until analysis. The phytoplankton identification was done using microscopy and a gridded Sedgewick-Rafter counter (Wildlife Supply Co, FL, USA) at 10x magnification. Further identification of *Planktothrix* spp was done using a hemacytometer at 40x magnification. The identification and BV estimation are outlined in detail in Chapter 3. The BV was computed from random images from representative depths and times throughout the sampling season. The total BV is the sum of the individual BV for each dominant cyanobacteria identified, Figure 4.2ab. The individual genera BV was estimated using the standard geometry body approximation [87]. The phycocyanin measured by the profiling fluorometer on the research station was calibrated with the concurrent water samples, Figure 4.2cd. The error bars were calculated from the standard deviation amongst each sample count multiplied by average BV.

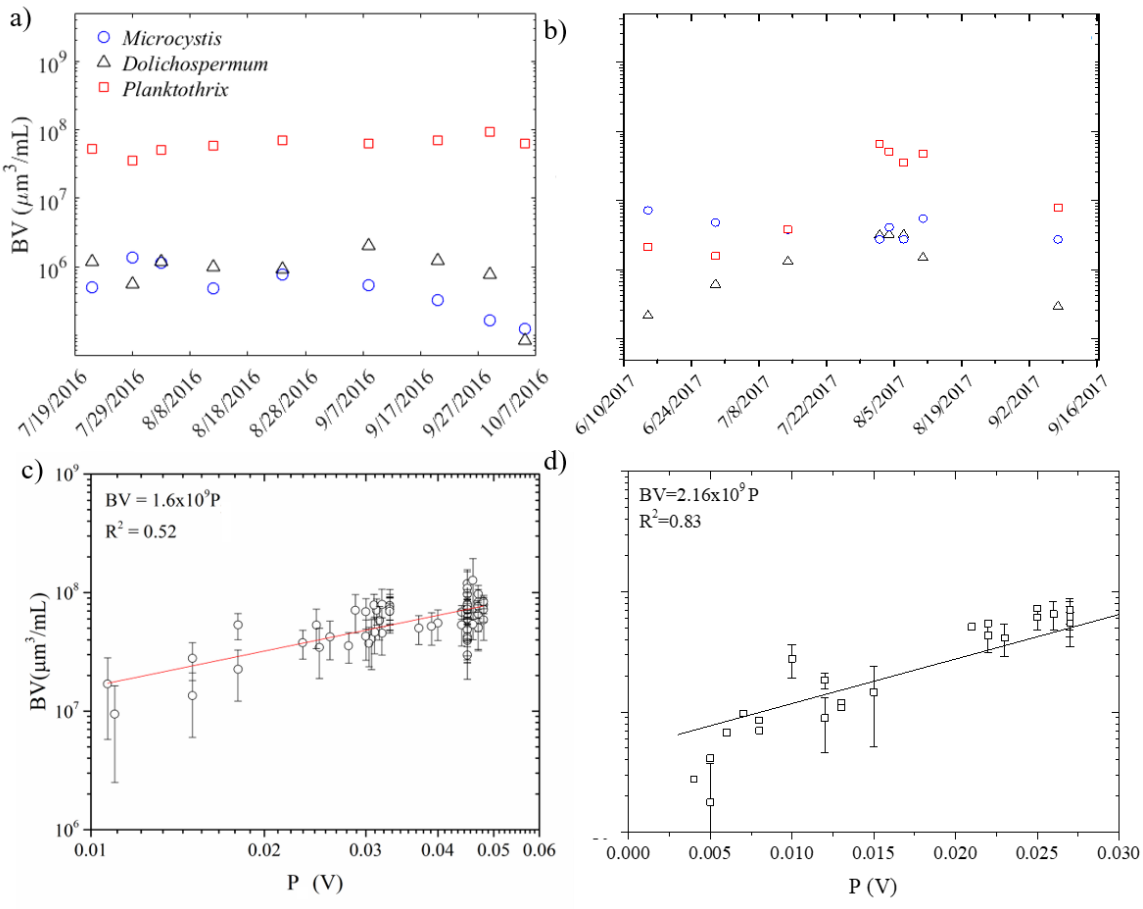

Figure 4.2: a,b) Time series of dominant cyanobacteria genera BV which makes up the total BV, where the circle represents *Microcystis* sp, the triangle represents *Dolichospermum* sp, and the square represents the *Planktothrix* sp. for a) Madison Lake and b) South Center Lake. c,d) Cyanobacteria biovolume calibration with the profiling phycocyanin probe. The symbols represent an average BV from samples taken from representative depths and dates throughout the sampling effort corresponding to the phycocyanin measured by the profiling fluorometer. The error bars represent the standard deviation of the cell counts of each genus multiplied by the average BV of individual

genera. Linear regression analyses for c) Madison Lake and d) South Center Lake yielded $BV=1.6x10^9P$, $R^2=0.52$ and $BV=2.16x10^9P$, $R^2=0.83$, respectively.

Toxin quantification

The total microcystin concentration was measured using EPA Method 546 using ADDA ELISA PN 520011, Microtiter Plate (96T) (Abraxis INC, Warminster, PA USA). The samples were collected from representative depths and times throughout the sampling season (the same used for the BV calibration in Figure 4.2) and stored in the freezer until analyzed. Directly prior to analysis, the samples were freeze-thaw cycled three times and then filtered using GF/C filters (Whatman, Maidstone, UK). All samples were measured in duplicate. The samples and standards were vortexed prior to analysis. The plates were analyzed using a BioTek EL800 96 well microplate reader set to a wavelength of 450 nm (Winooski, VT, USA).

Physical Lake Conditions

Using the meteorological data and vertical profiles measured by the research station, we estimated several parameters to characterize the physical lake conditions.

The diurnal surface mixed layer (SL) is the region of relatively constant temperature at the water surface. The depth of the diurnal surface mixed layer (h_{SL}) is defined as the depth of the layer where the temperature variation remain confined within 0.3 °C with respect to the surface temperature. The thermocline, instead, corresponds to the region of the maximum density gradient. The thermocline depth, z_T, is estimated from

the density profiles by determining the first moment of the density gradient [90,91], as shown in Equation 3.3.

The measured water temperatures were averaged temporally over the period of internal seiche for the estimation of the local density ρ. The period of vertical mode 1 internal seiche was estimated by the equation 3.4. All the meteorological and temperature data used and plotted hereinafter are averaged over the seasonal seiche period, (two and three hours for Madison Lake and South Center Lake, respectively) centered temporally on each measured profile to filter out the seiche variability and the associated internal waves.

The shear velocity, $u_* = (\tau_w/\rho_e)^{1/2}$, is the velocity scale derived from the shear stress at the water surface and is used here to quantify the effect of the wind on lake mixing and water column thermal structure. The shear stress is estimated as $\tau_w = C_D \rho_{air} U^2$, where ρ_{air} is the density of the air, C_D is the drag coefficient (assumed to be $1x10^{-3}$ for U <5 m/s and $1.5x10^{-3}$ for U >5 m/s [96] and U is the wind speed at 10 m extrapolated by $U = U_h[1-(C_D^{0.5}/\kappa)\ln(10/h_w)]$; assuming a logarithmic layer, h_w =1.5 m is the height of the wind sensor at the research station providing the local wind speed U_h, and κ=0.4 is the von Karman constant.

To quantify the strength of thermal stratification, the Schmidt stability, St, was estimated using the seiche averaged temperature profiles. St describes the resistance to mechanical mixing due to the potential energy of the density stratification in the water

column [93,108]. St is a measure of the amount of work per unit surface area needed to mix the water column to a uniform temperature, and it is defined in equation 3.5.

To quantify the mixing and the turbulence induced by wind in the water column, a specific Reynolds number is defined using length and velocity scales of the diurnal surface mixed layer, Re_{SL}, defined as:

$$\mathrm{Re}_{SL} = \frac{u_* h_{SL}}{\nu_{SL}} \tag{4.1}$$

where ν_{SL} which is the depth-averaged kinematic viscosity of the water in SL.

Results

Meteorological and Stratification Conditions

The physical lake conditions measured by the research station varied over the course of the study (Figure 4.3). The wind speed time series depicts a cyclic pattern throughout the seasons ranging from U = 0 to 6 m/s for both lakes, except for a high wind event on August 3, 2017, reaching a maximum of U = 9 m/s (Figure 4.3ab). In both lakes, the water temperature reached its maximum in the surface mixed layer during July (Figure 4.3cd). Madison Lake has a higher average temperature in the water column and a more variable thermocline, consistent with the lower $\overline{\mathrm{St}}$. South Center Lake has a much higher St than Madison Lake, with seasonally averaged values $\overline{\mathrm{St}}$ =183 and 24 J/m^2, respectively. After August 18, Madison Lake became weakly stratified and exhibited a polymictic behavior (data not shown). Overall, the measurements suggest dimictic conditions during the sampling season in South Center Lake, quantified by high St and a well-established

temperature gradient, as compared to a more polymictic condition in Madison Lake supported by its highly variable thermocline depth and significantly lower St.

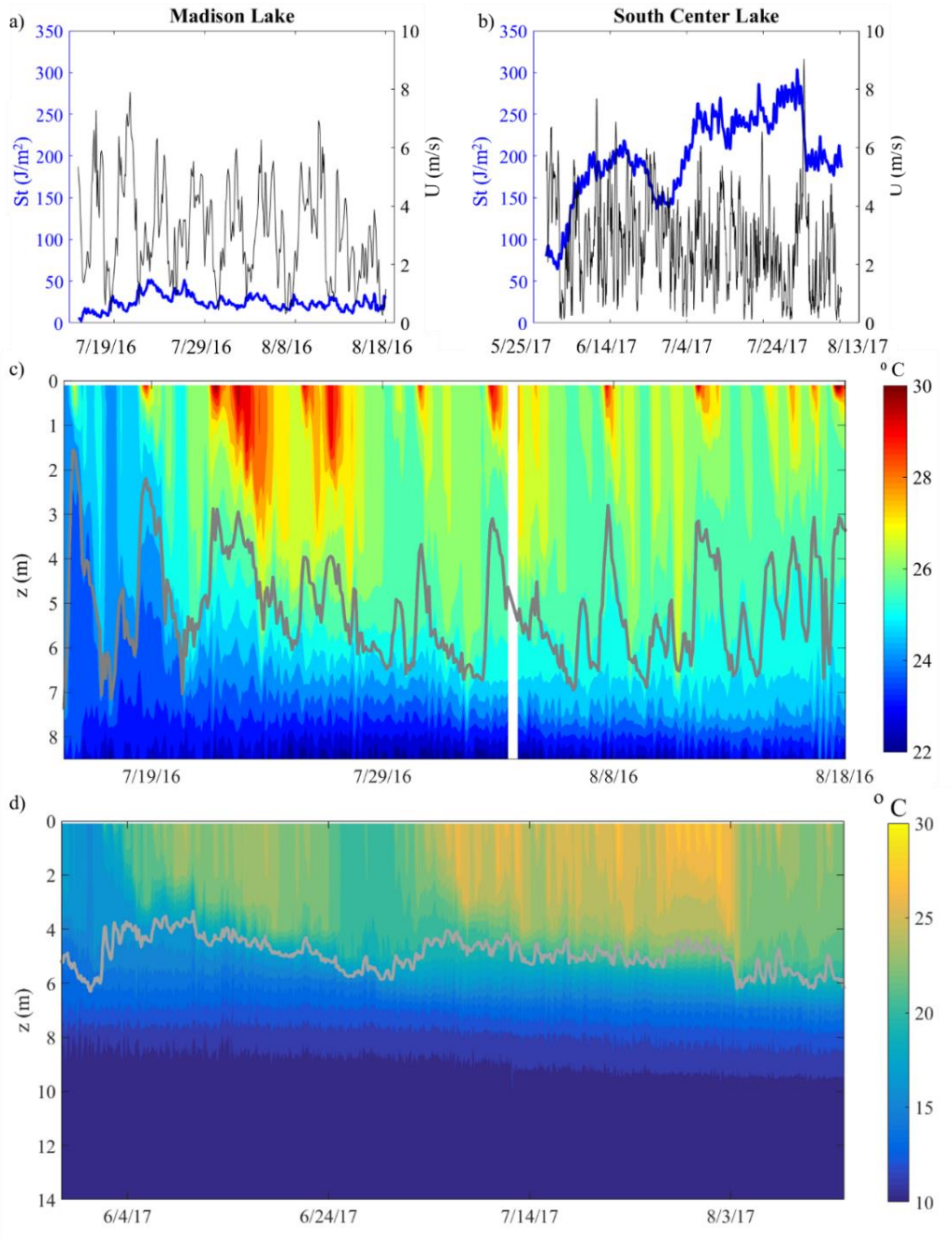

Figure 4.3: Time series of wind speed U , averaged over the period of vertical mode 1 internal seiche (thin solid line) and time series of Schmidt stability index (thick line) in a) Madison Lake and b) South Center Lake. Temperature contours and the time series of thermocline depths (solid lines) for c) Madison Lake and d) South Center Lake.

Water chemistry variability

Nitrate and phosphate concentrations were measured from discrete water samples from the epilimnion and hypolimnion throughout the season, Figure 4.4. The phosphate concentrations were depth-averaged above the thermocline ($[PO4]_e$) and below the thermocline ($[PO4]_h$). $[PO4]_e$ was relatively constant throughout the observation period for both lakes and was high compared to the $[PO4]_h$ in Madison Lake and comparable to $[PO4]_h$ in South Center Lake. The nitrate+nitiate concentrations measured in both the epilimnion and hypolimnion of the water column were all < 0.15 mg/L, which is typical of Minnesota lakes [19]. Madison Lake had higher phosphate concentrations than in South Center Lake, $\overline{[PO_4]_e}$=150 and 40 µg/L, respectively.

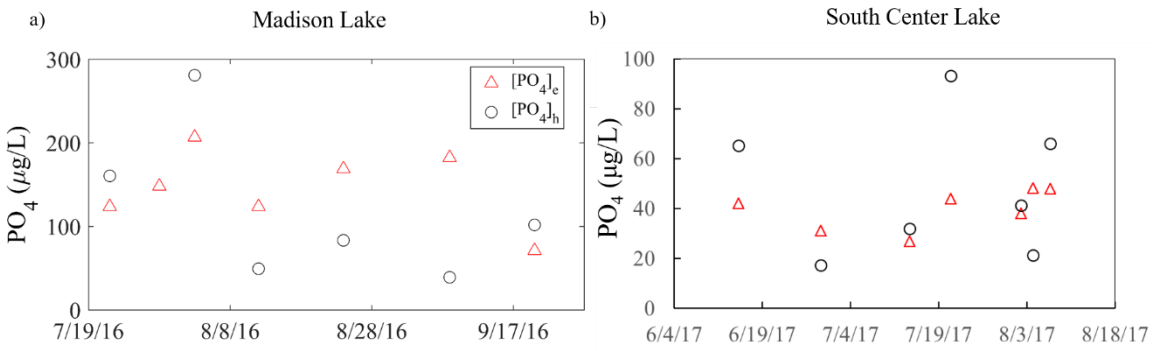

Figure 4.4: Time series of average PO_4 concentrations in the epilimnion (triangles) and hypolimnion (circles) for a) Madison Lake, and b) South Center Lake.

BV variability

The biovolume (BV) contours show the vertical and temporal evolution of cyanobacteria BV throughout the seasons monitored by the profiler in Madison Lake (Figure 4.5a), and South Center Lake (Figure 4.5b). Both lakes experienced high BV

above the thermocline beginning in mid-July of both years. In Madison Lake, cyanobacteria accumulation extended over a larger percentage of the observed water column, and the weaker temperature gradient at the thermocline did not confine the BV as well as that observed in South Center Lake, resulting in higher BV in the hypolimnion. In South Center Lake on August 3, 2017, during a high wind event, the BV abruptly increased above the thermocline, which was likely due to horizontal transport of cyanobacteria by the wind. This abrupt increase is also observed by comparing the water samples taken on August 2 and on August 4, when *Planktothrix* composition increases (Figure 4.2b). After the wind event high BV persisted for one week and then decreased.

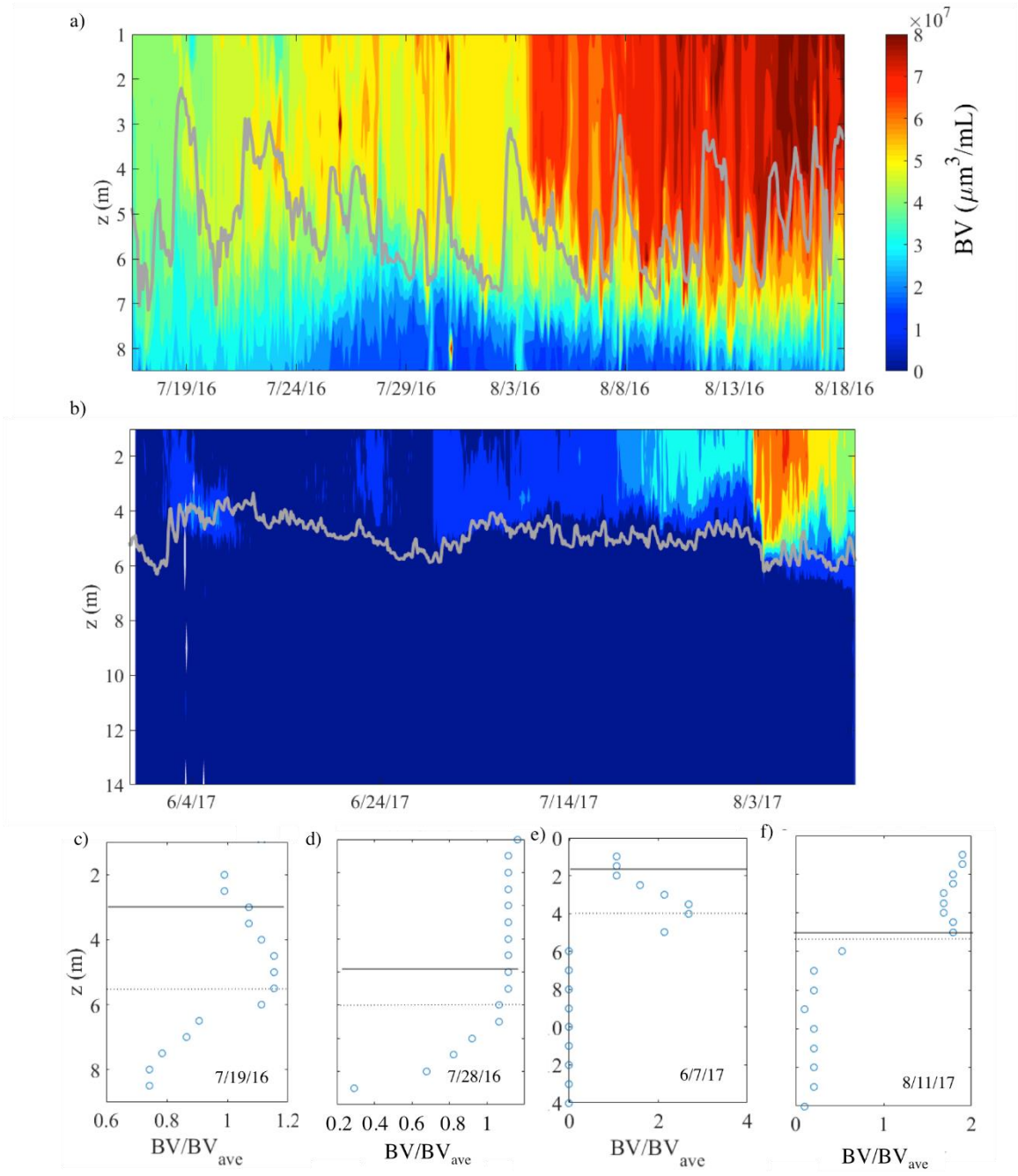

Figure 4.5: Temporal contour of BV water column profiles, where the gray line is the thermocline depth for a) Madison Lake and b) South Center Lake. c-f) Selected BV profiles from c,d)Madison Lake and e,f)South Center Lake. The dotted line is the thermocline depth and the solid line is the depth of the diurnal surface layer.

Overall, both Madison Lake and South Center lake are eutrophic lakes but had nitrite+nitrate concentrations <0.15 mg/L during the study periods. The main differences observed between these two lakes are 1) the higher phosphate concentrations in Madison lake, 2) the weaker thermal stability, or lower St, in Madison lake leading to a turnover in mid-August, 3) the higher BV concentrations in Madison Lake, though with a lower contribution by *Microcystis*.. Despite those differences both lakes show a significant increase in cyanobacteria biovolume in early August.

Quantification of BV vertical heterogeneity

Despite the difference cyanobacteria composition and lake thermal stratification, high biovolume remained confined above the thermocline, in both lakes. We however distinguish two types of BV profiles above z_T : 1) uniform distribution in the surface mixed layer, SL (Figure 4.5d-f) and 2) BV distribution with a local maximum (Figure 4.5c-e). Uniform distributions made up 64% and 56% of the BV profiles in Madison Lake and South Center Lake, respectively.

Table 4.1: Physical lake parameters consistent with BV distributions (uniform and peak) in Madison Lake and South Center Lake. μ is the average value based on n samples, outlined below, for the respective BV distribution conditions. All parameters were assessed as significant ($P<0.05$) based on single factor ANOVA analysis.

	Madison Lake		**South Center Lake**	
	μ (uniform) n=257	μ (peak) n=146	μ (uniform) n=523	μ (peak) n=403
h_{SL} (m)	4.50	2.58	3.31	1.91
h_{SL}/z_T	0.77	0.60	0.58	0.43
u*(m/s)	0.005	0.003	0.004	0.003
Re_{SL}	2.48×10^4	1.02×10^4	1.44×10^4	7.26×10^3

We examined physical lake parameters relevant to the diurnal surface mixed layer, where the highest BV values were observed (Table 4.1). These were the parameters that showed significant differences ($P>0.05$) between peak and uniform BV distribution. It is important to note that St and Lake Number, which were used to describe vertical heterogeneity in the entire water column (Chpater 3), were not found to be relevant in this analysis. In an effort to combine u* and h_{SL}, we created a specific Reynolds number Re_{SL} which is relevant to the surface mixed layer, using u_* as the characteristic velocity scale, h_{sl} as the characteristic length scale and the viscosity of the water in the surface mixed layer. The mean values for h_{SL}, h_{SL}/z_T, u_*, and Re_{SL} were larger for uniform distributions as compared to peak distributions in both lakes, suggesting stronger mixing due to high wind deepening the surface mixed layer. We compare the statistical distribution of each variable in Figure 4.6. As in Table 4.1, larger h_{SL}, h_{SL}/z_T, u_*, and Re_{SL}, correspond to

uniform distributions as compared to peak distributions. In an effort to understand the mechanisms governing cyanobacteria distribution in the water column, we combined results from both lakes and systematically compare the occurrence of uniform and peak distributions as a function of Re_{SL} (Figure 4.7).

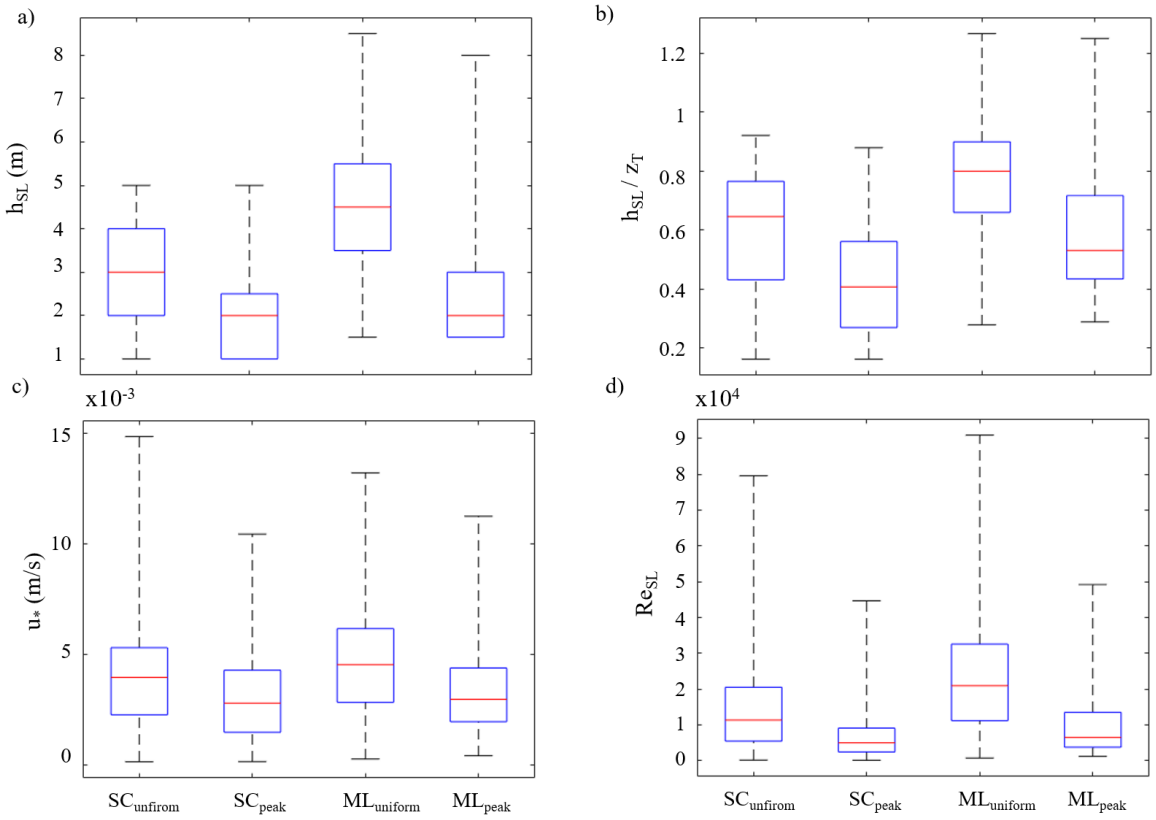

Figure 4.6. Comparison between physical lake parameters, a) h_{SL}, b) h_{SL}/z_T, c) u_*, b) Re_{SL}, versus uniform and peak BV distributions for South Center Lake and Madison Lake. The red line represents the median of the respective data sets. The top of the box represents the 75th percentile, the bottom of the box represents the 25th percentile and the whiskers represent range of the data set.

Uniform BV distributions were observed more frequently at larger Re_{SL}, with all distributions being uniform at Re_{SL} > 50,000 (Figure 4.7a). The percentage of uniform profiles versus the total number of profiles as a function of Re_{SL} ($N_{uniform}/N_{Re}$) are plotted in Figure 4.7b. Thus, given Re_{SL} from meteorological and thermal sensors, we can predict how frequently the BV distribution will be uniform or exhibiting a local peak in the epilimnion. For example, when $Re_{SL}>5x10^4$ the BV was always observed to be uniformly distributed. Conversely, for (lower) $Re_{SL}=7x10^3$ there is a 50% chance of finding a uniform or peak distribution. The relationship provided in Figure 7b in fact describes how often we expect significant BV vertical heterogeneities in the epilimnion as a function of easily measurable local meteorological and temperature parameters describing the turbulent regime in the diurnal surface layer.

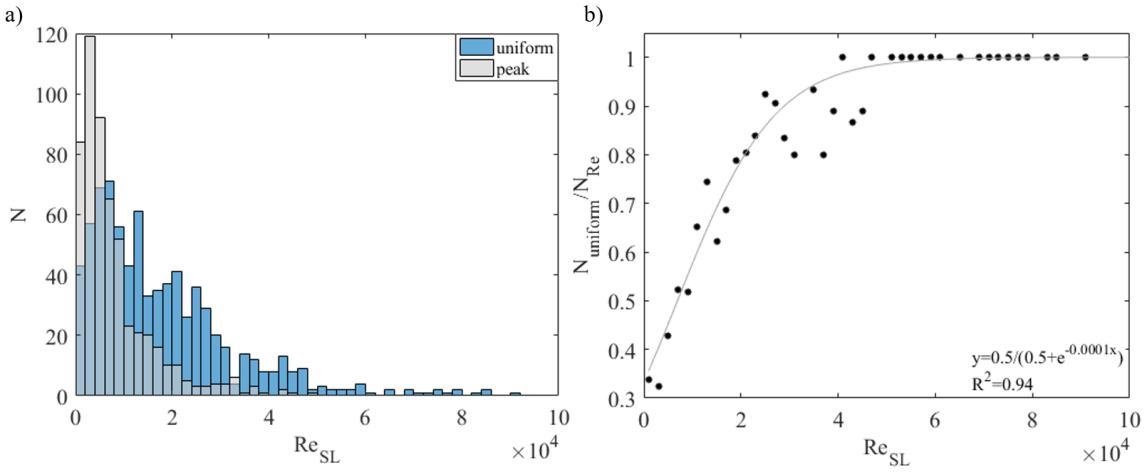

Figure 4.7. a) Frequency of peak (grey) and uniform (blue) BV distributions as a function of Re_{SL}, with bin size of 2000. b) Ratio of uniform distributions to total number of profiles as a function of Re_{SL}. These data represent all profiles for both lakes.

Microcystin and cyanobacteria biovolume vertical stratification

This section demonstrates the applicability of quantifying BV vertical heterogeneity to accurately predict Microcystin (MC) vertical distribution. BV and MC profiles corresponding to selected sampling dates and depths from the epilimnion to the hypolimnion are plotted in Figure 4.8. For all dates, a uniform BV distribution was observed in the surface layer, decaying with a steep gradient in proximity of the thermocline z_T. For both lakes, similar patterns in the distribution of BV and MC were observed. However, Madison Lake exhibits low MC concentrations that are close to the detection limit and are therefore more noisy profiles. The vertical Microcystin distributions extracted from the water samples qualitatively agree with the BV profiles for all the monitored days: MC is fairly homogeneous in the surface mixed layer and negligible below the thermocline, which is then used to normalize the depth (Figure 4.9).

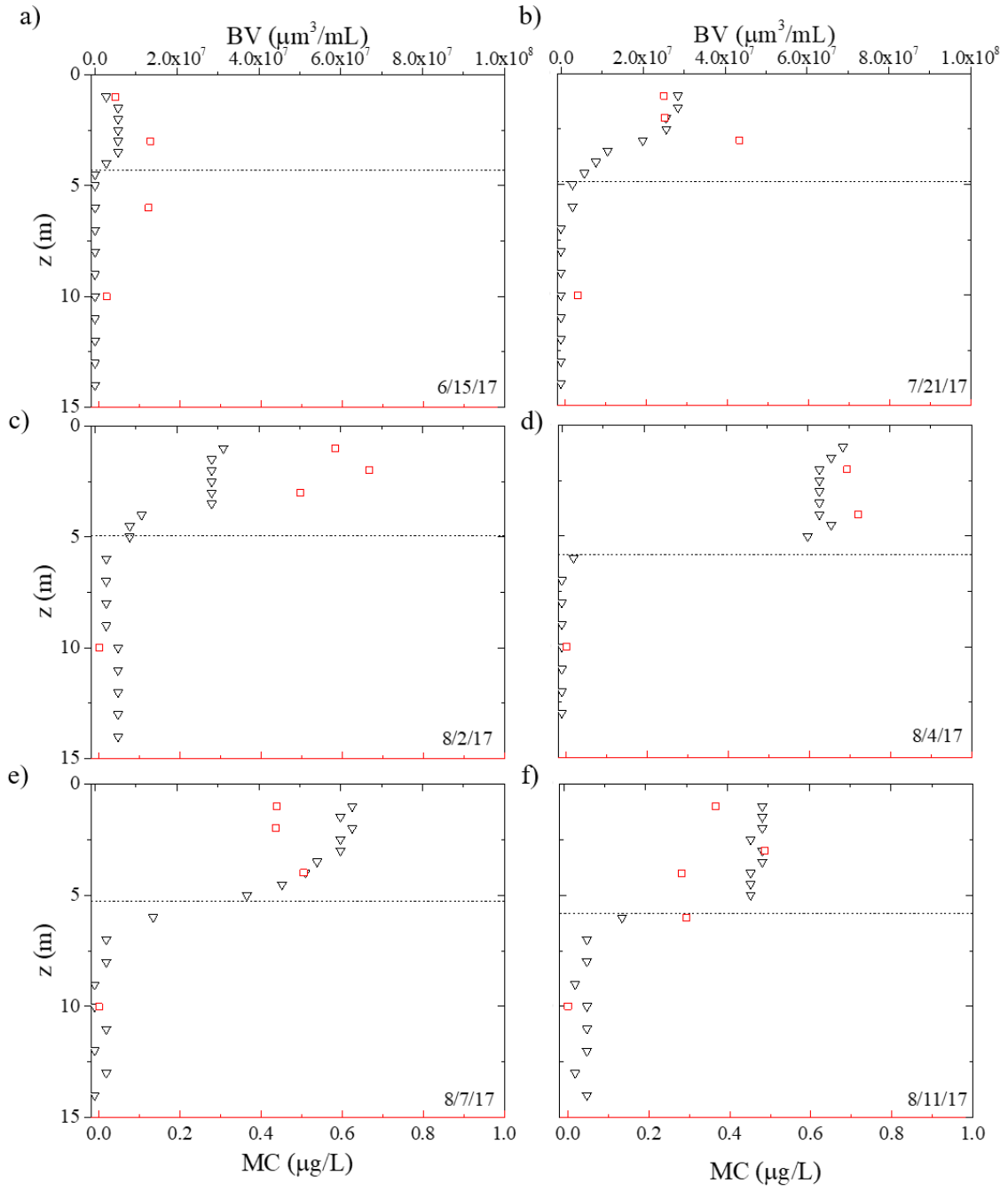

Figure 4.8: Depth profiles of BV (inverted triangle symbol) and the corresponding profiles of MC (square symbol) in South Center Lake. Each MC data point is an average of duplicate samples. The dashed line represents the thermocline depth.

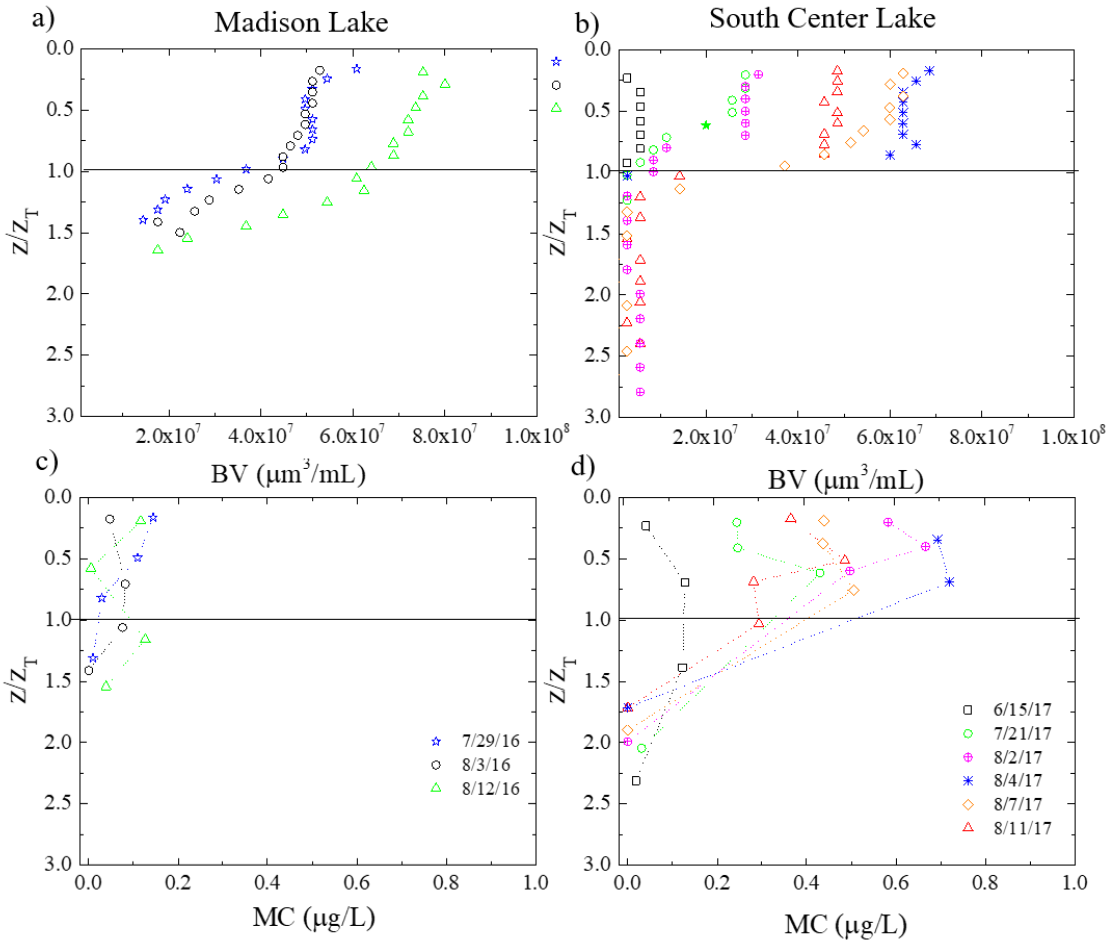

Figure 4.9: Vertical BV and MC profiles normalized by the thermocline depth z_T from samples throughout the season in Madison Lake (a,c) and South Center Lake (b, d). . Each MC data point is an average of duplicate samples. The horizontal line represents the thermocline depth.

Based on the above observations, we explore the overall relationship between MC and BV measured from the discrete samples (Figure 4.10). A linear correlation between MC and BV emerged from both South Center Lake and Madison Lake data. The data encompassed a wide range of depths, atmospheric conditions, BV and MC concentrations,

and composition of cyanobacteria. The correlation, quantified over the entire measuring season, was statistically more robust in South Center Lake (R^2=0.84) in comparison to Madison Lake (R^2=0.31).

More interestingly, temporal variability in the ratio of average MC in the epilimnion, to average BV in the epilimnion (MC_{ep} /BV_{ep}) were observed consistently in the two seasons (Figure 4.11). In both lakes, the maximum MC_{ep} /BV_{ep} preceded the maximum BV in the epilimnion (Figure 4.11ab). This trend was observed over a similar time span (from July 14th to August 11th) in the two lakes, despite the different years and different environmental conditions. In South Center Lake the maximum ratio occurs at the beginning of the BV_{ep} growth (Figure 4.11b). Note that in Madison Lake the first MC sample was taken on July 14, which did not allow to cover the same seasonal MC_{ep} /BV_{ep} evolution as compared to South Center Lake. Based on the two lakes data, it is likely that we missed the Microcystin peak along with the onset of BV_{ep} growth.

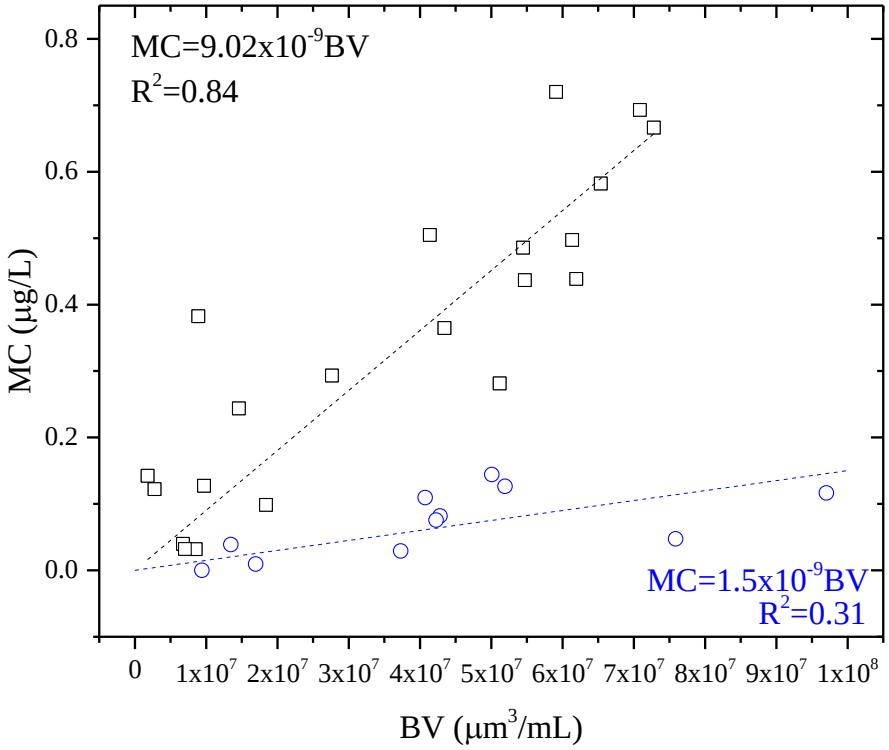

Figure 4.10: Concentration of MC versus BV in South Center Lake (square symbol) and Madison Lake (circle symbol). The data points represent the average of replicate of MC.

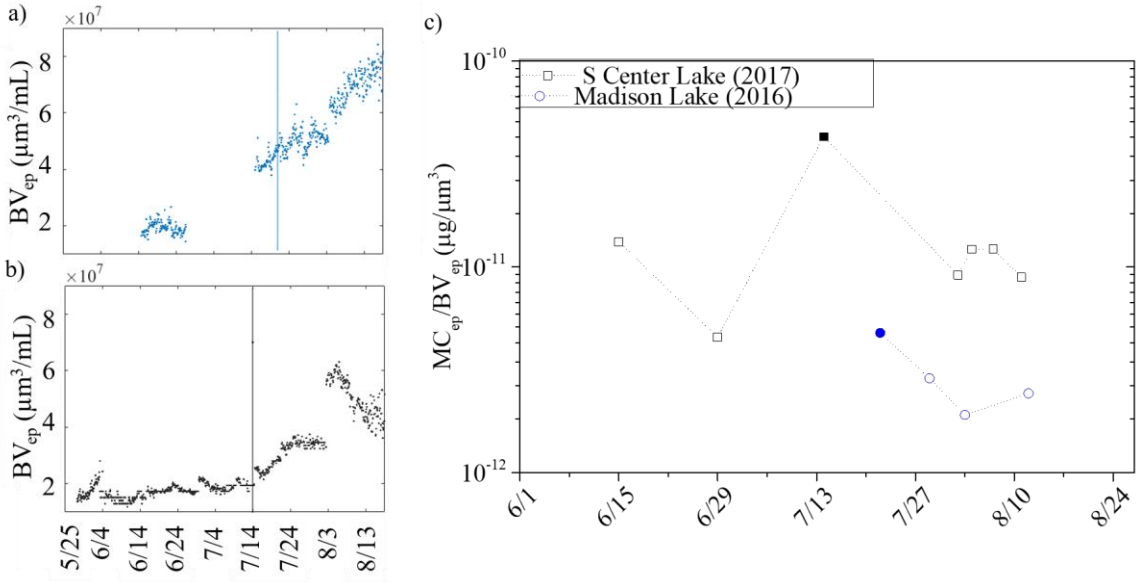

Figure 4.11:Average biovolume in the epilimnion, BV_{ep} , for a) Madison Lake and b) South Center Lake. c) The time series of MC_{ep}/BV_{ep} for Madison lake (square) and South Center lake (circle). The maxima MC_{ep}/BV_{ep} are the filled symbols in c) and correspond to the dates marked by the vertical lines in panels a-b).

Discussion

The objective of our study was to explore possible relationships among distributions of cyanobacteria biovolume (BV), microcystin concentrations (MC), lake physical parameters, and meteorological conditions in two eutrophic stratified lakes. While Chapter 3 showed that cyanobacteria BV is significant only above the thermocline during stratification where cyanobacteria are exposed to high phosphate, temperature and light, there is still further vertical variability to explain within this region. We distinguish two distributions 1) uniformly distributed BV in the diurnal surface mixed layer and 2) local maxima of the BV profile in the epilimnion. These different distributions have been shown

to depend on physical lake parameters, describing the lake thermal structure and the wind speed forcing, which control mixing in the surface layer. In particular, under large shear velocity u_* the water in the epilimnion is mixed to a homogeneous temperature which extends deeper in the water column, increasing the surface mixed layer depth h_{SL}. Inspired by the term $u_* h_{SL}$ consistently increasing with surface mixing and with uniform BV distribution, we defined a Reynolds number $Re_{SL} = u_* h_{SL}/ \nu_{SL}$ for wind-induced turbulence in the diurnal surface mixed layer. Uniform BV distributions are observed under highly dynamic lake conditions, characterized by large values of u_*, h_{SL}, and Re_{SL}, demonstrating that uniform BV distributions are governed by mechanical mixing, while the cyanobacteria behaved more like passive tracers. Conversely, peak BV distributions correspond to more calm conditions, lower values of u_*, h_{SL}, and Re_{SL}, implying that cyanobacteria may be able to actively choose their location in the water column, forming high BV layers both near the surface or at the thermocline, and obeying their physiological drivers. Wang et al. (2016) determined that the greatest influence of wind to cyanobacteria blooms is by direct transport throughout the water column and less by indirect nutrient transport from shear of the sediments or direct disturbance or shear on individual cells. This direct transport impact was based on the critical wind speed of >2-3 m/s to disperse *Microcystis* surface blooms in the water column [109]. Additionally, the vertical distribution of cyanobacteria is particularly sensitive to wind as compared to other phytoplankton with vertical heterogeneity of *Microcystis* being highly correlated with strong winds in Lake Taihu [74]. To incorporate both thermal structure and wind, we developed a relationship in polymictic and dimictic lakes that may predict the probability of the BV distribution type as a function

of Re_{SL}. For a given Re_{SL} we know the probability of a single point sample being representative of the BV in SL i.e. a uniform distribution. Conversely, if there is a peak distribution a single point sample may not be representative of the max BV in the water column, as peaks can contain BV significantly higher than the depth-averaged when BV_{max} was shown to be up to 2 times the BV_{ave} (Figure 4.5). Understanding the BV distribution above the thermocline is important in determining, how representative a single point sample is, based on a ratio of easily measurable local meteorological and temperature parameters.

The distribution of MC is consistent with the distribution of BV during the stratified period in each lake. BV and MC were concentrated above the thermocline and are highly correlated over different depths, dates, and local physical conditions. Graham and Jones [107] also showed uniform distributions of MC and cyanobacteria biomass concentrated above the thermocline and declining in deeper layers. Likewise, there was a high correlations between local cyanobacteria BV and microcystin concentrations, [107,110]. This said, the total MC concentrations were lower in Madison Lake, likely due to the difference in cyanobacterial composition. There was much lower *Microcystis* sp biovolume contrbution in Madison Lake, while the total BV was dominated by *Planktothrix.* Although it is a microcystin producing genera, *Planktothrix* biovolume has been shown to not be correlated with MC [110]. Additionally, high Anatoxin concentrations in Madison Lake were measured by MPCA during our sampling period (though in different locations in the lake). Anatoxin is not produced by *Microcystis* but by *Dolichospermum* along with other cyanobacteria not dominant here. Chia et al. [111] showed that exposure to anatoxin

reduced the MC production of *Microcystis*. A nationwide study of 1161 lakes found that it was very rare for there to be co-production of cyanotoxins in cyanobacteria blooms [112].

The correlation between MC and BV concentrations and distributions allows for the use of the model describing BV vertical heterogeneities discussed in Chapter 3 to predict MC vertical distributions. This work extends that model by describing BV distributions specifically above the thermocline. Our modeling framework allows us to use easily measurable, local, thermal and meteorological conditions in the water column, as a predictor for BV and MC vertical distributions, and thus as a guideline for water sampling strategies.

The temporal variations of cyanobacteria biovolume in the epilimnion (BV_{ep}) were appreciable during the monitoring period. We observed that the peak of MC_{ep} /BV_{ep} occurred before the maximum BV_{ep}, with MC_{ep} /BV_{ep} decreasing as the high BV_{ep} persisted. In South Center Lake, this peak coincided with the onset of significant BV_{ep} increase. The MC concentrations were similar prior to the maximum BV concentrations as after the onset of high BV concentrations. Overall, it was notable that the trends of MC_{ep} /BV_{ep} between Madison Lake and South Center Lake were not only identical in shape but occurred on the same dates one year apart and under two different stratification conditions. This trend of MC_{ep} /BV_{ep} can also provide insight about the relationships between physiological conditions and metabolic activities of cyanobacteria in lakes (like nitrogen regulation, allopathy and the defense against grazing [14,106]. Long et al. [113] showed a correlation between *Microcystis* growth rate and microcystin production in N-limited cultures. Similarly, Orr and Jones (1998) showed that toxin production was associated with

periods of cell concentration increases not in the stationary or death phase in N-limited cultures. These results are relevant to both lakes, in fact exhibiting low inorganic nitrogen. These observations are notable because the maximum MC_{ep} /BV_{ep} occurred in time periods just before the period of precipitous BV growth in the epilimnion, which is when the physical signs of harmful algal blooms are less recognizable to the public and to biomass monitoring systems. Understanding and confirming the temporal lag between BV growth and MC peak concentration remains critical to prevent health hazards.

Conclusion

A high frequency, high resolution, long-term monitoring station was deployed during summer months, in a eutrophic, polymictic Minnesota lake in 2016 and a eutrophic, dimictic Minnesota lake in 2017. Although the two lakes exhibited different stratification conditions, nutrient concentrations, and cyanobacteria compositions; similar trends in both lakes unveiled functional relationship between a) wind-induced hydrodynamic mixing, b) current thermal stratification, c) cyanobacteria biovolume, BV, vertical distribution, and d) Microcystin, MC, distribution. This resulted in the production of a framework that can predict total water column heterogeneity and distribution above the thermocline of both cyanobacterial BV and MC.

The temporal and vertical heterogeneities of nitrate and phosphate do not describe the variability in BV or MC, both showing cyanobacteria rich layers above the thermocline. The BV distribution was observed to be further influenced by wind-induced mixing in the epiliminion, frequently able to homogenize the diurnal surface layer layer (SL) in terms of water temperature, biovolume and Microcystin. A quantitative relationship was developed

to determine the probability of observing a uniform distribution in the SL as a function of the ratio of easily measurable local environmental parameters. Uniform BV distributions were associated with SL Reynolds number Re_{SL}>50,000 values consistent with greater mixing in the diurnal surface mixed layer. At lower values, cyanobacteria are inferred to be able to move along the water column, driven by physiology and not passively advected. This understanding is important for directing sampling efforts because it narrows the scope of BV heterogeneity above the thermocline and suggests a more (or less) detailed vertical sampling protocol to capture (or neglect) potential peaks and compute representative averages at minimal cost. This is of utmost importance because BV and MC distributions in each layer of the water column were reasonably correlated with each other. Such correlation suggest that high MC occurs with high BV, which is not surprising given the combination of both intra- and extra- cellular Microcystin. Particularly interesting is the MC production per unit of biovolume, quantified by the term, MC_{ep} /BV_{ep} (averaged in the epiliminion). Its temporal variations were monitored in both lakes and showed a maximum value occurring before the maximum BV, corresponding to the onset of BV growth (especially evident from South Center Lake data). This observation is notable because the maximum MC_{ep} /BV_{ep} occurs before substantial BV accumulation, when the physical signs of HABs are less recognizable to the public and surface monitoring efforts. The results presented here shed new light on the complexity of BV and microcystin distributions and have important implications for future management and monitoring strategies.

Chapter 5

Conclusions and Recommendations

Conclusions

This dissertation increases the understanding of abiotic environmental conditions, i.e. different mixing scales, on the physiology and distribution of cyanobacteria in nutrient invariant eutrophic systems using field and laboratory studies.

Chapter 2 outlined the effect of variable small-scale turbulence conditions on cultured *Microcystis* in controlled laboratory experiments. In this experimental setup, we successfully mimicked natural conditions in controlled lab setting. Although there was no significant change in growth kinetics, during either long and short term studies, small-scale turbulence was observed to affect metabolic photosynthesis of *Microcystis* by inducing a reduction in net oxygen production and uptake, and a moderation of the carbon uptake. These effects were observed in different growth phases of the *Microcystis*, even if the actual population growth rate estimated from the cell concentration was only slightly

modulated by turbulence (−5% and 11% for Re_λ = 33 and Re_λ = 15, respectively, as compared to stagnant conditions). Therefore, small-scale turbulence influences the photosynthetic metabolism of *Microcystis,* which is not manifested in population growth. This chapter highlighted the importance of physical drivers even in simplified laboratory conditions. However, cyanobacteria live in the context of many different mixing scales with variable temperature and light conditions. Thus the next chapters explore large-scale fluid motion and environmental drivers in lake systems affecting cyanobacteria distributions.

Chapters 3 and 4 use the custom, newly fabricated, high resolution, high frequency profiling water quality monitoring station. Chapter 3 introduced the research station, which has been deployed in a polymictic eutrophic and a dimictic eutrophic lake. Cyanobacteria blooms in eutrophic lakes were observed to be driven by prolonged warm surface water temperatures and strong thermal stratification stability. From the polymictic lake in the initial study, BV persisted in the surface layer during strong stratification conditions but was distributed homogenously throughout the water column when the stratification weakened. From these BV profiles, a relationship was developed between BV heterogeneity in the water column vs St and T_s that is verified in a dimictic eutrophic lake the following year. In fact, although this study was conducted during a different summer, in a different lake with different a) nutrient and stratification conditions, b) cyanobacteria conditions and c) meteorological events including an extreme wind event; it still describes BV heterogeneity using StC_pT_s. This relationship is relevant to sampling protocols of cyanobacteria blooms in lakes (i.e. remote sensing, photic zone integrated sampling and

fixed point samples) as it informs if the sample depth is representative of the entire water column; allowing for the extrapolation of single point monitoring. In Madison Lake, the polymictic lake, the depth of maximum cyanobacteria biomass is above the thermocline depth and in the photic zone, with sub-surface maxima localized at depths where photosynthetically active radiation is approximately 10 $\mu E/m^2s$. Under hyper/eutrophic nutrients invariant conditions, as investigated in this work, predictive tools should include the easily measurable local meteorological and physical lake conditions as drivers of BV temporal and vertical heterogeneities.

Chapter 4 uses the same research station to extend the discussion of chapter 3 by quantifying and describing BV distribution above the thermocline and MC distribution in the water column. Although the two lakes exhibited different stratification conditions, nutrient concentrations, and cyanobacteria compositions; similar trends in both lakes unveiled functional relationship between a) wind-induced hydrodynamic mixing, b) current thermal stratification, c) cyanobacteria biovolume, BV, vertical distribution, and d) Microcystin, MC, distribution. A quantitative relationship was developed to determine the probability of observing a uniform distribution in the SL as a function of the ratio of easily measurable local environmental parameters. Uniform BV distributions were associated with SL Reynolds number Re_{SL}>50,000 values consistent with greater mixing in the diurnal surface mixed layer. This understanding is important for directing sampling efforts because it narrows the scope of BV heterogeneity above the thermocline, and suggests a more (or less) detailed vertical sampling protocol to capture (or neglect) potential peaks and compute representative averages at minimal cost. This is of utmost importance because

BV and MC distributions in each layer of the water column were reasonably correlated with each other. This correlation between MC and BV distributions allows for the use of the relationships describing BV to also describe MC distributions using easily measurable physical lake parameters. Finally, MC_{ep} /BV_{ep} variations are observed in both polymictic and dimictic lakes. The observed maximum occurred before the maximum BV and specifically during the onset BV growth (especially evident in South Center Lake). This observation is notable because the maximum MC_{ep} /BV_{ep} occurs before substantial BV accumulation, when the physical signs of HABs are less recognizable to the public and surface monitoring efforts. The results presented here shed new light on the complexity of BV and microcystin distributions and have important implications for future management and monitoring strategies.

Recommendations

HAB are gaining attention from scientists, local water resource managers, and federal agencies. This new attention is driving new funding sources for more monitoring efforts and advances in monitoring technology to resolve HAB dynamics to manage risks. However, strategies for monitoring efforts can be disparate and non-standard in lakes among research studies ([70,71,73,78–81]), either because of specific locations of interest, conventional sampling protocols, or individual monitoring staff choices. However conclusion about abundance and distribution are still made. It is the mission of this thesis to enhance the understanding of drivers for HAB in lakes with histories of eutrophic invariant nutrient conditions and better direct sampling efforts for HAB monitoring. From this body of work and the conclusions outlined above, it is important to understand physical

mixing, temperature and the combination of conditions in order to fully resolve HAB dynamics in lakes and to direct future sampling efforts. This thesis showed that easily measurable lake parameters can be used to predict overall BV vertical heterogeneity by measuring thermal stability in the entire water column. From these results, we showed that cyanobacteria distribution can be driven by St and T_s for both strongly stratified and weakly stratified lakes. When the lake is weakly stratified the BV is uniformly mixed, conversely when the lake is stratified the cyanobacteria are accumulating above the thermocline. Thus, when deciding on sampling locations, you must first understand the stratification conditions 1) If the BV is uniformly distributed, any sample in the water column will be representative, 2) if it is strongly stratified the BV is above the thermocline and the maximum BV therein can be up to 2.2 times the BV depth average. In this second case, we must understand how the BV is distributed above the thermocline, either in local maxima or if the BV is uniformly distribution in the surface mixed layer. In order to do this, you can use local meteorological and temperature conditions more specific to the mixing layer. When Re_{SL} are high, i.e. >50,000, the BV is uniform above the thermocline and thus fewer samples are necessary. However, when mixing conditions are lower i.e. Re_{SL} =7500, local cyanobacteria maxima form and thus more samples must be taken to capture possible maxima peaks. These results do not predict the depth of BV peaks for both lakes because there is an evolution of different types of cyanobacteria that we observed. These different genera have different eco-physiological traits that determine ideal growth conditions, thus this prediction is composition dependent. The body of work presented in this thesis describes vertical heterogeneity of bulk cyanobacteria based on the traits they all share,

which is buoyancy regulation. These trends transcend BV concentration magnitude as they are all relative to BV distribution therefore we were able to describe both South Center and Madison Lake over the season even when the BV was low during May and high in mid August. As shown in Chapter 4, BV vertical distribution is well correlated with MC distribution and misguided sampling may under represent microcystin concentrations, which has implications for public safety.

Bibliography

[1] W.W. Carmichael, The toxins of cyanobacteria, Sci. Am. 270 (1994) 78–86.

[2] R.W. Zurawell, H. Chen, J.M. Burke, E.E. Prepas, Hepatotoxic Cyanobacteria: A Review of the Biological Importance of Microcystins in Freshwater Environments, Journal of Toxicology and Environmental Health, Part B. 8 (2005) 1–37. doi:10.1080/10937400590889412.

[3] G.A. Codd, L.F. Morrison, J.S. Metcalf, Cyanobacterial toxins: risk management for health protection, Toxicology and Applied Pharmacology. 203 (2005) 264–272. doi:10.1016/j.taap.2004.02.016.

[4] E. Mantzouki, P.M. Visser, M. Bormans, B.W. Ibelings, Understanding the key ecological traits of cyanobacteria as a basis for their management and control in changing lakes, Aquatic Ecology. 50 (2016) 333–350. doi:10.1007/s10452-015-9526-3.

[5] C.S. Reynolds, R.L. Oliver, A.E. Walsby, Cyanobacterial dominance: The role of buoyancy regulation in dynamic lake environments, New Zealand Journal of Marine and Freshwater Research. 21 (1987) 379–390. doi:10.1080/00288330.1987.9516234.

[6] C.M. Hodges, S.A. Wood, J. Puddick, C.G. McBride, D.P. Hamilton, Sensor manufacturer, temperature, and cyanobacteria morphology affect phycocyanin fluorescence measurements, Environmental Science and Pollution Research. 25 (2018) 1079–1088. doi:10.1007/s11356-017-0473-5.

[7] T. Kutser, L. Metsamaa, A.G. Dekker, Influence of the vertical distribution of cyanobacteria in the water column on the remote sensing signal, Estuarine, Coastal and Shelf Science. 78 (2008) 649–654. doi:10.1016/j.ecss.2008.02.024.

[8] Y. Song, B. Qiu, The CO_2 -concentrating mechanism in the bloom-forming cyanobacterium *Microcystis aeruginosa* (Cyanophyceae) and effects of UVB

radiation on its operation [1], Journal of Phycology. 43 (2007) 957–964. doi:10.1111/j.1529-8817.2007.00391.x.
[9] A. Wilkinson, M. Hondzo, M. Guala, Effect of Small-Scale Turbulence on the Growth and Metabolism of <i>Microcystis aeruginosa</i>, Advances in Microbiology. 06 (2016) 351–367. doi:10.4236/aim.2016.65034.
[10] J.A. Elliott, Is the future blue-green? A review of the current model predictions of how climate change could affect pelagic freshwater cyanobacteria, Water Research. 46 (2012) 1364–1371. doi:10.1016/j.watres.2011.12.018.
[11] H.W. Paerl, J. Huisman, Climate change: a catalyst for global expansion of harmful cyanobacterial blooms, Environmental Microbiology Reports. 1 (2009) 27–37. doi:10.1111/j.1758-2229.2008.00004.x.
[12] H.W. Paerl, Nuisance phytoplankton blooms in coastal, estuarine, and inland waters1: Nuisance blooms, Limnology and Oceanography. 33 (1988) 823–843. doi:10.4319/lo.1988.33.4part2.0823.
[13] A. Holland, S. Kinnear, Interpreting the Possible Ecological Role(s) of Cyanotoxins: Compounds for Competitive Advantage and/or Physiological Aide?, Marine Drugs. 11 (2013) 2239–2258. doi:10.3390/md11072239.
[14] P.T. Orr, G.J. Jones, Relationship between microcystin production and cell division rates in nitrogen-limited Microcystis aeruginosa cultures, Limnology and Oceanography. 43 (1998) 1604–1614. doi:10.4319/lo.1998.43.7.1604.
[15] L. Song, W. Chen, L. Peng, N. Wan, N. Gan, X. Zhang, Distribution and bioaccumulation of microcystins in water columns: A systematic investigation into the environmental fate and the risks associated with microcystins in Meiliang Bay, Lake Taihu, Water Research. 41 (2007) 2853–2864. doi:10.1016/j.watres.2007.02.013.
[16] P.M. Visser, B.W. Ibelings, M. Bormans, J. Huisman, Artificial mixing to control cyanobacterial blooms: a review, Aquatic Ecology. (2015). doi:10.1007/s10452-015-9537-0.
[17] C. Wagner, R. Adrian, Cyanobacteria dominance: Quantifying the effects of climate change, Limnology and Oceanography. 54 (2009) 2460–2468. doi:10.4319/lo.2009.54.6_part_2.2460.
[18] T. Wynne, R. Stumpf, Spatial and Temporal Patterns in the Seasonal Distribution of Toxic Cyanobacteria in Western Lake Erie from 2002–2014, Toxins. 7 (2015) 1649–1663. doi:10.3390/toxins7051649.
[19] M. Lindon, S. Heiskary, Blue-green algal toxin (microcystin) levels in Minnesota lakes, Lake and Reservoir Management. 25 (2009) 240–252. doi:10.1080/07438140903032424.
[20] H.W. Paerl, W.S. Gardner, K.E. Havens, A.R. Joyner, M.J. McCarthy, S.E. Newell, B. Qin, J.T. Scott, Mitigating cyanobacterial harmful algal blooms in aquatic ecosystems impacted by climate change and anthropogenic nutrients, Harmful Algae. 54 (2016) 213–222. doi:10.1016/j.hal.2015.09.009.

[21] M.H. Dehghani, Removal of cyanobacterial and algal cells from water by ultrasonic waves — A review, Journal of Molecular Liquids. 222 (2016) 1109–1114. doi:10.1016/j.molliq.2016.08.010.
[22] H.C.P. Matthijs, P.M. Visser, B. Reeze, J. Meeuse, P.C. Slot, G. Wijn, R. Talens, J. Huisman, Selective suppression of harmful cyanobacteria in an entire lake with hydrogen peroxide, Water Research. 46 (2012) 1460–1472. doi:10.1016/j.watres.2011.11.016.
[23] I. van Gremberghe, F. Leliaert, J. Mergeay, P. Vanormelingen, K.V. der Gucht, A.-E. Debeer, G. Lacerot, L. De Meester, W. Vyverman, Lack of Phylogeographic Structure in the Freshwater Cyanobacterium Microcystis aeruginosa Suggests Global Dispersal, PLoS ONE. 6 (2011) e19561. doi:10.1371/journal.pone.0019561.
[24] C.C. Carey, B.W. Ibelings, E.P. Hoffmann, D.P. Hamilton, J.D. Brookes, Eco-physiological adaptations that favour freshwater cyanobacteria in a changing climate, Water Research. 46 (2012) 1394–1407. doi:10.1016/j.watres.2011.12.016.
[25] H.W. Paerl, R.S. Fulton, P.H. Moisander, J. Dyble, Harmful freshwater algal blooms, with an emphasis on cyanobacteria, The Scientific World Journal. 1 (2001) 76–113.
[26] H.W. Paerl, T.G. Otten, Harmful Cyanobacterial Blooms: Causes, Consequences, and Controls, Microbial Ecology. 65 (2013) 995–1010. doi:10.1007/s00248-012-0159-y.
[27] World Health Organization, Guidelines for water quality, Vol.1, 3rd edition incorporating 1st and 2nd addenda., (2008).
[28] S. Jahnichen, T. Ihle, T. Petzoldt, J. Benndorf, Impact of Inorganic Carbon Availability on Microcystin Production by Microcystis aeruginosa PCC 7806, Applied and Environmental Microbiology. 73 (2007) 6994–7002. doi:10.1128/AEM.01253-07.
[29] D.P. Singh, M.B. Tyagi, A. Kumar, J.K. Thakur, A. Kumar, Antialgal activity of a hepatotoxin-producing cyanobacterium, Microcystis aeruginosa, World Journal of Microbiology and Biotechnology. 17 (2001) 15–22.
[30] N. Gan, Y. Xiao, L. Zhu, Z. Wu, J. Liu, C. Hu, L. Song, The role of microcystins in maintaining colonies of bloom-forming Microcystis spp.: Microcystis colony maintenance by microcystins, Environmental Microbiology. 14 (2012) 730–742. doi:10.1111/j.1462-2920.2011.02624.x.
[31] Z. Wu, L. Song, R. Li, Different tolerances and responses to low temperature and darkness between waterbloom forming cyanobacterium Microcystis and a green alga Scenedesmus, Hydrobiologia. 596 (2008) 47–55. doi:10.1007/s10750-007-9056-7.
[32] Y. Yamamoto, H. Nakahara, Competitive dominance of the cyanobacterium Microcystis aeruginosa in nutrient-rich culture conditions with special reference to dissolved inorganic carbon uptake, Phycological Research. 53 (2005) 201–208. doi:10.1111/j.1440-183.2005.00387.x.
[33] M. Lürling, I. Roessink, On the way to cyanobacterial blooms: Impact of the herbicide metribuzin on the competition between a green alga (Scenedesmus) and a cyanobacterium (Microcystis), Chemosphere. 65 (2006) 618–626. doi:10.1016/j.chemosphere.2006.01.073.

[34] M. Zhang, F. Kong, X. Shi, P. Xing, X. Tan, Differences in Responses to Darkness between *Microcystis aeruginosa* and *Chlorella pyrenoidosa*, Journal of Freshwater Ecology. 22 (2007) 93–99. doi:10.1080/02705060.2007.9664149.
[35] M. Li, P. Nkrumah, M. Xiao, Biochemical composition of Microcystis aeruginosa related to specific growth rate: insight into the effects of abiotic factors, Inland Waters. 4 (2014) 357–362. doi:10.5268/IW-4.4.710.
[36] S.M.E. Daley, A.D. Kappell, M.J. Carrick, R.L. Burnap, Regulation of the Cyanobacterial CO2-Concentrating Mechanism Involves Internal Sensing of NADP+ and α-Ketogutarate Levels by Transcription Factor CcmR, PLoS ONE. 7 (2012) e41286. doi:10.1371/journal.pone.0041286.
[37] G. Sandrini, H.C.P. Matthijs, J.M.H. Verspagen, G. Muyzer, J. Huisman, Genetic diversity of inorganic carbon uptake systems causes variation in CO2 response of the cyanobacterium Microcystis, The ISME Journal. 8 (2014) 589–600. doi:10.1038/ismej.2013.179.
[38] J.-C. Kehr, E. Dittmann, Biosynthesis and Function of Extracellular Glycans in Cyanobacteria, Life. 5 (2015) 164–180. doi:10.3390/life5010164.
[39] Z. Yang, L. Geng, W. Wang, J. Zhang, Combined effects of temperature, light intensity, and nitrogen concentration on the growth and polysaccharide content of Microcystis aeruginosa in batch culture, Biochemical Systematics and Ecology. 41 (2012) 130–135. doi:10.1016/j.bse.2011.12.015.
[40] R.H. Regel, J.D. Brookes, G.G. Ganf, R.W. Griffiths, The influence of experimentally generated turbulence on the Mash01 unicellular Microcystis aeruginosa strain, Hydrobiologia. 517 (2004) 107–120.
[41] M. Hondzo, T.A. Warnaars, Coupled Effects of Small-Scale Turbulence and Phytoplankton Biomass in a Small Stratified Lake, Journal of Environmental Engineering. 134 (2008) 954–960. doi:10.1061/(ASCE)0733-9372(2008)134:12(954).
[42] A. Chengala, M. Hondzo, D.G. Mashek, Fluid motion mediates biochemical composition and physiological aspects in the green alga Dunaliella primolecta Butcher, Limnology & Oceanography: Fluids & Environments. 3 (2013) 74–88. doi:10.1215/21573689-2326826.
[43] P.R. Kenis, J.W. Hoyt, FRICTION REDUCTION BY ALGAL AND BACTERIAL POLYMERS, 1971.
[44] I.R. Jenkinson, J. Sun, Drag increase and drag reduction found in phytoplankton and bacterial cultures in laminar flow: Are cell surfaces and EPS producing rheological thickening and a Lotus-leaf Effect?, Deep Sea Research Part II: Topical Studies in Oceanography. 101 (2014) 216–230.
[45] B. Qiu, K. Gao, EFFECTS OF CO2 ENRICHMENT ON THE BLOOM-FORMING CYANOBACTERIUM MICROCYSTIS AERUGINOSA (CYANOPHYCEAE): PHYSIOLOGICAL RESPONSES AND RELATIONSHIPS WITH THE AVAILABILITY OF DISSOLVED INORGANIC CARBON1, Journal of Phycology. 38 (2002) 721–729. doi:10.1046/j.1529-8817.2002.01180.x.
[46] J. Jiménez, Ocean Turbulence at millimeter scales, Scientia Marina. 61 (1997) 47–56.

[47] M. Guala, A. Liberzon, A. Tsinober, W. Kinzelbach, An experimental investigation on Lagrangian correlations of small-scale turbulence at low Reynolds number, Journal of Fluid Mechanics. 574 (2007) 405. doi:10.1017/S0022112006004204.
[48] P. Doron, L. Bertuccioli, J. Katz, T.R. Osborn, Turbulence Characteristics and Dissipation Estimates in the Coastal Ocean Bottom Boundary Layer from PIV Data, Journal of Physical Oceanography. 31 (2001) 2108–2134. doi:10.1175/1520-0485(2001)031<2108:TCADEI>2.0.CO;2.
[49] B.L. O'Connor, M. Hondzo, Dissolved oxygen transfer to sediments by sweep and eject motions in aquatic environments, Limnology and Oceanography. 53 (2008) 566–578.
[50] D. Dvoretsky, S. Dvoretsky, E. Peshkova, M. Temnov, Optimization of the process of cultivation of microalgae chlorella vulgaris biomass with high lipid content for biofuel production, Chemical Engineering Transactions. (2015005) 361–366. doi:10.3303/CET1543061.
[51] S.E. Kingsland, Modeling nature, University of Chicago Press, 1995.
[52] Murray R. Badger, Kristin Palmqvist, J.-W. Yu, Measurement of CO2 and HCO3− fluxes in cyanobacteria and microalgae during steady-state photosynthesis, Physiologia Plantarum. 90 (1994) 529–536.
[53] P.L. Brezonik, W.A. Arnold, Water chemistry: an introduction to the chemistry of natural and engineered aquatic systems, Oxford University Press, New York, 2011.
[54] M.A. Crayton, Toxic cyanobacteria blooms: a field/laboratory guide, Olympia: Office of Environmental Health Assessments, Washington State Department of Health. (1993).
[55] S.G. Saddoughi, S.V. Veeravalli, Local isotropy in turbulent boundary layers at high Reynolds number, Journal of Fluid Mechanics. 268 (1994) 333. doi:10.1017/S0022112094001370.
[56] W.H. Thomas, C.H. Gibson, Effects of small-scale turbulence on microalgae, Journal of Applied Phycology. 2 (1990) 71–77.
[57] S. Fraisse, M. Bormans, Y. Lagadeuc, Turbulence effects on phytoplankton morphofunctional traits selection: Functional traits selected by turbulence, Limnology and Oceanography. 60 (2015) 872–884. doi:10.1002/lno.10066.
[58] L. Chen, F. Mao, G.C. Kirumba, C. Jiang, M. Manefield, Y. He, Changes in metabolites, antioxidant system, and gene expression in Microcystis aeruginosa under sodium chloride stress, Ecotoxicology and Environmental Safety. 122 (2015) 126–135. doi:10.1016/j.ecoenv.2015.07.011.
[59] K. Gasljevic, K. Hall, D. Chapman, E.F. Matthys, Drag-reducing polysaccharides from marine microalgae: species productivity and drag reduction effectiveness, Journal of Applied Phycology. 20 (2008) 299–310. doi:10.1007/s10811-007-9250-z.
[60] H. Xu, H. Cai, G. Yu, H. Jiang, Insights into extracellular polymeric substances of cyanobacterium Microcystis aeruginosa using fractionation procedure and parallel factor analysis, Water Research. 47 (2013) 2005–2014. doi:10.1016/j.watres.2013.01.019.

[61] A.M. Dolman, J. Rücker, F.R. Pick, J. Fastner, T. Rohrlack, U. Mischke, C. Wiedner, Cyanobacteria and Cyanotoxins: The Influence of Nitrogen versus Phosphorus, PLoS ONE. 7 (2012) e38757. doi:10.1371/journal.pone.0038757.
[62] M.T. Dokulil, K. Teubner, Cyanobacterial dominance in lakes, Hydrobiologia. 438 (2000) 1–12.
[63] V. Huber, C. Wagner, D. Gerten, R. Adrian, To bloom or not to bloom: contrasting responses of cyanobacteria to recent heat waves explained by critical thresholds of abiotic drivers, Oecologia. 169 (2012) 245–256. doi:10.1007/s00442-011-2186-7.
[64] O. Kerimoglu, K. Rinke, Stratification dynamics in a shallow reservoir under different hydro-meteorological scenarios and operational strategies: NONWINTER STRATIFICATION DYNAMICS, Water Resources Research. 49 (2013) 7518–7527. doi:10.1002/2013WR013520.
[65] H.W. Paerl, J. Huisman, Climate change: a catalyst for global expansion of harmful cyanobacterial blooms, Environmental Microbiology Reports. 1 (2009) 27–37. doi:10.1111/j.1758-2229.2008.00004.x.
[66] Y. Cha, S.S. Park, K. Kim, M. Byeon, C.A. Stow, Probabilistic prediction of cyanobacteria abundance in a Korean reservoir using a Bayesian Poisson model, Water Resources Research. 50 (2014) 2518–2532. doi:10.1002/2013WR014372.
[67] A.E. Walsby, C.S. Reynolds, R.L. Oliver, J. Kromkamp, M.M. Gibbs, The role of buoyancy in the distribution of *Anabaena* sp. in Lake Rotongaio, New Zealand Journal of Marine and Freshwater Research. 21 (1987) 525–526. doi:10.1080/00288330.1987.9516250.
[68] J. You, K. Mallery, J. Hong, M. Hondzo, Temperature effects on growth and buoyancy of Microcystis aeruginosa, Journal of Plankton Research. 40 (2018) 16–28. doi:10.1093/plankt/fbx059.
[69] M.-È. Garneau, T. Posch, G. Hitz, F. Pomerleau, C. Pradalier, R. Siegwart, J. Pernthaler, Short-term displacement of *Planktothrix rubescens* (cyanobacteria) in a pre-alpine lake observed using an autonomous sampling platform, Limnology and Oceanography. 58 (2013) 1892–1906. doi:10.4319/lo.2013.58.5.1892.
[70] A. Cantin, B.E. Beisner, J.M. Gunn, Y.T. Prairie, J.G. Winter, Effects of thermocline deepening on lake plankton communities, Canadian Journal of Fisheries and Aquatic Sciences. 68 (2011) 260–276. doi:10.1139/F10-138.
[71] Y. Cuypers, B. Vinçon-Leite, A. Groleau, B. Tassin, J.-F. Humbert, Impact of internal waves on the spatial distribution of Planktothrix rubescens (cyanobacteria) in an alpine lake, The ISME Journal. 5 (2011) 580–589. doi:10.1038/ismej.2010.154.
[72] A.E. Walsby, F. Schanz, Light-dependent growth rate determines changes in the population of Planktothrix rubescens over the annual cycle in Lake Zürich, Switzerland, New Phytologist. 154 (2002) 671–687. doi:10.1046/j.1469-8137.2002.00401.x.
[73] S.W. Chung, J. Imberger, M.R. Hipsey, H.S. Lee, The influence of physical and physiological processes on the spatial heterogeneity of a Microcystis bloom in a stratified reservoir, Ecological Modelling. 289 (2014) 133–149. doi:10.1016/j.ecolmodel.2014.07.010.

[74] H.-S. Cao, F.-X. Kong, L.-C. Luo, X.-L. Shi, Z. Yang, X.-F. Zhang, Y. Tao, Effects of Wind and Wind-Induced Waves on Vertical Phytoplankton Distribution and Surface Blooms of *Microcystis aeruginosa* in Lake Taihu, Journal of Freshwater Ecology. 21 (2006) 231–238. doi:10.1080/02705060.2006.9664991.
[75] X. Wu, F. Kong, Effects of Light and Wind Speed on the Vertical Distribution of *Microcystis aeruginosa* Colonies of Different Sizes during a Summer Bloom, International Review of Hydrobiology. 94 (2009) 258–266. doi:10.1002/iroh.200811141.
[76] A. Wilkinson, M. Hondzo, M. Guala, Effect of Small-Scale Turbulence on the Growth and Metabolism of <i>Microcystis aeruginosa</i>, Advances in Microbiology. 06 (2016) 351–367. doi:10.4236/aim.2016.65034.
[77] S. Missaghi, M. Hondzo, C. Sun, M. Guala, Influence of fluid motion on growth and vertical distribution of cyanobacterium Microcystis aeruginosa, Aquatic Ecology. 50 (2016) 639–652. doi:10.1007/s10452-016-9583-2.
[78] M. Bormans, P.W. Ford, L. Fabbro, G. Hancock, Onset and persistence of cyanobacterial blooms in a large impounded tropical river, Australia, Marine and Freshwater Research. 55 (2004) 1. doi:10.1071/MF03045.
[79] C.A. Klausmeier, E. Litchman, Algal games: The vertical distribution of phytoplankton in poorly mixed water columns, Limnology and Oceanography. 46 (2001) 1998–2007. doi:10.4319/lo.2001.46.8.1998.
[80] A. Pannard, M. Bormans, Y. Lagadeuc, Phytoplankton species turnover controlled by physical forcing at different time scales, Canadian Journal of Fisheries and Aquatic Sciences. 65 (2008) 47–60. doi:10.1139/f07-149.
[81] B. Simmonds, S.A. Wood, D. Özkundakci, D.P. Hamilton, Phytoplankton succession and the formation of a deep chlorophyll maximum in a hypertrophic volcanic lake, Hydrobiologia. 745 (2015) 297–312. doi:10.1007/s10750-014-2114-z.
[82] M. Lindon, R. Valley, S. Mackenthum, Sentinel Lake Assessment Report Madison Lake (07-0044) Blue Earth County, Minnesota, (2010).
[83] J.D. Wehr, R.G. Sheath, J.P. Kociolek, eds., Freshwater algae of North America: ecology and classification, Second edition, Elsevier/AP, Academic Press is an imprint of Elsevier, Amsterdam ; Boston, 2015.
[84] L. Brient, M. Lengronne, E. Bertrand, D. Rolland, A. Sipel, D. Steinmann, I. Baudin, M. Legeas, B. Le Rouzic, M. Bormans, A phycocyanin probe as a tool for monitoring cyanobacteria in freshwater bodies, J. Environ. Monit. 10 (2008) 248–255. doi:10.1039/B714238B.
[85] J.-M.E. Kasinak, B.M. Holt, M.F. Chislock, A.E. Wilson, Benchtop fluorometry of phycocyanin as a rapid approach for estimating cyanobacterial biovolume, Journal of Plankton Research. 37 (2015) 248–257. doi:10.1093/plankt/fbu096.
[86] Y. Kong, I. Lou, Y. Zhang, C.U. Lou, K.M. Mok, Using an online phycocyanin fluorescence probe for rapid monitoring of cyanobacteria in Macau freshwater reservoir, Hydrobiologia. 741 (2014) 33–49. doi:10.1007/s10750-013-1759-3.
[87] H. Hillebrand, C.-D. Dürselen, D. Kirschtel, U. Pollingher, T. Zohary, BIOVOLUME CALCULATION FOR PELAGIC AND BENTHIC MICROALGAE, Journal of Phycology. 35 (1999) 403–424. doi:10.1046/j.1529-8817.1999.3520403.x.

[88] J.D. Strickland, T.R. Parsons, A practical handbook of seawater analysis, (1972).
[89] T.R. Parsons, Y. Maita, C.M. Lalli, A manual of chemical and biological methods for seawater analysis, 1st ed, Pergamon Press, Oxford [Oxfordshire] ; New York, 1984.
[90] M. Hondzo, H.G. Stefan, Long-term lake water quality predictors, Water Research. 30 (1996) 2835–2852. doi:10.1016/0043-1354(95)00286-3.
[91] J.C. Patterson, P.F. Hamblin, J. Imberger, Classification and dynamic simulation of the vertical density structure of lakes1: Dynamic simulation of lakes, Limnology and Oceanography. 29 (1984) 845–861. doi:10.4319/lo.1984.29.4.0845.
[92] G. Flaim, E. Eccel, A. Zeileis, G. Toller, L. Cerasino, U. Obertegger, Effects of re-oligotrophication and climate change on lake thermal structure, Freshwater Biology. 61 (2016) 1802–1814. doi:10.1111/fwb.12819.
[93] S.B. Idso, On the concept of lake stability1, Limnology and Oceanography. 18 (1973) 681–683. doi:10.4319/lo.1973.18.4.0681.
[94] D.C. Rolland, S. Bourget, A. Warren, I. Laurion, W.F. Vincent, Extreme variability of cyanobacterial blooms in an urban drinking water supply, Journal of Plankton Research. 35 (2013) 744–758. doi:10.1093/plankt/fbt042.
[95] J. Imberger, J.C. Patterson, Physical limnology, in: J. Hutchinson W,, T.Y. Wu (Eds.), Advances in Applied Mechanics, Academic Press, 1990: pp. 303–475.
[96] J.S. Read, D.P. Hamilton, I.D. Jones, K. Muraoka, L.A. Winslow, R. Kroiss, C.H. Wu, E. Gaiser, Derivation of lake mixing and stratification indices from high-resolution lake buoy data, Environmental Modelling & Software. 26 (2011) 1325–1336. doi:10.1016/j.envsoft.2011.05.006.
[97] C.J. Lorenzen, Extinction of Light in the Ocean by Phytoplankton, ICES Journal of Marine Science. 34 (1972) 262–267. doi:10.1093/icesjms/34.2.262.
[98] T.T. Wynne, R.P. Stumpf, M.C. Tomlinson, J. Dyble, Characterizing a cyanobacterial bloom in Western Lake Erie using satellite imagery and meteorological data, Limnology and Oceanography. 55 (2010) 2025–2036. doi:10.4319/lo.2010.55.5.2025.
[99] S. Diehl, S. Berger, R. Ptacnik, A. Wild, PHYTOPLANKTON, LIGHT, AND NUTRIENTS IN A GRADIENT OF MIXING DEPTHS: FIELD EXPERIMENTS, Ecology. 83 (2002) 399–411. doi:10.1890/0012-9658(2002)083[0399:PLANIA]2.0.CO;2.
[100] H. Wang, Z. Zhang, D. Liang, H. du, Y. Pang, K. Hu, J. Wang, Separation of wind's influence on harmful cyanobacterial blooms, Water Research. 98 (2016) 280–292. doi:10.1016/j.watres.2016.04.037.
[101] A. Pannard, B.E. Beisner, D.F. Bird, J. Braun, D. Planas, M. Bormans, Recurrent internal waves in a small lake: Potential ecological consequences for metalimnetic phytoplankton populations: Vertical internal modes in a small lake, Limnology and Oceanography: Fluids and Environments. 1 (2011) 91–109. doi:10.1215/21573698-1303296.
[102] D. Planas, S. Paquet, Importance of climate change-physical forcing on the increase of cyanobacterial blooms in a small, stratified lake, Journal of Limnology. 75 (2016). doi:10.4081/jlimnol.2016.1371.

[103] K.D. JöHnk, J. Huisman, J. Sharples, B. Sommeijer, P.M. Visser, J.M. Stroom, Summer heatwaves promote blooms of harmful cyanobacteria, Global Change Biology. 14 (2008) 495–512. doi:10.1111/j.1365-2486.2007.01510.x.
[104] C.L. Marti, J. Imberger, L. Garibaldi, B. Leoni, Using time scales to characterize phytoplankton assemblages in a deep subalpine lake during the thermal stratification period: Lake Iseo, Italy: PHYTOPLANKTON ASSEMBLAGES IN LAKE ISEO, Water Resources Research. 52 (2016) 1762–1780. doi:10.1002/2015WR017555.
[105] Z.E. Taranu, R.W. Zurawell, F. Pick, I. Gregory-Eaves, Predicting cyanobacterial dynamics in the face of global change: the importance of scale and environmental context, Global Change Biology. 18 (2012) 3477–3490. doi:10.1111/gcb.12015.
[106] A. Holland, S. Kinnear, Interpreting the Possible Ecological Role(s) of Cyanotoxins: Compounds for Competitive Advantage and/or Physiological Aide?, Marine Drugs. 11 (2013) 2239–2258. doi:10.3390/md11072239.
[107] J.L. Graham, J.R. Jones, Microcystin in Missouri reservoirs, Lake and Reservoir Management. 25 (2009) 253–263. doi:10.1080/07438140903143239.
[108] G. Flaim, E. Eccel, A. Zeileis, G. Toller, L. Cerasino, U. Obertegger, Effects of re-oligotrophication and climate change on lake thermal structure, Freshwater Biology. 61 (2016) 1802–1814. doi:10.1111/fwb.12819.
[109] I.T. Webster, P.A. Hutchinson, Effect of wind on the distribution of phytoplankton cells in lakes revisited, Limnology and Oceanography. 39 (1994) 365–373. doi:10.4319/lo.1994.39.2.0365.
[110] B. Pawlik-Skowrońska, T. Skowroński, J. Pirszel, A. Adamczyk, Relationship between cyanobacterial bloom composition and anatoxin-A and microcystin occurrence in the eutrophic dam reservoir (SE Poland), 2004.
[111] M.A. Chia, M.K. Cordeiro-Araújo, A.S. Lorenzi, M. do C. Bittencourt-Oliveira, Does anatoxin-a influence the physiology of Microcystis aeruginosa and Acutodesmus acuminatus under different light and nitrogen conditions?, Environmental Science and Pollution Research. 23 (2016) 23092–23102. doi:10.1007/s11356-016-7538-8.
[112] K.A. Loftin, J.L. Graham, E.D. Hilborn, S.C. Lehmann, M.T. Meyer, J.E. Dietze, C.B. Griffith, Cyanotoxins in inland lakes of the United States: Occurrence and potential recreational health risks in the EPA National Lakes Assessment 2007, Harmful Algae. 56 (2016) 77–90. doi:10.1016/j.hal.2016.04.001.
[113] B.M. Long, G.J. Jones, P.T. Orr, Cellular Microcystin Content in N-Limited Microcystis aeruginosa Can Be Predicted from Growth Rate, Applied and Environmental Microbiology. 67 (2001) 278–283. doi:10.1128/AEM.67.1.278-283.2001.
[114] I.R. Falconer, Health effects associated with controlled exposures to cyanobacterial toxins, in: H.K. Hudnell (Ed.), Cyanobacterial Harmful Algal Blooms: State of the Science and Research Needs, Springer New York, New York, NY, 2008: pp. 607–612. doi:10.1007/978-0-387-75865-7_27.
[115] D. van der Merwe, Freshwater cyanotoxins, in: Biomarkers in Toxicology, Elsevier, 2014: pp. 539–548. doi:10.1016/B978-0-12-404630-6.00031-2.

[116] R. Banker, S. Carmeli, O. Hadas, B. Teltsch, R. Porat, A. Sukenik, IDENTIFICATION OF CYLINDROSPERMOPSIN IN APHANIZOMENON OVALISPORUM (CYANOPHYCEAE) ISOLATED FROM LAKE KINNERET, ISRAEL1, Journal of Phycology. 33 (1997) 613–616. doi:10.1111/j.0022-3646.1997.00613.x.
[117] R.P. Barbiero, E.B. Welch, Contribution of benthic blue-green algal recruitment to lake populations and phosphorus translocation, Freshwater Biology. 27 (1992) 249–260. doi:10.1111/j.1365-2427.1992.tb00537.x.
[118] V. Istv´novics, K. Pettersson, M.A. Rodrigo, D. Pierson, J. Padis´k, W. Colom, *Gloeotrichia echinulata* , a colonial cyanobacterium with a unique phosphorus uptake and life strategy, Journal of Plankton Research. 15 (1993) 531–552. doi:10.1093/plankt/15.5.531.
[119] J.B. Aavad, Bloom formation of Gloeotrichia echinulata and Aphanizomenon flos-aquae in a shallow, eutrophic, Danish lake, Hydrobiologia. 289 (1994) 193–197. doi:10.1007/BF00007420.
[120] R.A. Osgood, A hypothesis on the role of Aphanizomenon in translocating phosphorus, Hydrobiologia. 169 (1988) 69–76. doi:10.1007/BF00007934.
[121] K. Pettersson, E. Herlitz, V. Istv�novics, The role of Gloeotrichia echinulata in the transfer of phosphorus from sediments to water in Lake Erken, Hydrobiologia. 253 (1993) 123–129. doi:10.1007/BF00050732.
[122] Y. Lara, A. Lambion, D. Menzel, G. Codd, A. Wilmotte, A cultivation-independent approach for the genetic and cyanotoxin characterization of colonial cyanobacteria, Aquatic Microbial Ecology. 69 (2013) 135–143. doi:10.3354/ame01628.
[123] C.S. Reynolds, The Ecology of Phytoplankton, Cambridge University Press, 2006. https://books.google.com/books?id=gDz5jGsPWZYC.
[124] J.M. Rinta-Kanto, E.A. Konopko, J.M. DeBruyn, R.A. Bourbonniere, G.L. Boyer, S.W. Wilhelm, Lake Erie Microcystis: Relationship between microcystin production, dynamics of genotypes and environmental parameters in a large lake, Harmful Algae. 8 (2009) 665–673. doi:10.1016/j.hal.2008.12.004.

Appendix A

Cyanobacteria Composition: Temporal and Vertical Variability

Introduction

The goal of the chapter is to outline the change in cyanobacteria composition in time and space from the two lakes sampled. It is also used as a guide for the identification and importance of the different cyanobacteria genera I observed throughout my field investigations. Although many remote sensing and monitoring strategies measure phycocyanin, like the research station used here, this only captures bulk cyanobacteria. However, there are many different types of cyanobacteria, which are capable of forming HAB each with their own biological niches, physiological advantages, and cyanotoxins that they produce [4,5]. Because of this, management strategies have to take into account not only bulk phycocyanin but also collect information about specific cyanobacteria taxa to adequately combat HAB risks. For example, there are well known cyanotoxins produced

by cyanobacteria that can affect human health, such as microcystin, saxitoxin, anatoxin, cylindrospermopsin and more [1,114,115]. The cyanobacteria that produce these toxins range in buoyancy regulation, light affinity, temperature, and nutrient requirements, including the ability for some cyanobacteria to fix nitrogen. All of these disparate needs make monitoring and management strategies difficult.

Methods

Site Descriptions

The samples outlined here are taken at the research station locations from 2016 and 2017 described in the previous chapters. Both lakes were chosen because they are eutrophic and have a long monitoring history [19]. The research station was anchored in 9.2 m and 16.5 m Madison Lake and South Center Lake, respectively. During the study period, the phosphate concentrations were 150 and 40 µg/L in the epilimnion in Madison Lake and South Center Lake, respectively. The nitrate concentrations were all below detection <0.15mg/L. The wind speed in both lakes ranged from 0-6 m/s and showed diurnal variability. The air temperature in both summers was similar but because of the depth of the research station was shallower in Madison Lake the water temperature was warmer throughout the water column. Madison Lake is a polymictic lake and the research station observed lake turnover in mid August. South Center Lake stayed stratified throughout the observation period. The Schmidt stability index was much higher in South Center Lake than in Madison Lake at 200 and 20 J/m^2, respectively.

Sample Handling

The collection, identification, and enumeration of the cyanobacteria composition is described in detail previously in this thesis. Whole water samples were taken at the research site every meter from the surface to the depth of research station on a weekly basis in both lakes. The samples were stored in Lugols Iodine and stored in the fridge until analyzed. All identification and enumeration is done using microscopy and the BV analysis was done from micrographs using ImageJ, according to the methods outlined previously in this thesis. A summary is in Table A.1.

Table A.1: Comparison of measured and reported biovolumes for the dominant cyanobacteria genera in Madison and South Center Lake. Measured cellular biovolume (μm^3/cell) for *Microcystis* spp. and *Dolichospermum* spp. are described as the average cellular biovolume (± standard deviation). The biovolume measured and reported for *Planktothrix* spp. is filament length (µm) and is described as averaged filament lengths (± standard deviation). The reported biovolumes were measured and reported by the corresponding cited literature.

	Genus	**Measured, Madison Lake**	**Measured, South Center Lake**	**Reported**	**Citation**
BV_{mic} (μm^3/cell)	*Microcystis* spp.	147 (±1.84)		25.8-65.4	Torres et al., 2016
				54-343	Yamamoto et al., 2009
(μm^3/colony)		$5.15x10^5$ ($\pm 4.58x10^5$)	$2.4x10^5$ ($\pm 1.3x10^5$)	-	-
BV_{dol} (μm^3/cell)	*Dolichospermum* spp.	113 (±17.7)	199(±2)	47.683	Kong et al., 2014
				70-300	Yamamoto et al., 2009
Filament length (µm)	*Planktothrix* spp.	253 (± 219)	191(± 66)	77-594	Torres et al., 2016
				30-400	Yamamoto et al., 2009
BV_{plk} (μm^3/ filament)		$7.5x10^3$ ($\pm 6.5x10^3$)	$4.5x10^3$ ($\pm 1.6x10^3$)	-	-

Results

Image Library and Cyanobacteria Identification Guide

Although the cyanobacteria outlined above were dominant, other species were observed during the sampling period in both lakes. Cyanobacteria come in different colony types, morphologies and sizes. The micrograph below was taken from a bloom at the boat launch from Madison Lake in July 2016, Figure A.1. This is a good example of the breadth of cyanobacteria that can be observed in Minnesota Lakes. There are at least 6 different types of cyanobacteria in this sample, all six are capable of cyanotoxin production. The following section will outline each type, the morphology and ecology associated with them to aid in future identification efforts.

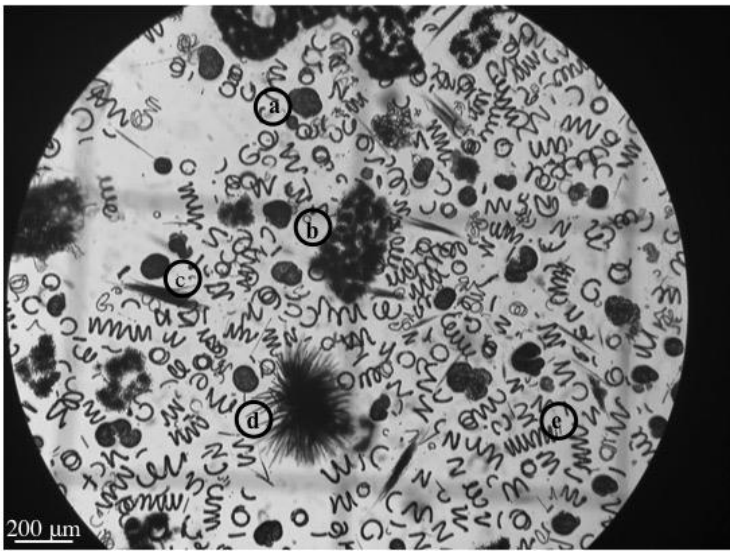

Figure A.1: Micrograph taken from a concentrated sample from a bloom at the boat launch in Madison Lake, July 2016, where a) *Woronchinia,* b) *Microcystis*, c)*Aphanizomenon,* d)*Gloeotrichia*, and e)*Dolichospermum.* Image was acquired at the St Anthony Falls Lab by Anne Wilkinson.

Non-Dominant Species

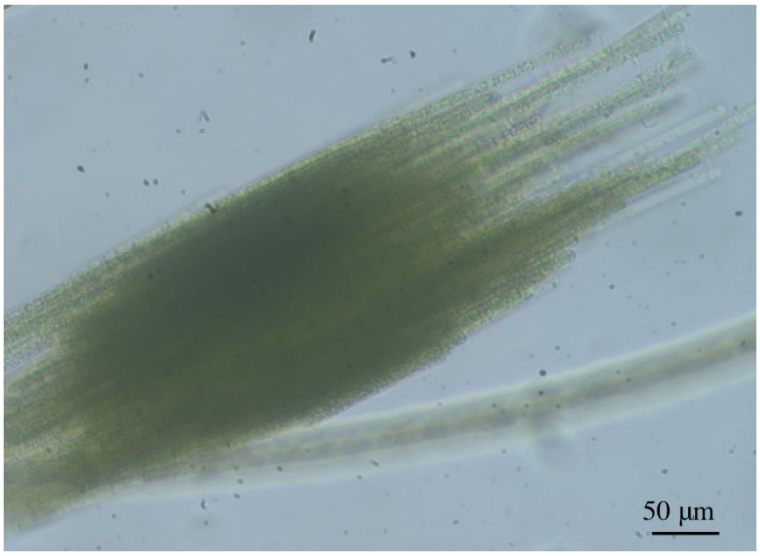

Figure A.2: Micrograph of *Aphanizomenon* colony at 400x magnification taken from Lake Erie in August 2015. Image was acquired at the Ohio State University Stone Lab, Algae Identification Workshop (2015) by Anne Wilkinson.

Aphanizomenon is a colonial, filamentous bloom forming cyanobacteria. Colonies appear as tight stacks of filaments, Figure A.2. Blooms of *Aphanizomenon* are distinct and easily recognizable on the surface because individual colonies can become large enough to see with the naked eye. They look like a pile of grass clippings floating on the water. These blooms are particularly dangerous because they produce cylindrospermopsin, a potent nerve toxin [116].

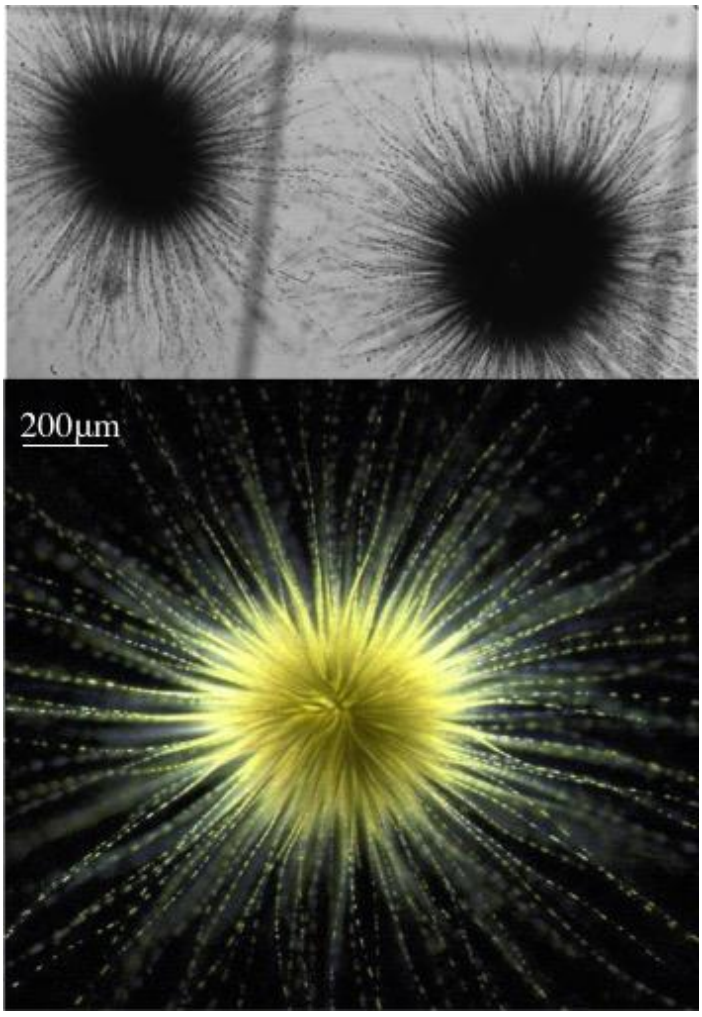

Figure A.3: Micrographs of *Gloeotrichia* sp colony taken from the sampling site at Madison Lake in July 2016. Images were acquired at the St Anthony Falls Lab by Anne Wilkinson.

Gloeotrichia and *Aphanizomenon* are phylogenetically related ([24]. *Gloeotrichia* colonies are very large and distinctive, Figure A.3. Colonies form when individual filaments attached in a central point and extend radially to create spheres on the order of millimeters in diameter. *Gloeotrichia* are a special type of cyanobacteria because they rely on benthic recruitment, as opposed to epilimnetic growth, like the other types of

cyanobacteria observed here [117,118]. Additionally, *Gloeotrichia* and *Aphanizomenon* grow from spores in the sediment and can accumulate biomass in benthos before migrating to the surface [119]. This migration is responsible for the movement of particulate phosphorous and nitrogen in the water column [117,118,120,121]. Thus, *Gloeotrichia* are common in lakes with very high phosphate concentrations, and is why we observed them in Madison Lake during early July [119]. They are a microcystin producing genera, as well.

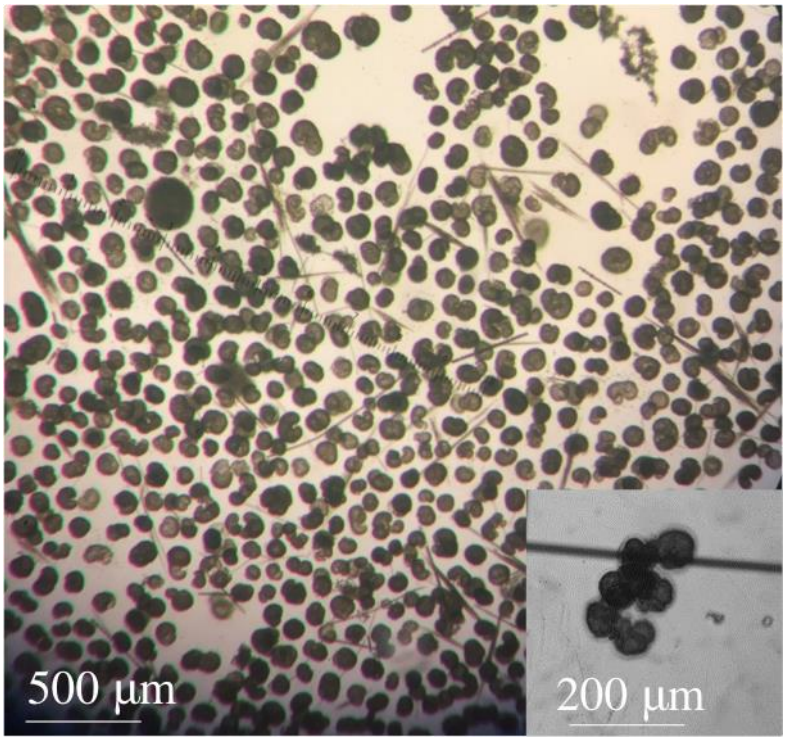

Figure A.4: Micrographs of *Woronchinia* colonies taken from South Center Lake in August 2017. Images were acquired at the St Anthony Falls Lab by Anne Wilkinson.

Woronchinia form spherical colonies from cells in a mucilaginous matrix, Figure A.4. This genera form surface bloom at the surface of eutrophic and mesotrophic lakes. High microcystin have been measured during these blooms [122].

Dominant Species

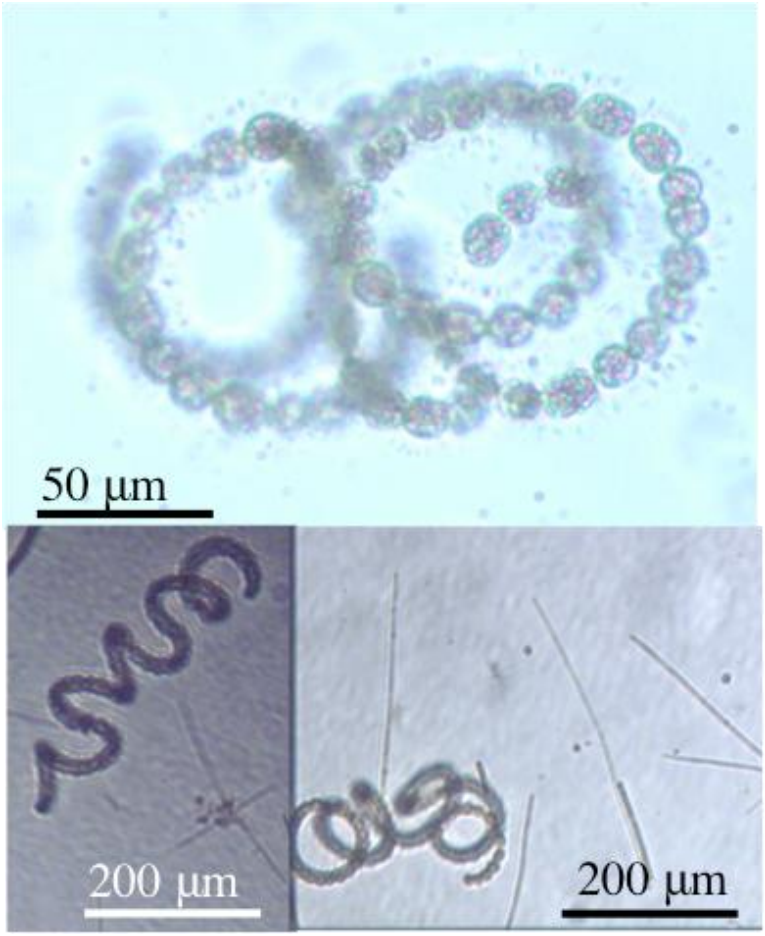

Figure A.5: Micrographs of *Dolichospermum* sp colonies taken from Lake Erie August 2015, the sampling site at Madison Lake in July 2016, and the sampling site at South Center Lake in July 2017. Images were acquired at the St Anthony Falls Lab and at the Ohio State University Stone Lab, Algae Identification Workshop by Anne Wilkinson.

Dolichospermum, formerly known as *Anabaena,* forms helical filaments of individual cells, Figure A.6. *Dolichospermum* are highly buoyant and bloom forming [123]. This genus is a good competitor under low nitrogen supplies as it can fix nitrogen

using special cells called heterocyst [4,123]. However, N-fixation takes a lot of energy and with *Dolichospermum's* high light affinity, this genera is very vulnerable to mixing [4]. Conversely, the increasing temperatures and strong stratification will improve the formation of HAB even in low N environments because of the access to light to power N-fixation and growth. *Dolichospermum* produce both micrcocystin and anatoxin [4]. Anatoxin was observed by the MPCA in Madison Lake during 2016. It is a potent yet very unstable neurotoxin [115].

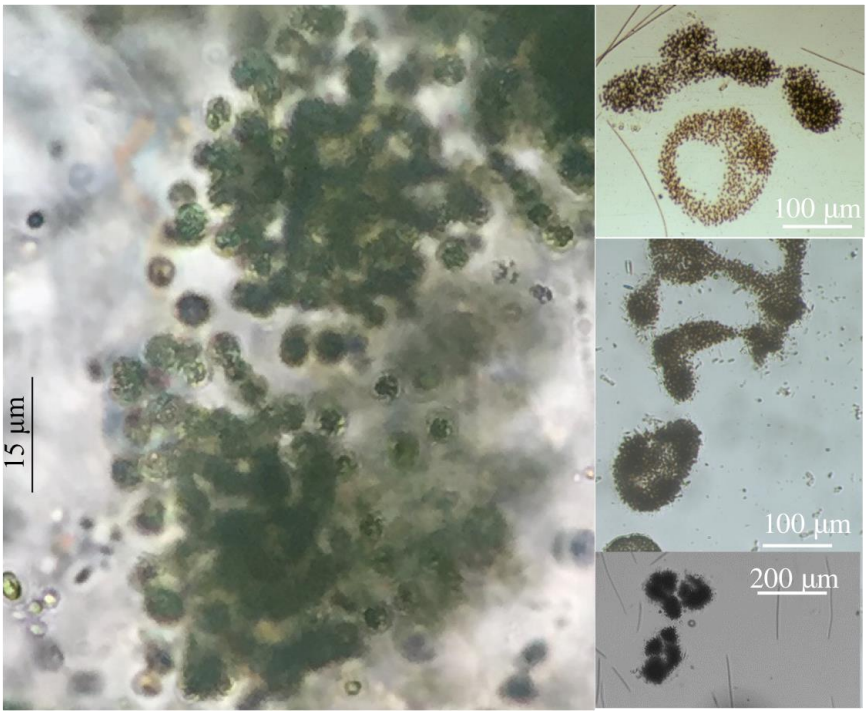

Figure A.6: Micrographs of *Microcystis* sp colonies taken from Lake Erie August 2015, the sampling site at Madison Lake in July 2016. Images were acquired at the St Anthony Falls Lab and at the Ohio State University Stone Lab, Algae Identification Workshop by Anne Wilkinson.

Microcystis are probably the most common and widely reported on cyanobacteria on the planet [1]. They are responsible for some of the largest blooms in the world including Lake Taihu in China and Lake Erie in US [100]. They are so well studied because they can achieve large mono-genera blooms quickly at the surface of nutrient rich warm water bodies [11,124]. This is because they highest buoyancy regulation of any other type of cyanobacteria described here [100]. They also are notable because they can produce the most potent cyanotoxin, microcystin which is its namesake [1,114]. Colonies of *Microcystis* are large (up to a mm in diameter), amorphous, and dense assemblages of individual cells, Figure A.6.

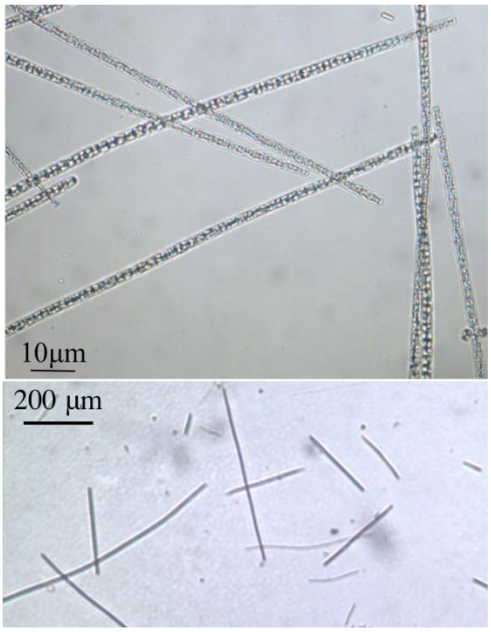

Figure A.7: Micrographs of *Planktothrix* sp filaments taken from Lake Erie August 2015, and the sampling site at Madison Lake in July 2016. Images were acquired at the St Anthony Falls Lab and at the Ohio State University Stone Lab, Algae Identification Workshop by Anne Wilkinson.

Planktothrix form thin filaments, Figure A.7. *Planktothrix* are metalminetic species because of weak buoyancy regulation and low light affinity [4]. They are capable of forming layers in the metalimnion because of their special light harvesting ability [4,123]. They are capable of adjusting their pigments in response to variable light conditions in the metalimnion [4,101]. Additionally they can persist under lower light in deeper layers or more turbid waters because they require very little energy to sustain cell function and structure [4]. *Planktothrix* are often observed after bloom collapses, like we saw in Madison Lake, because of their flexible living conditions, i.e. low light, low energy, lower temperature and lower phosphate requirements [4,69,72]. However, this behavior requires long lake retention times because of this ability to outcompete fast growing algae. *Planktothrix* are also capable of producing microcystin [61]. Because of their metalimnetic behavior, blooms of *Planktothrix* are difficult to observe from the surface, additionally the pigments of *Planktothrix* are not as distinct as the high light affinity cyanobacteria thus blooms do not appear as blue-green but the water may just appear a turbid brown color when present.

Table A.2: Comparison of different cyanobacteria genera, morphology, cyanotoxins and ecological niches.

Genus	Morphology	Cyanotoxins	Niche
Aphanizomenon	Colonies of tightly stacked parallel filaments	Cylindrospermopsin, Anatoxin, Saxitoxin, Geosmin	N fixer, growth in the benthos
Gloeotrichia	Spherical colonies of radial filaments	Microcystin	N fixer, growth in the benthos
Woronchinia	Mucilaginous spherical/kidney shaped colonies	Microcystin	Non-N fixer, Highly buoyant, high light affinity
Dolichospermum	Helical filaments of spherical cells	Microcystin, Cylindrospermopsin, Anatoxin, Saxitoxin, Geosmin	N-fixer, highly buoyant, high light affinity
Microcystis	Large dense amorphous colonies of spherical cells	Microcsytin	Non-N fixer, Highly buoyant, high light affinity
Planktothrix	Thin filaments	Microcystin	N-fixer, weak buoyancy regulation, low light affinity

Cyanobacteria Composition Temporal Variability

The time evolution of algae in both lakes are expressed in two ways, i.e. biovolume concentration, BV (μm^3/mL) and cell concentration, N (cell/mL), to demonstrate the importance of reporting consistent cyanobacteria biomass. As discussed in the previous

chapters, using just the cell concentration did not yield an acceptable calibration with the phycocyanin sensor because of the change in cyanobacteria composition and the different morphology of each genera as discussed below. The BV shows the change in composition based on the measurable BV from each genera, the shape of the individual genera trends do not change in N but the relative numbers amongst do because the average BV/cell per genera is different.

In Madison Lake, Microcystis slowly declines throughout the observation period, Figure A.8. *Dolichospermum* peaks at 9/8/16 and then declines. *Planktothrix* numbers stay consistent throughout the season. *Planktothrix* has a consistently higher BV than the other two genera. This difference between the N times series is because the BV/filament is an order of magnitude higher than that for *Dolichospermum*. In South Center Lake, *Microcystis* briefly peaks in mid July, Figure A.9. *Dolichospermum* peaks on 8/3/17 as well and then declines. *Planktothrix* peaks sharply at 8/3/17 and remains high. Not only did the composition change with time, there is also vertical variability associated with the different sampling locations.

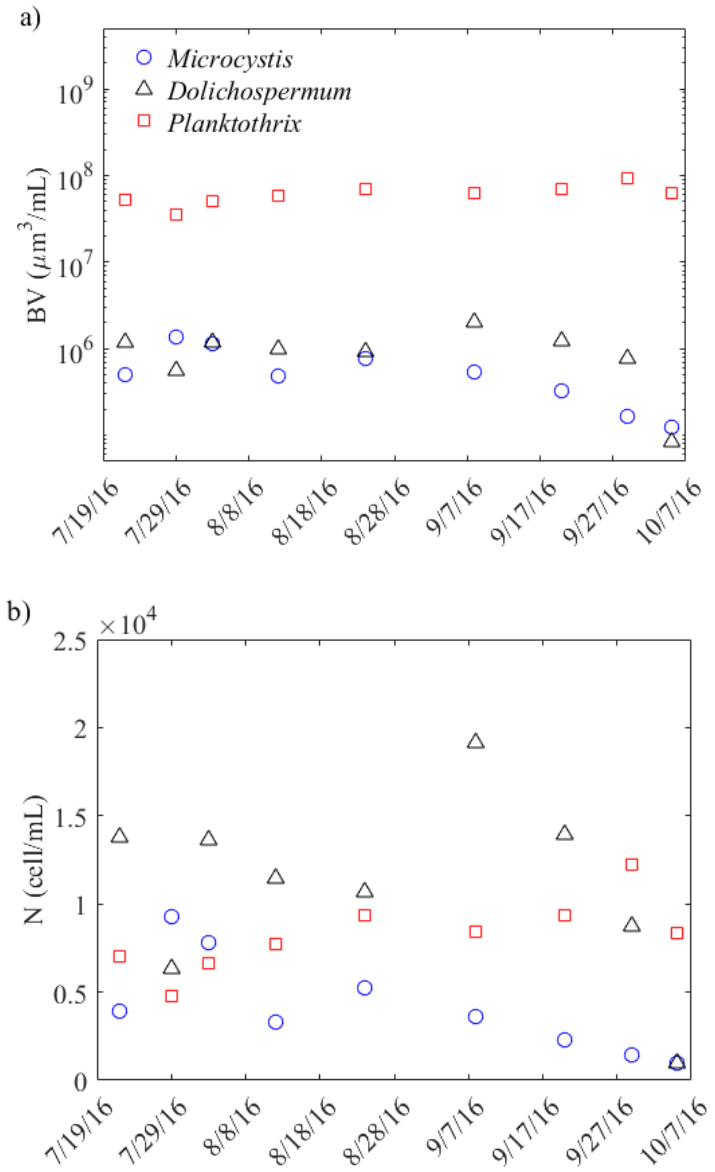

Figure A.8:a) Time series of depth averaged dominant cyanobacteria genera BV concentrations for Madison Lake, 2016. The circle represents *Microcystis* sp, the triangle represents *Dolichospermum* sp, and the square represents the *Planktothrix* sp.b) Time series of depth average dominant cyanobacteria genera cell concentrations, where the circle represents *Microcystis* sp, the triangle represents *Dolichospermum* sp, and the square represents the *Planktothrix* sp

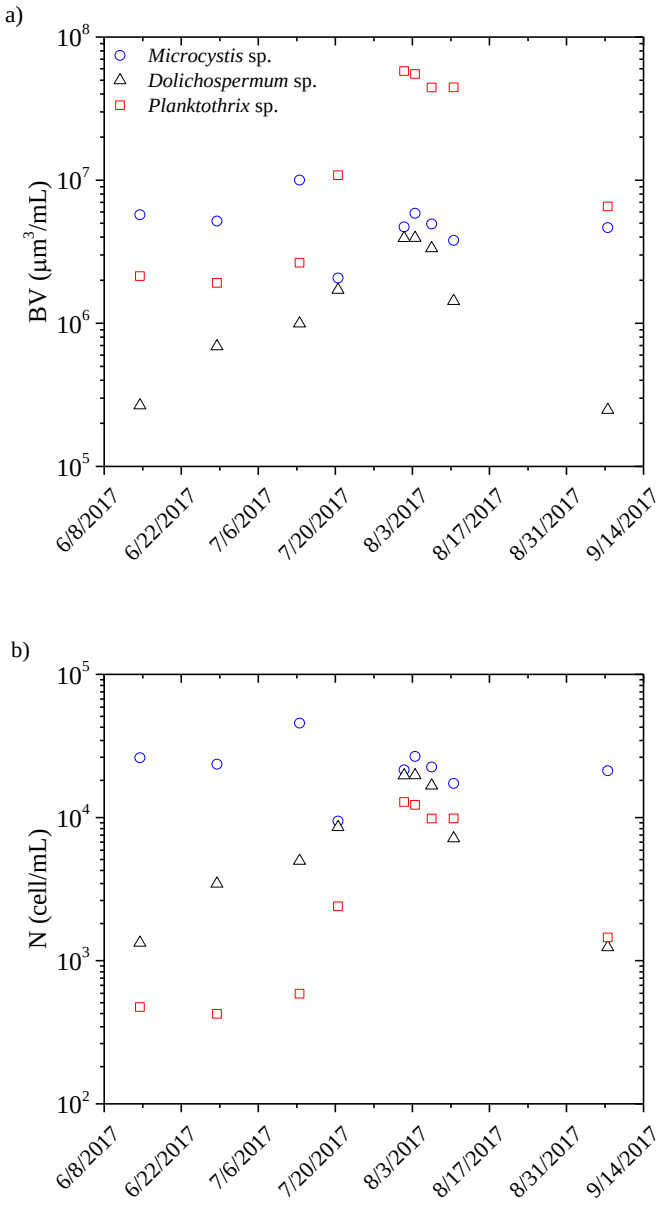

Figure A.9: a) Time series of average BV of dominant cyanobacteria genera in the epilimnion, where the circle represents *Microcystis* sp, the triangle represents *Dolichospermum* sp, and the square represents the *Planktothrix* sp. b) Time series of average cell concentrations of dominant cyanobacteria genera in the epilimnion, where the

circle represents *Microcystis* sp, the triangle represents *Dolichospermum* sp, and the square represents the *Planktothrix* sp

Cyanobacteria Vertical Distribution

Madison Lake

Before 8/13 the BV is more stratified and shows some confinement by the thermocline, which is not the case during the weakly stratified period after, Figure A.10. The *Dolichospermum* and *Microcystis* showed are more vertical heterogeneity than *Planktothrix* i) usually peaking near the surface and ii) are more confined above the thermocline.

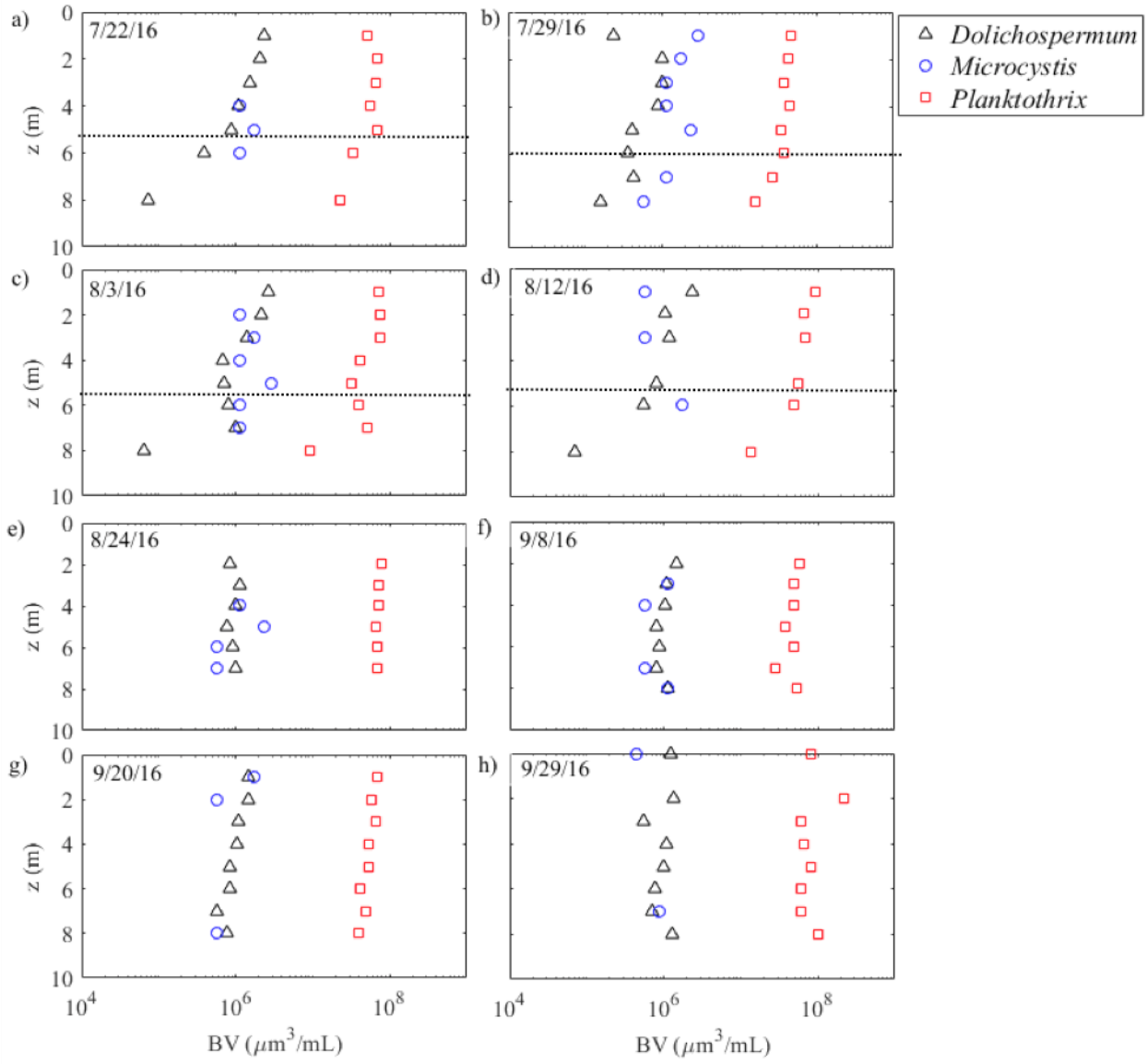

Figure A.10: Depth profiles of dominant cyanobacteria BV in Madison Lake at different sampling dates throughout 2016, where the circle represents *Microcystis* sp, the triangle represents *Dolichospermum* sp, and the square represents the *Planktothrix* sp. The dotted line is the thermocline depth.

South Center Lake

The profiles here only show depths above the thermocline because in South Center Lake the other depths are 0 um^3/mL for all genera, Figure A.11. We can see that before 8/2/17 *Microcystis* more prevalent in the surface layer and both *Microcystis* and *Dolichospermum* are uniformly mixed in the surface layer. After 8/2/17 the *Planktothrix* but shows the same distribution in the water column as the other genera.

Overall, we can see the differences between Madison Lake and South Center Lake are prevalent by the shape of the BV profiles not only in the entire column but also in the surface layer. Namely in Madison Lake, the BV extends deeper in the water column and has less of a confining effect of the thermocline because of the lower stability index.

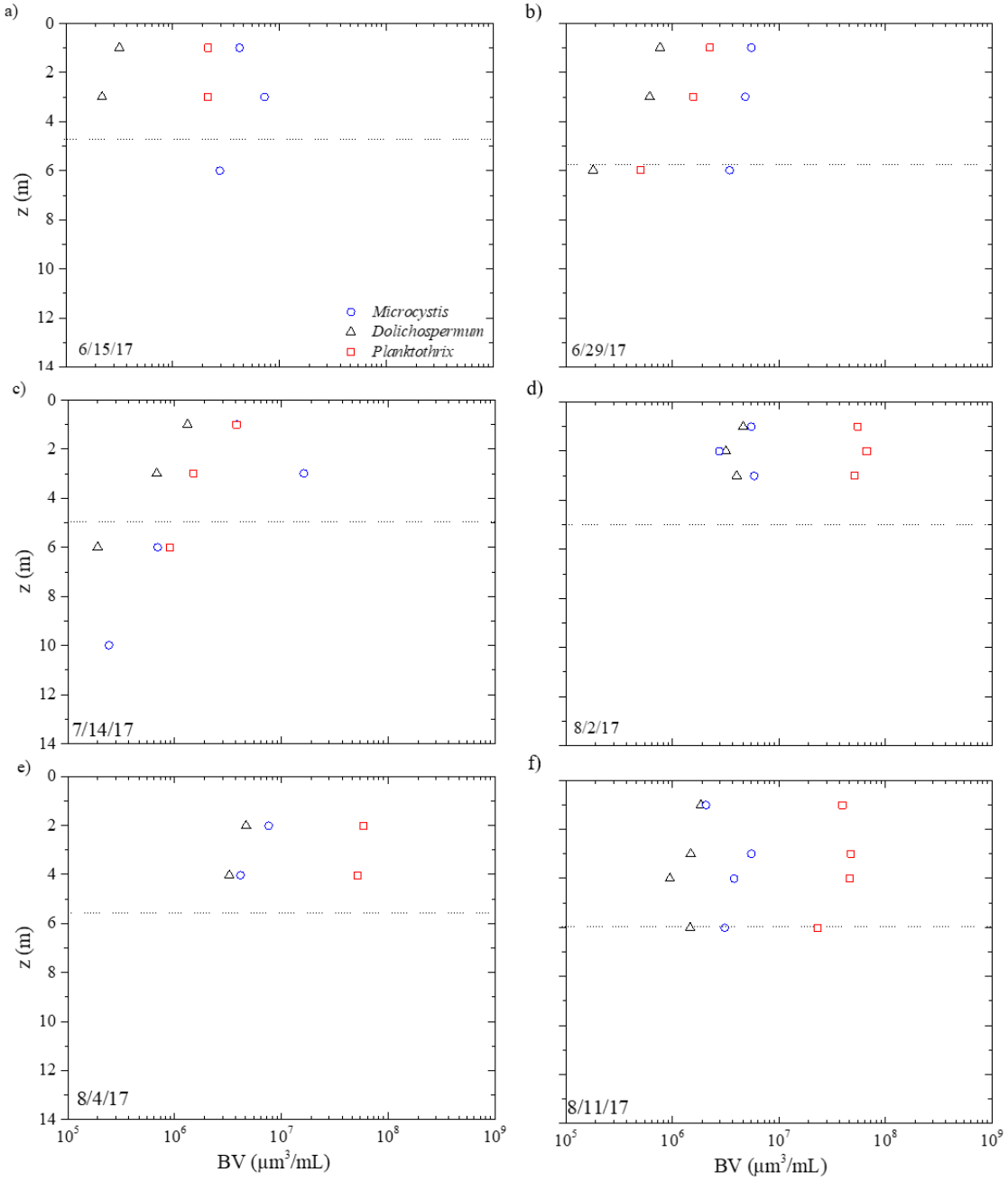

Figure A.11: Depth profiles of dominant cyanobacteria BV in South Center Lake at different sampling dates throughout 2017, where the circle represents *Microcystis* sp, the

triangle represents *Dolichospermum* sp, and the square represents the *Planktothrix* sp. The dotted line represents the thermocline depth.

Conclusion

As outlined in the identification section there are different types of cyanobacteria capable of forming toxic HAB, which have different ecological niches. It is important for management strategies to understand the behaviors of these different cyanobacteria under both polymictic and dimictic conditions in eutrophic lakes. Both lakes have the same genera, *Dolichospermum, Microcystis* and *Planktothrix*, but in different relative concentrations. *Planktothrix* represented the highest BV in both lakes. Both show vertical heterogeneities, which reflect those observed by the research station and are driven by physical lake conditions.

Appendix B

Packing Lists for Field Work

General Packing List

- ☐ Hydrolab box
  - pH fluid 7,10
  - specific conductivity
  - DI
  - Cup
  - Electrolyte and pellets
  - Aluminum foil
- ☐ Inverter
- ☐ Batteries
- ☐ Labtop
- ☐ Charger
- ☐ Connector
- ☐ Van dorn
- ☐ Bottles
- ☐ Notebook
- ☐ Sharpee
- ☐ Label tape
- ☐ Plankton net
- ☐ Tooth brush-to clean probe
- ☐ Life jacket
- ☐ Depth finder
- ☐ Phone cases
- ☐ Secchi disk
- ☐ Laser site
- ☐ Tools
- ☐ Extra rope
- ☐ Tow rope
- ☐ Labtop for SKAMP
- ☐ SKAMP
- ☐ Mask and fins
- ☐ Sunscreen
- ☐ Water
- ☐ Buckets
- ☐ Cooler
- ☐ Paddles
- ☐ Straps

Deployment Buoy Packing List

Buoy

- □ Computer
- □ WIFI hotspot
- □ Hydrolab
- □ Battery
- □ Met Station instruments
    - o Rain gauge
    - o PAR sensor
    - o Antenna
    - o cup and vane
- □ hydrolab
- □ counter weight
- □ rope
- □ Deck Counter weight
    - o Level
    - o Bolts ruler
    - o weights

anchors

- □ ropes anchors(3 75 ft long)
- □ chain
- □ anchors(3)
    - o sand anchors(2)
    - o heavy(1)
- □ buoys (3)
- □ ropes buoys(from v tanks)

Thermistor Chain

- □ 2 carabineers
- □ weight
- □ rope .25 in
- □ chain
- □ buoy(red)

Extras

- □ canoe
- □ life jackets x 6
- □ tape measure
- □ waders x2
- □ depth finders
- □ maps
- □ extra rope
- □ bottles
- □ van dorn sampler
- □ cooler
- □ swim suit
- □ mask
- □ safl shirt
- □ blue straps
- □ big white rope from the back of the truck
- □ reflective tape and sign
- □ gloves
- □ extra carabineers
- □ C batteries for sonde

tools

- □ drills (2)
- □ batteries
- □ Bens tool kit
- □ Light bolts +washers
- □ Tube of silicone
- □ Silicone gun
- □ Compass
- □ Knives
- □ Wrenches for all the nuts and bolts

Appendix C

Protocols for Phycocyanin Analysis

Phycocyanin Fluorometer Analysis

1. Vacuum-filter samples with GF/F phycocyanin analyses
2. To quantify phycocyanin, filters were first ground in 10 mL
   of 50 mM phosphate buffer (40 mL of concentrated buffer
   in 960 mL distilled water; pH 7.0+0.1) under reduced light using a smooth Teflon grinder in a centrifuge tube for 1 min.
3. 10 mL aliquot of phosphate buffer was used to rinse the grinder into the centrifuge tube, bringing the total extract volume to 20 mL
4. Extraction: samples were stored in darkness at 4C for 2 h and then placed in a dark cabinet
   for another 2 h to warm to room temperature (21C) prior to analysis. Thus, the total extraction time was 4h.
5. Filtered extracts were analyzed for phycocyanin using a Turner Designs Trilogy fluorometer fitted with an orange module (Turner Designs #7200-044) that accommodated a four-sided clean, clear 10 mm, glass square cuvette

NOTE

All extractions and sample processing must be done under reduced laboratory lightand absolutely no exposure to sunlight.

Calibration

1. Raw fluorescence units (RFUs) were converted to phycocyanin concentrations using a standard curve

[concentrations (mg L21): 0, 10, 50, 100, 500, 1000 and
2000]
created with phycocyanin dissolved in phosphate buffer. Prior to creating our standard curve

Sample Storage

Filters can be stored in the dark at 2C until processed.

NOTE
The extract temperature should be approximately the same as the temperature during standard curve development since colder extract temperatures cause higher fluorescence measurements

Kasinak J. Plankton Res. (2015) 37(1): 248–257. First published online October 29, 2014 doi:10.1093/plankt/fbu096

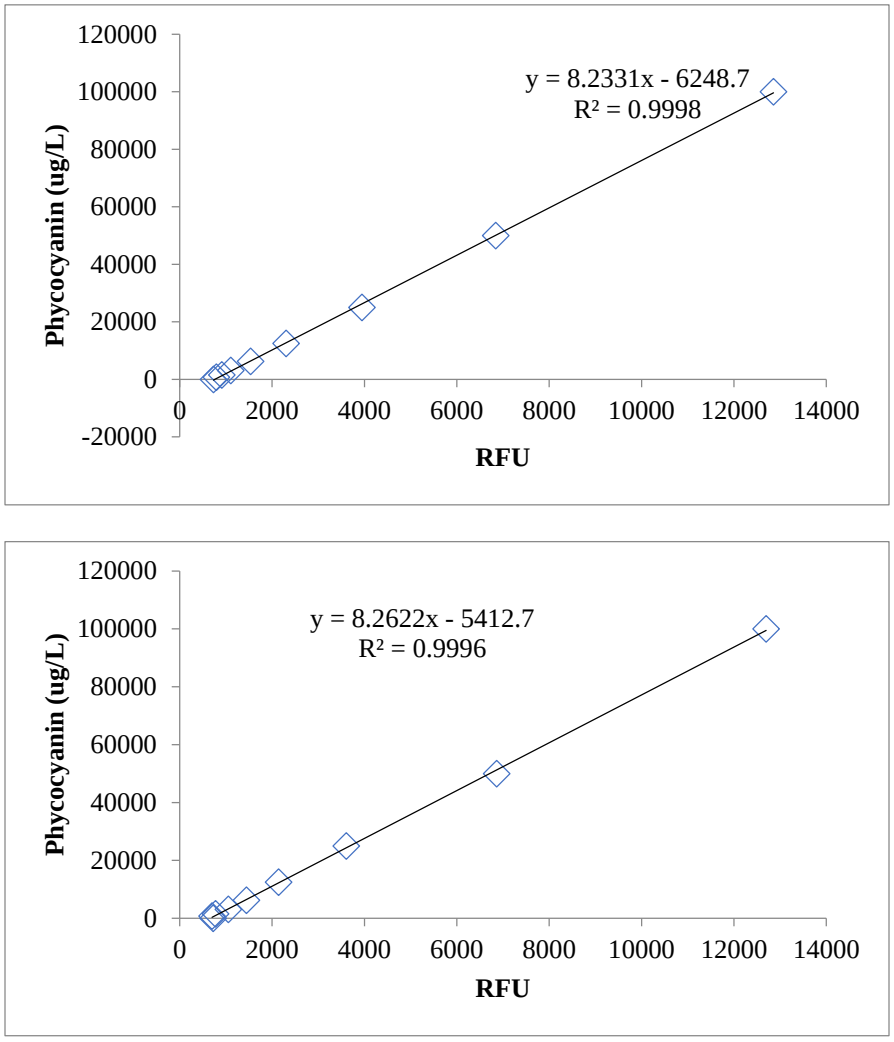

Figure C.1:Sample calibrations of Phycocyanin (µg/L) vs RFU from Madison Lake 2016.

Appendix D

Protocols for Calibration of the Phycocyanin Probe

Breaking colonies

1. Place a glass test tube in the microwave with cap barely screwed on
    a. Every 5s to ensure no overflow
    b. Repeat 3 times
2. On touch mode vortex the test tube on setting 4 for about 30s
    a. Use a hot pad if needed
3. Remove 10ul and count under the hemacytometer

Calibrating the phycocyanin probe on the hydrolab

1. Lake water with concentrated phytoplankton samples >53um colonies collected from Bray Park boat launch Monday 5/9/16 set by the window
2. Selected colonies (all that I could to obtain the highest concentration) from the top of the 3 jars in (1) with an eyedropper and filled to 300mL(just enough to cover the sensor with lake water described in (1)
3. Place the probes in the calibration cup, filled with the known concentration of colonies
4. Twirl the cup attached to the stand in between the window and the probe(in the same place everytime)
5. Wait until the signal plateaus about 15s so that there is no time for rising past the sensing zone
6. Repeat (3-5) for 4 dilutions of (1) 250,100,50, tap water

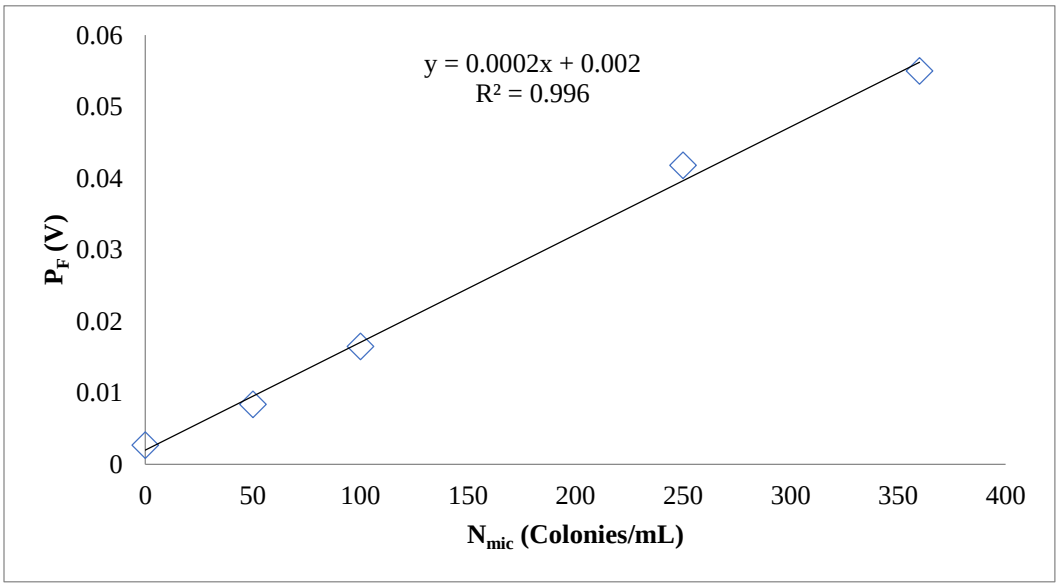

Figure D.1:Calibration of phycocyanin probe vs from samples collected from a *Microcystis* bloom on 5/26/16 measured in the lab.

Table D.1: Calibration and cell/colony data from samples collected from a *Microcystis* bloom on 5/26/16.

nominal dilution	**original stock**	**DI water**	**hydrolab voltage**	**N_{mic} (Colonies/mL)**	**Unicellular (cell/mL)**	**cell/colony**
360	300	0	0.055	360	870,000	2416.667
250	208	92	0.0418	234	590,000	2360
100	120	180	0.0165	-	-	-
50	150	150	0.0084	-	-	-
0	0	300 (tap water)	0.0027	-	-	-

Appendix E

Code to Import and Display Data from Vista Data Vision

```
clear

%[filename,pathname] = uigetfile('*.csv');
filename='vdv_05_11 _2017_10_23_2017profile.csv';
pathname='./'
delimiter = ',';
startRow = 7;

%% Format string for each line of text:
%   column1: date strings (%s)
%   column2: double (%f)
% For more information, see the TEXTSCAN documentation.
formatSpec = '%s%f%f%f%f%f%f%f%[^\n\r]';

%% Open the text file.
fileID = fopen([pathname,filename],'r');

%% Read columns of data according to format string.
% This call is based on the structure of the file used to generate this
% code. If an error occurs for a different file, try regenerating the
code
% from the Import Tool.
dataArray = textscan(fileID, formatSpec, 'Delimiter', delimiter,
'EmptyValue' ,NaN,'HeaderLines' ,startRow-1, 'ReturnOnError', false);
```

```
%% Close the text file.
fclose(fileID);

%% Post processing for unimportable data.
% No unimportable data rules were applied during the import, so no post
% processing code is included. To generate code which works for
% unimportable data, select unimportable cells in a file and regenerate
the
% script.

%% Convert the contents of column with dates to serial date numbers
using date format string (datenum).
%dataArray{1} = datenum(dataArray{1},'mm/dd/yyyy HH:MM');
dataArray{1} = datenum(dataArray{1},'yyyy-mm-dd HH:MM:SS');

%% Allocate imported array to column variable names download all in
order time depth, LDO % PAR pH phycocyanin Temp
time = dataArray{:, 1};
depth  = dataArray{:, 2};
LDO_AVG_ = dataArray{:, 3};
LDO_AVG_perc = dataArray{:, 4};
PAR= dataArray{:, 5};
PH = dataArray{:, 6};
phycocyanin_Avg_Volts = dataArray{:, 7};
 SpCond_Avg = dataArray{:, 8};
Temp_Avg = dataArray{:, 9};
% SpCond_Avg = dataArray{:, 8};
% Temp_Avg = dataArray{:, 9};

%2016-07-19 00:02:03,   1  ,   12.51, 155.7 , 10.19 ,  8.84 , 0.026 ,
0.273  , 26.17
%               date, depth,   LDO  , LDO % , PAR   ,  PH    , phy  ,
SPcond  , Tavg




%
%

%% Clear temporary variables
clearvars filename delimiter startRow formatSpec fileID dataArray ans;

%%Identify good periods for profiles

%% contour plot for profiles
clear depth2 depth3 Indecies phyco_reshaped
%change this to switch parameters to plot
measurement = phycocyanin_Avg_Volts;
measurement2 = Temp_Avg;
measurement3 = PH;
```

```
measurement4 = LDO_AVG_perc;
measurement5 = PAR;



 depth2 = round(depth/.5)*.5;%round to 0.5
 Indecies = find(depth2==1);%find the indices of the starting depth
 measurement_reshaped = i*ones(max(Indecies(2:end)-Indecies(1:end-1)),
length(Indecies));%creates empty matrices to fill for each variable
 measurement_reshape2 = i*ones(max(Indecies(2:end)-Indecies(1:end-1)),
length(Indecies));%creates empty matrices to fill for each variable
measurement_reshape3 = i*ones(max(Indecies(2:end)-Indecies(1:end-1)),
length(Indecies));%creates empty matrices to fill for each variable
measurement_reshape4 = i*ones(max(Indecies(2:end)-Indecies(1:end-1)),
length(Indecies));%creates empty matrices to fill for each variable
measurement_reshape5 = i*ones(max(Indecies(2:end)-Indecies(1:end-1)),
length(Indecies));%creates empty matrices to fill for each variable

 depth3 = i*ones(max(Indecies(2:end)-Indecies(1:end-1)),
length(Indecies));
 time2 = NaN(max(Indecies(2:end)-Indecies(1:end-1)), length(Indecies));
 for ii = 1:length(Indecies)-1
     measurement_reshaped(1:-Indecies(ii)+Indecies(ii+1),ii) =
measurement(Indecies(ii):Indecies(ii+1)-1); %take data from starting
depth to ending depth for each profile into reshaped matrix  each
column is a depth profile at each start time of the profile
     measurement_reshaped2(1:-Indecies(ii)+Indecies(ii+1),ii) =
measurement2(Indecies(ii):Indecies(ii+1)-1); %take data from starting
depth to ending depth for each profile into reshaped matrix  each
column is a depth profile at each start time of the profile
     measurement_reshaped3(1:-Indecies(ii)+Indecies(ii+1),ii) =
measurement3(Indecies(ii):Indecies(ii+1)-1); %take data from starting
depth to ending depth for each profile into reshaped matrix  each
column is a depth profile at each start time of the profile
     measurement_reshaped4(1:-Indecies(ii)+Indecies(ii+1),ii) =
measurement4(Indecies(ii):Indecies(ii+1)-1); %take data from starting
depth to ending depth for each profile into reshaped matrix  each
column is a depth profile at each start time of the profile
     measurement_reshaped5(1:-Indecies(ii)+Indecies(ii+1),ii) =
measurement5(Indecies(ii):Indecies(ii+1)-1); %take data from starting
depth to ending depth for each profile into reshaped matrix  each
column is a depth profile at each start time of the profile



     depth3(1:-Indecies(ii)+Indecies(ii+1),ii) =
depth2(Indecies(ii):Indecies(ii+1)-1); %reshape depth matrix to match
phyco matrix
     time2(:,ii) = time(Indecies(ii)); %make the start time of each
profile the time for every depth sample of the same profile
     if ii == length(Indecies)-1
         ii = ii+1;  %this section captures the last depth profile, but
does the same as above
```

```
        measurement_reshaped(1:-Indecies(ii)+length(depth2)+1,ii) =
measurement(Indecies(ii):end);
        measurement_reshaped2(1:-Indecies(ii)+length(depth2)+1,ii) =
measurement2(Indecies(ii):end);
        measurement_reshaped3(1:-Indecies(ii)+length(depth2)+1,ii) =
measurement3(Indecies(ii):end);
        measurement_reshaped4(1:-Indecies(ii)+length(depth2)+1,ii) =
measurement4(Indecies(ii):end);
        measurement_reshaped5(1:-Indecies(ii)+length(depth2)+1,ii) =
measurement5(Indecies(ii):end);
        depth3(1:-Indecies(ii)+length(depth2)+1,ii) =
depth2(Indecies(ii):end);
        time2(:,ii) = (time(Indecies(ii)));
    end
 end
% depth3(find(depth3==i)) = 10; %changes the extra depths that we
padded each profile with to match all profile lengths to numbers that
apear off the contour graph so they don't interfere with the image

%phyco2=reshape(phycocyanin_Avg_Volts, 14, 150); (1:145) (157:end)
%
contourf(time2(:,157:end),depth3(:,157:end),phyco_reshaped(:,157:end));

%% plots
% measurement = phycocyanin_Avg_Volts;
% measurement2 = Temp_Avg;
% measurement3 = PH;
% measurement4 = LDO_AVG_perc;
% measurement5 = PAR;
 kk=0;
timsbreaks = [0,0];
for ii= 1:length(time)-1
    if abs(time(ii+1)-time(ii))>0.1667
       kk=kk+1;
       timsbreaks(kk,:) = [time(ii) time(ii+1)];

    end
end
y=[1,14];

figure % substract 0.5m to the deptgh
contourf(time2,real(depth3-0.5),real(measurement_reshaped5),0:10:900);
%  xlim([datenum('12-Jul-2016 13:02:03') time2(end)])
datetick('x','mm/dd','keeplimits','keepticks')
colorbar
colormap jet
        title('PAR')
        xlabel('Time')
        ylabel('Depth')
        set(gca,'YDir','rev')
        ylim([1 13.5])
        %phycocyanin
        %caxis([0.004 0.04])
```

```
      ax.XTickLabelRotation=90;
     hold on
%fill(timsbreaks(4,:),y','w');
for ii=1:length(timsbreaks)
    ANW =[timsbreaks( ii,:);timsbreaks(ii,:)];  BNW = [y;y(2),y(1)];
   H= fill(ANW(:),BNW(:),'w');
   uistack(H)
end
set(gcf, 'renderer', 'painter');

hold off


% make a row vector of y

figure
contourf(time2,real(depth3),real(measurement_reshaped),0:0.002:0.03);
% xlim([datenum(2017,5,11) datenum(2017,7,30)])
datetick('x','mm/dd','keeplimits','keepticks')
colorbar
colormap jet
        title('Phycocyanin Times Series Depth Profile')
        xlabel('Time')
        ylabel('Depth')
        set(gca,'YDir','rev')
        ylim([1 14])
        caxis([0 0.02])
       ax.XTickLabelRotation=90;
hold on
%fill(timsbreaks(4,:),y','w');
for ii=1:length(timsbreaks)
    ANW =[timsbreaks( ii,:);timsbreaks(ii,:)];  BNW = [y;y(2),y(1)];
   H= fill(ANW(:),BNW(:),'w');
   uistack(H)
end
set(gcf, 'renderer', 'painter');
hold off

figure
contourf(time2,real(depth3),real(measurement_reshaped4),0:30:200);
%  xlim([datenum('12-Jul-2016 13:02:03') time2(end)])
datetick('x','mm/dd','keeplimits','keepticks')
colorbar
colormap jet
        title('LDO %')
        xlabel('Time')
        ylabel('Depth')
        set(gca,'YDir','rev')
        ylim([1 14])
       % caxis([20 27])
        %temperature
        %caxis([22 27])
       ax.XTickLabelRotation=90;
```

```
           hold on
%fill(timsbreaks(4,:),y','w');
for ii=1:length(timsbreaks)
    ANW =[timsbreaks( ii,:);timsbreaks(ii,:)];  BNW = [y;y(2),y(1)];
   H= fill(ANW(:),BNW(:),'w');
   uistack(H)
end
set(gcf, 'renderer', 'painter');

hold off

figure
contourf(time2,real(depth3),real(measurement_reshaped3),30);
%  xlim([datenum('12-Jul-2016 13:02:03') time2(end)])
datetick('x','mm/dd','keeplimits','keepticks')
colorbar
colormap jet
        title('pH')
        xlabel('Time')
        ylabel('Depth')
        set(gca,'YDir','rev')
        ylim([1 14])
        caxis([6 9])
        %temperature
        %caxis([22 27])
       ax.XTickLabelRotation=90;
           hold on
%fill(timsbreaks(4,:),y','w');
for ii=1:length(timsbreaks)
    ANW =[timsbreaks( ii,:);timsbreaks(ii,:)];  BNW = [y;y(2),y(1)];
   H= fill(ANW(:),BNW(:),'w');
   uistack(H)
end
set(gcf, 'renderer', 'painter');

hold off


figure
contourf(time2,real(depth3),real(measurement_reshaped2),30);

datetick('x','mm/dd','keeplimits','keepticks')
colorbar
colormap jet
        title('T')
        xlabel('Time')
        ylabel('Depth')
        set(gca,'YDir','rev')
        ylim([1 14])
        caxis([5 30])
        %temperature
        %caxis([22 27])
       ax.XTickLabelRotation=90;
```

```
            hold on
%fill(timsbreaks(4,:),y','w');
for ii=1:length(timsbreaks)
    ANW =[timsbreaks( ii,:);timsbreaks(ii,:)];  BNW = [y;y(2),y(1)];
   H= fill(ANW(:),BNW(:),'w');
   uistack(H)
end
set(gcf, 'renderer', 'painter');

hold off


%% env conditions

%[filename,pathname] = uigetfile('*.csv');
filename='vdv_05_11_2017_10-23_2017weather.csv'
pathname='./'
delimiter = ',';
startRow = 7;


%1 Time,MadisonLake_5Min: 24 Hour
%2 Rainfall[mm],MadisonLake_5Min:
%3 AirTemp_Avg[Â°C],MadisonLake_5Min:
%4 batt_volt_Avg[Volts],MadisonLake_5Min:
%5 DewPt_Avg[Â°C],MadisonLake_5Min:
%6 PAR_Den_Avg[umol/s/m2],MadisonLake_5Min:
%7 PTemp_Avg[Â°C],MadisonLake_5Min:
%8 Rain_Tot[mm],MadisonLake_5Min:
%9 RH_Avg[%RH],MadisonLake_5Min:
%10 WaterTemp_0.1m_Avg[Â°C],MadisonLake_5Min:
%11 WaterTemp_0.5m_Avg[Â°C],MadisonLake_5Min:
%12 WaterTemp_1.0m_Avg[Â°C],MadisonLake_5Min:
%13 WaterTemp_1.5m_Avg[Â°C],MadisonLake_5Min:
%14 WaterTemp_2.0m_Avg[Â°C],MadisonLake_5Min:
%15 WaterTemp_2.5m_Avg[Â°C],MadisonLake_5Min:
%16 WaterTemp_3.5m_Avg[Â°C],MadisonLake_5Min:
%17 WaterTemp_4.5m_Avg[Â°C],MadisonLake_5Min:
%18 WaterTemp_5.5m_Avg[Â°C],MadisonLake_5Min:
%19 WaterTemp_6.5m_Avg[Â°C],MadisonLake_5Min:
%20 WaterTemp_7.5m_Avg[Â°C],MadisonLake_5Min:
%21 WaterTemp_8.5m_Avg[Â°C],MadisonLake_5Min:
%22 WindDir_Avg[Â°],MadisonLake_5Min:
%23 WindDir_StDev[Â°],MadisonLake_5Min:
%24 WindSpeed_Avg[m/s]
%2016-07-19
00:00:00,0,24,12.76,19.07,0.959,24.62,0,73.91,26.94,26.98,25.37,24.98,2
4.77,24.67,24.47,23.96,23.86,23.66,23.54,22.64,105.2,9.3,2.149

formatSpec =
'%s%f%f%f%f%f%f%f%f%f%f%f%f%f%f%f%f%f%f%f%f%f%f%f%f%f%[^\n\r]';

%% Open the text file.
```

```
fileID = fopen([pathname,filename],'r');

%% Read columns of data according to format string.
% This call is based on the structure of the file used to generate this
% code. If an error occurs for a different file, try regenerating the
code
% from the Import Tool.
dataArray = textscan(fileID, formatSpec, 'Delimiter', delimiter,
'EmptyValue' ,NaN,'HeaderLines' ,startRow-1, 'ReturnOnError', false);

%% Close the text file.
fclose(fileID);

%% Post processing for unimportable data.
% No unimportable data rules were applied during the import, so no post
% processing code is included. To generate code which works for
% unimportable data, select unimportable cells in a file and regenerate
the
% script.

%% Convert the contents of column with dates to serial date numbers
using date format string (datenum).
%dataArray{1} = datenum(dataArray{1},'mm/dd/yyyy HH:MM');
dataArray{1} = datenum(dataArray{1},'yyyy-mm-dd HH:MM:SS');

%% Allocate imported array to column variable names download all in
order time depth, LDO % PAR pH phycocyanin Temp
timeb = dataArray{:, 1};
rain_ = dataArray{:, 2};
Tair = dataArray{:, 3};
PARair = dataArray{:, 7};
RH= dataArray{:, 10};
t1 = dataArray{:, 11};
t2 = dataArray{:, 12};
t10 = dataArray{:, 13};
t11 = dataArray{:, 14};
t12 = dataArray{:, 15};
t3 = dataArray{:, 16};
t4 = dataArray{:, 17};
t5 = dataArray{:, 18};
t6  = dataArray{:, 19};
t7 = dataArray{:, 20};
t8 = dataArray{:, 21};
t9 = dataArray{:, 22};
wdir = dataArray{:, 23};
wspd = dataArray{:, 25};
dept=[0.1 1 2 3 4 5 6 7 8 10 12 14];

% SpCond_Avg = dataArray{:, 8};
% Temp_Avg = dataArray{:, 9};

tarray=cat(2,t1,t2,t3,t4,t5,t6,t7,t8,t9,t10,t11,t12);
%% Clear temporary variables
```

```
clearvars filename delimiter startRow formatSpec fileID dataArray ans;

%% plots
 kk=0;
timbbreaks = [0,0];
for ii= 1:length(timeb)-1
    if abs(timeb(ii+1)-timeb(ii))>0.1667
       kk=kk+1;
       timsbreaks(kk,:) = [timeb(ii) timeb(ii+1)];

    end
end
figure
contourf(timeb,dept,tarray',30)
datetick('x','mm/dd HH PM','keeplimits','keepticks')
colorbar
colormap jet
title('T_t_h_e_r_m_i_s_t_o_r')
xlabel('Time')
ylabel('Depth')
set(gca,'YDir','rev')
ylim([1 14])
%phycocyanin
caxis([10 35])
ax.XTickLabelRotation=90;



figure;
subplot(6,1,1),plot(timeb,PARair,'r')
datetick('x','mm/dd','keeplimits','keepticks')
xlabel('Time')
ylabel('Light (PAR air)')
subplot(6,1,2),plot(timeb,Tair,'k')
hold on
subplot(6,1,2),plot(timeb,t2 ,'r')
datetick('x','mm/dd','keeplimits','keepticks')
xlabel('Time')
legend('T air','T water at 1 m')
ylabel('T')
set(gca,'ylim',[20,35])
subplot(6,1,3),plot(timeb,wspd ,'k')
datetick('x','mm/dd','keeplimits','keepticks')
xlabel('Time')
ylabel('U [m/s]')
set(gca,'ylim',[0,11])
subplot(6,1,4),plot(timeb,RH ,'b')
datetick('x','mm/dd','keeplimits','keepticks')
xlabel('Time')
ylabel('RH')
subplot(6,1,5),plot(time2(1,:),cianoave,'b')
hold on
subplot(6,1,5),plot(time2(1,:),cianomax,'r')
```

```
datetick('x','mm/dd','keeplimits','keepticks')
xlabel('Time')
legend('Cave','Cmax')
ylabel('Phycocyanin Voltage')
subplot(6,1,6),plot(time2(1,:),measurement_reshaped4(1,:),'r')
hold on
subplot(6,1,6),plot(time2(1,:),measurement_reshaped4(7,:),'b')
datetick('x','mm/dd','keeplimits','keepticks')
xlabel('Time')
legend('z=1m p1','z=4m p7')
ylabel('Dissolved Oxygen LDO%')
```